

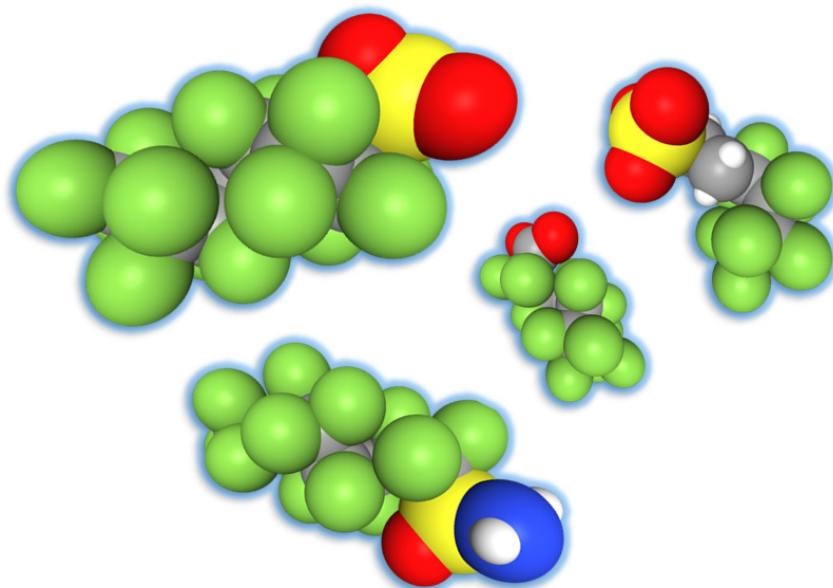


DOCTORAL THESIS NO. 2021:75
FACULTY OF NATURAL RESOURCES AND AGRICULTURAL SCIENCES

Binding of per- and polyfluoroalkyl substances (PFASs) in soil

Effects of solution chemistry, soil properties,
and PFAS structure

HUGO DE CAMPOS PEREIRA



Binding of per- and polyfluoroalkyl substances (PFASs) in soil

Effects of solution chemistry, soil properties,
and PFAS structure

Hugo de Campos Pereira

Faculty of Natural Resources and Agricultural Sciences

Department of Soil and Environment

Uppsala



SWEDISH UNIVERSITY
OF AGRICULTURAL
SCIENCES

DOCTORAL THESIS

Uppsala 2021

Acta Universitatis Agriculturae Sueciae
2021:75

Cover: Ball-and-stick models of the PFASs perfluorooctane sulfonate (PFOS), perfluorooctanoate (PFOA), 6:2 fluorotelomer sulfonate (6:2 FTSA), and perfluorooctane sulfonamide (FOSA). Green represents fluorine, grey carbon, white hydrogen, yellow sulfur, red oxygen, and blue nitrogen.

Creator: H. de Campos Pereira, modified from the PubChem computational tool (pubchem.ncbi.nlm.nih.gov/)

ISSN 1652-6880

ISBN (print version) 978-91-7760-827-1

ISBN (electronic version) 978-91-7760-828-8

© 2021 Hugo de Campos Pereira, Swedish University of Agricultural Sciences

Uppsala

Print: SLU Service/Repro, Uppsala 2021

Binding of per- and polyfluoroalkyl substances (PFASs) in soil. Effects of solution chemistry, soil properties, and PFAS structure

Abstract

The large environmental mobility and persistence of per- and polyfluoroalkyl substances (PFASs) along with confirmed or suspected toxicities make the substances one of the great challenges of our time in the fields of chemical management and environmental risk assessment. In order to risk assess PFAS-contaminated sites, improved quantitative and mechanistic understanding of the partitioning and retention in soil is crucial.

The overall aim of this thesis was to improve the understanding of how PFASs are bound to soil and components therein, including soil organic matter (SOM) and iron (hydr)oxides. The focus was on investigating the role of soil/sorbent net charge and solution pH on binding, and the mechanisms that govern this partitioning behavior.

The effect of soil/sorbent net charge, solution pH, and solid-phase properties on binding was investigated in batch experiments. The surface net charge of sorbents was quantified by geochemical modeling and ζ -potential measurements. Spectroscopic techniques (X-ray absorption, ^{13}C nuclear magnetic resonance) were employed to increase mechanistic understanding.

The driving force for the overall binding of a certain PFAS substance to mineral soils and organic soil horizons was identified as hydrophobic interaction, whereas electrostatic interaction was the main process responsible for the binding onto the positively charged iron (hydr)oxide ferrihydrite. The quality of SOM influenced the binding of PFASs to organic soil materials, in particular that of longer-chained PFASs. Binding of PFASs to soil and to isolated SOM and ferrihydrite was inversely related to solution pH and soil/sorbent net charge, in a manner that suggests that the electronegative fluorine atoms by charge interaction contribute to the binding's overall pH-/charge-dependency.

Extrapolation of organic carbon-normalized binding in organic soil materials to mineral soils underestimated the binding onto the latter, as did an equilibrium partitioning approach based on the surface net charge of SOM. The possible presence of black carbon or other high-affinity binding sites in the mineral soils could not be ruled out, why a component additivity approach (SOM, ferrihydrite) could not be tested properly for these materials. To conclude, this highlights the need for additional experimental binding data that allow the development of more accurate geochemical models with the ability to simulate and predict the binding and leaching of PFASs in the terrestrial environment.

Keywords: PFOS, PFOA, sorption, leaching, XANES, ^{13}C NMR

Author's address: Hugo de Campos Pereira, Swedish University of Agricultural Sciences, Department of Soil and Environment, P.O. Box 7014, 750 07 Uppsala, Sweden.
E-mail: hugo.pereira@slu.se

Bindning av högfluorerade ämnen (PFAS) i mark. Effekter av lösningskemi, markegenskaper, och PFAS-ämnens struktur

Sammanfattning

PFAS-ämnens stora rörlighet och beständighet i miljön tillsammans med bekräftade eller misstänkta negativa hälsoeffekter gör dem till en av vår tids stora utmaningar inom kemikaliehantering och miljöriskbedömning. För att bättre kunna riskbedöma PFAS-förorenade områden är det avgörande med en bättre förståelse av deras fördelning och fastläggningsmekanismer i mark.

Det övergripande syftet med denna avhandling var att öka förståelsen för hur PFAS-ämnen binds i mark och till enskilda komponenter däri, såsom till exempel organiskt material (OM) och järnoxidtytor. Fokus låg på att undersöka vilken roll som pH-värdet samt jordars eller sorbenters nettoladdning har för fastläggningen av olika PFAS-ämnen, samt vilka mekanismer som ligger bakom fastläggningen.

Effekten av nettoladdning och lösnings-pH på bindningen av PFAS undersöktes i skakförsök, där jordarnas/sorbenternas nettoladdning kvantifierades genom geokemisk modellering samt mätning av ζ -potentialen. ^{13}C -kärnmagnetisk resonansspektroskopi användes för karakterisering av organiska jordar, och röntgenabsorption användes för att få ökad mekanistisk förståelse för bindningsmekanismer till järnoxidtytor.

Hydrofoba interaktioner identifierades som drivande för den övergripande bindningen av PFAS-ämnen i mark och till isolerat organiskt material, medan elektrostatiske interaktioner var den huvudsakliga mekanism som drev bindningen till den positivt laddade järn(hydr)oxiden ferrihydrit. Kvaliteten hos det organiska materialet påverkade bindningen av PFAS-ämnen till organiska jordmaterial, i synnerhet vad gäller mer långkedjade PFAS. Förändringar i pH och sorbentnettoladdning gav en större effekt på bindningen av mera långkedjade PFAS-ämnen jämfört med mera kortkedjade ämnen. Detta tyder på att det finns ett bidrag från de elektronegativa fluoratomerna i molekylens svans, utöver bidraget från den funktionella huvudgruppen, till bindningens övergripande pH- och laddningsberoende i mark samt till isolerat organiskt material och ferrihydrit.

Extrapolering av bindningsstyrka normaliserad mot innehållet av organiskt kol i isolerat organiskt material till mineraljordar underskattade bindningen av PFAS-ämnen; detsamma gjorde ett angreppssätt baserat på det organiska materialets ytnettoladdning. Närvaro av bindningsställen av högaffinitetstyp kunde inte uteslutas för mineraljordsmaterialen, varför ett komponent-additivt angreppssätt (OM, ferrihydrit) inte tillfredsställande kunde testas för dessa jordar. Sammanfattningsvis behövs det mer experimentell bindningsdata för PFAS-ämnen i mark som tillåter utveckling av mer precisa geokemiska modeller med förmågan att simulera och förutsäga ämnens fastläggning och utlakning i markmiljön.

Nyckelord: PFOS, PFOA, sorption, utlakning, XANES, ^{13}C NMR

Författarens adress: Hugo de Campos Pereira, Sveriges lantbruksuniversitet, Inst. mark och miljö, Box 7014, 750 07 Uppsala, Sverige. *E-post:* hugo.pereira@slu.se

Till António, Carin och Hannes

Contents

List of publications.....	9
Abbreviations	13
1. Introduction.....	15
1.1 Per- and polyfluoroalkyl substances	15
1.2 Risk assessment of PFASs.....	17
2. Aim, objectives and hypotheses.....	21
2.1 Overall aim.....	21
2.2 Specific objectives	21
2.3 Hypotheses	21
3. Materials and Methods.....	23
3.1 Background for the structure of the experimental work	23
3.2 Overview of the experimental work.....	23
3.3 Batch mode partitioning experiments.....	25
3.3.1 pH-dependent binding experiments.....	25
3.3.2 Sorption isotherms.....	27
3.3.3 Desorption isotherms.....	28
3.3.4 Quantification of sorbent surface net charge	30
3.4 Chemical analysis.....	30
3.4.1 Studied PFASs and their quantification	30
3.4.2 Analysis of aqueous PFAS concentrations.....	31
3.4.3 Analysis of total PFAS concentrations in soil	31
3.4.4 PFAS instrumental analysis.....	31
3.4.5 Quality assurance and quality control.....	32
3.4.6 Supporting analyses	33
3.5 Data treatment	33
3.6 ¹³ C NMR spectroscopy	34
3.6.1 Background	34
3.6.2 Experiment and data treatment	35
3.7 X-ray absorption spectroscopy	36
3.7.1 Background	36
3.7.2 Experiment and data treatment	37

4.	Results and Discussion	39
4.1	pH- and charge-dependent binding of PFASs	39
4.2	Effect of PFAS structure on binding	42
4.2.1	Overall binding as affected by PFAS structure	42
4.2.2	pH- and charge-dependent binding as affected by PFAS structure	44
4.3	Binding of PFASs to isolated soil components	48
4.3.1	Binding to soil organic matter	48
4.3.2	Binding to ferrihydrite	52
4.4	Binding of PFASs to soils	55
4.4.1	Overview	55
4.4.2	Overall binding behavior	57
4.4.3	The role of soil properties	58
4.4.4	Binding as related to the calculated net charge of SOM	61
4.4.5	A binding component not related to pH/charge?	62
5.	Conclusions	65
	Implications and future research	67
	References	69
	Popular science summary	79
	Populärvetenskaplig sammanfattning	81
	Acknowledgments	83

List of publications

This thesis is based on the work contained in the following papers, referred to by Roman numerals in the text:

- I. H. Campos Pereira, M. Ullberg, D.B. Kleja, J.P. Gustafsson, L. Ahrens. (2018) Sorption of perfluoroalkyl substances (PFASs) to an organic soil horizon - Effect of cation composition and pH. *Chemosphere* 207, 183–191. DOI: 10.1016/j.chemosphere.2018.05.012
- II. H. Campos-Pereira, J. Makselon, D.B. Kleja, I. Prater, I. Kögel-Knabner, L. Ahrens, J.P. Gustafsson. Binding of per- and polyfluoroalkyl substances (PFASs) by organic soil materials with different structural composition – charge- and concentration-dependent sorption behavior. Submitted manuscript.
- III. H. Campos-Pereira, D.B. Kleja, C. Sjöstedt, L. Ahrens, W. Klysubun, J.P. Gustafsson. (2020). The adsorption of per- and polyfluoroalkyl substances (PFASs) onto ferrihydrite is governed by surface charge. *Environmental Science and Technology* 54, 15722–15730. DOI: 10.1021/acs.est.0c01646
- IV. H. Campos-Pereira, J. Kikuchi, D.B. Kleja, A. Enell, M. Pettersson, L. Ahrens, J.P. Gustafsson. Effect of pH and soil chemistry on the leaching potential of perfluoroalkyl substances (PFASs) in a wide range of temperate horizons. Manuscript.

Papers I and III are published open access using CC BY-NC-ND 4.0 (Paper I) and CC BY 4.0 (Paper III) licenses, respectively.

The contribution of Hugo de Campos Pereira (HCP) to the papers included in this thesis was as follows:

- I. HCP reevaluated the data of M. Ullberg's master thesis project, wrote the original manuscript draft, and edited and reviewed the manuscript with feedback and support of all co-authors.
- II. HCP collected the soils and planned the study together with J.P. Gustafsson and D.B. Kleja, performed the experimental and analytical work (PFASs) together with J. Makselon, analyzed the data together with J. Makselon, and wrote the original draft of the manuscript with feedback and support of all co-authors.
- III. HCP planned the study together with J.P. Gustafsson, performed the experimental and analytical work, analyzed and evaluated the data, wrote the original manuscript draft, and edited and reviewed the manuscript with the support of all co-authors.
- IV. HCP planned the study together with J.P. Gustafsson, collected soils S2, S4 and S8, performed the experimental and analytical work (PFASs), evaluated the data, and wrote the original draft of the manuscript with feedback and support of all co-authors.

Additional papers

In addition to the papers included in the thesis, the author has contributed to the following peer-reviewed publications:

Nouhi, S., Ahrens, L., **Campos Pereira, H.**, Hughes, A.V., Campana, M., Gutfreund, P., Palsson, G.K., Vorobiev, A., Hellsing, M.S. (2018). Interactions of perfluoroalkyl substances with a phospholipid bilayer studied by neutron reflectometry, *Journal of Colloid and Interface Science*, 511, pp. 474–481. DOI: 10.1016/j.jcis.2017.09.102

Sörengård, M., **Campos-Pereira, H.**, Ullberg, M., Lai, F.Y., Golovko, O., Ahrens, L. (2019). Mass loads, source apportionment, and risk estimation of organic micropollutants from hospital and municipal wastewater in recipient catchments, *Chemosphere*, 234, pp. 931–941. DOI: 10.1016/j.chemosphere.2019.06.041

Abbreviations

Technical terms.

AFFF	Aqueous film-forming foam
Alhox	Aluminum (hydr)oxide
DOC	Dissolved organic carbon
FA	Fulvic acid
FASAs	Fluoroalkyl sulfonamides
Fh	Ferrihydrite
FTSAs	Fluorotelomer sulfonates
HA	Humic acid
IC	Inorganic carbon
IS	Internal standard
LoQ	Limit of quantification
MS/MS	Tandem mass spectrometry
NMR	Nuclear magnetic resonance
OC	Organic carbon
PFASs	Per- and polyfluoroalkyl substances
PFCAs	Perfluorocarboxylates
PFSAs	Perfluorosulfonates
PZC	Point of zero charge
SOM	Soil organic matter
Stdev	Standard deviation
UPLC	Ultra-performance liquid chromatography
XANES spectroscopy	X-ray absorption near-edge structure spectroscopy

Per- and polyfluoroalkyl substances (PFASs) included in this thesis.

Acronym		Molecular formula	CAS number
<u>PFCAs</u>	<u>Perfluorocarboxylates</u>		
PFBA	Perfluorobutanoate	$C_3F_7COO^-$	375-22-4 ^a
PFPeA	Perfluoropentanoate	$C_4F_9COO^-$	2706-90-3 ^a
PFHxA	Perfluorohexanoate	$C_5F_{11}COO^-$	307-24-4 ^a
PFHpA	Perfluoroheptanoate	$C_6F_{13}COO^-$	375-85-9 ^a
PFOA	Perfluorooctanoate	$C_7F_{15}COO^-$	335-67-1 ^a
PFNA	Perfluorononanoate	$C_8F_{17}COO^-$	375-95-1 ^a
PFDA	Perfluorodecanoate	$C_9F_{19}COO^-$	335-76-2 ^a
PFUnDA	Perfluoroundecanoate	$C_{10}F_{21}COO^-$	2058-94-8 ^a
PFDoDA	Perfluorododecanoate	$C_{11}F_{23}COO^-$	307-55-1 ^a
PFTeDA	Perfluorotetradecanoate	$C_{13}F_{27}COO^-$	376-06-7 ^a
<u>PFASs</u>	<u>Perfluorosulfonates</u>		
PFBS	Perfluorobutane sulfonate	$C_4F_9SO_3^-$	45187-15-3
PFHxS	Perfluorohexane sulfonate	$C_6F_{13}SO_3^-$	108427-53-8
PFOS	Perfluorooctane sulfonate	$C_8F_{17}SO_3^-$	45298-90-6
<u>FASAs</u>	<u>Fluoroalkyl sulfonamides</u>		
FOSA	Perfluorooctane sulfonamide	$C_8F_{17}SO_2NH_2$	754-91-6
EtFOSA	<i>N</i> -ethyl perfluorooctane sulfonamide (Sulfluramid)	$C_8F_{17}SO_2NHC_2H_5$	4151-50-2
<u>FTSAs</u>	<u>Fluorotelomer sulfonates</u>		
6:2 FTSA	6:2 fluorotelomer sulfonate	$C_6F_{13}C_2H_4SO_3^-$	27619-97-2 ^a
8:2 FTSA	8:2 fluorotelomer sulfonate	$C_8F_{17}C_2H_4SO_3^-$	39108-34-4 ^a

^aThe CAS number is given for the undissociated species of the chemical.

1. Introduction

Per- and polyfluoroalkyl substances (PFASs) constitute one of the great challenges of our time in the fields of chemical management and environmental risk assessment. The organofluorine chemicals have quickly emerged as a group of contaminants of serious environmental concern. Across the globe, the occurrence of PFASs has caused authorities to restrict or shut down raw water sources for drinking water production (Andersson et al. 2019; NC Policy Watch 2020; New York State Dept. of Environmental Conservation 2020). Exposure to certain PFASs have been linked to adverse health effects in humans and other animals (Kim et al. 2021; Blake et al. 2018; Borg et al. 2013; Johansson et al. 2008), including various types of cancers (Steenland & Winquist 2021; Bartell & Vieira 2021). However, their environmental risk assessment is severely hampered by an incomplete understanding of the mechanisms and processes that dictate their behavior in the soil medium, in particular as regards their binding and leaching. Thus, up to date, no standard protocol exists to assess leaching of PFASs from contaminated sites, and consequently, assessment of their environmental transport, fate and risks remains a great challenge. In this thesis, the binding behavior in soil and to components therein was investigated for a range of different PFAS chemistries, with the aim of contributing to an increased knowledge to improve their environmental risk assessment.

1.1 Per- and polyfluoroalkyl substances

The use of organofluorine chemistry took pace in the 1940's with the Teflon[®] industry being an early important area for its applications (Kissa 2001). The manmade chemicals poly- and perfluoroalkyl substances (Figure 1) have

been produced since the 1950's (3M Company, *History of PFAS and 3M*, 2021) and comprises a group of more than 4,700 different compounds (Kissa 2001; OECD 2018). Their excellent surface-active (surfactant) properties and extreme persistence to degradation make them useful in a variety of applications that require durability and repellency to oil and water. PFASs are used, or have been used, in applications such as aqueous film-forming foams (AFFF) for fire extinction, medical devices, metal-plating, photo-resistors, polymer production, anti-reflective coatings for semi-conductors, and additives in hydraulic fluids (Paul et al. 2009; Buck et al. 2011; Herzke et al. 2012; Goldenman et al. 2019). In addition, their application is widespread in everyday consumer products such as cosmetics (Schultes et al. 2018), non-stick pans, water-repellent textiles, food packaging and paper products (Lindstrom et al. 2011).

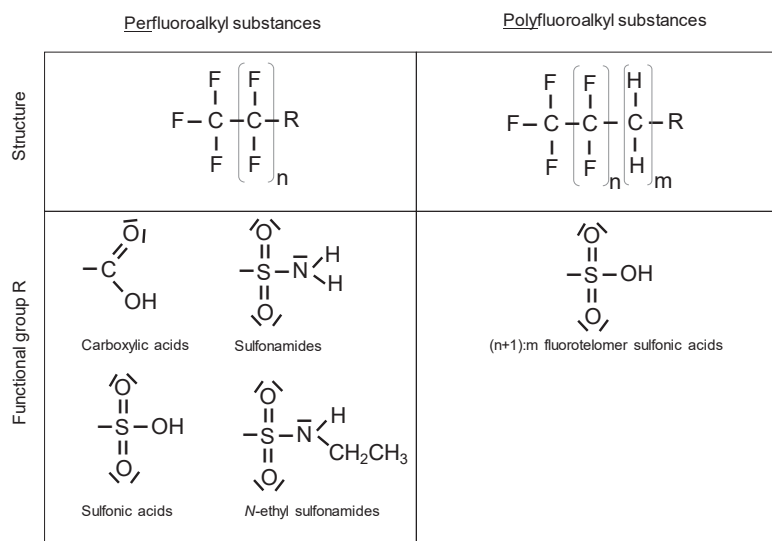


Figure 1. Chemical structures of some important PFAS subclasses that are commonly found in the terrestrial and aquatic environment. The carboxylic and (fluorotelomer) sulfonic acids are expected to be fully ionized at ambient pH values (Rayne & Forest 2009b, 2010; Barzen-Hanson et al. 2017b) and thus, in the environment, they are present as anions.

However, physicochemical properties that make PFASs useful for us humans, such as for example their extreme persistence to degradation, also contribute to making them substances of environmental concern. The carbon–fluorine bond is one of the strongest chemical bounds there are (O’Hagan 2008), and hence it is easy to understand why PFASs popularly are termed “forever-chemicals”. As a rule, PFASs do not occur naturally, and yet, they are found in the blood of nearly every human on earth (Lindstrom et al. 2011; Ludwicki et al. 2015) and are ubiquitously detected in the living and nonliving environment, including in the most remote environments on earth (Muir et al. 2019). Highly contaminated so-called hotspot areas are often associated with fire-fighting training activities, i.e. grounds where PFASs-containing AFFF historically has been released uncontrollably into the environment in large quantities. These historical uncontrolled emissions now constitute a severe contamination of soil and groundwater resources worldwide. Perfluorooctane sulfonate (PFOS) and perfluorooctane carboxylate (PFOA), for which at present the largest body of environmental fate and toxicological data exists, are together with their derivatives, salts and related compounds identified as PBT chemicals (i.e. persistent bioaccumulative and toxic) according to the REACH legislation of the European Union (ECHA, 2021), and as POPs (i.e., persistent organic pollutants) under the Stockholm Convention (2009 and 2020, respectively). As such, there is an ongoing global elimination of their use. In addition, perfluorohexane sulfonate (PFHxS), its salts and related compounds are under consideration for inclusion in the Stockholm Convention (2019).

1.2 Risk assessment of PFASs

The challenge of managing the environmental occurrence of PFASs is closely linked to the human right of having access to clean and safe drinking water (UN 2010). Drinking water is, for the general population, one of the principal routes of PFAS exposure (Sunderland et al. 2019), as conceptualized in Figure 2. The Swedish Food Agency has listed 11 PFASs (Table 1) for which the summed concentration should not exceed a guideline value of 90 ng L⁻¹ in the finished drinking water (Ankarberg & Lindberg 2016). The Swedish government has given as a task to the authority of the Swedish Geotechnical Institute to derive guideline values for PFASs in soil and groundwater, a

work that is currently ongoing (Pettersson et al., 2015). While such environmental guideline values are not legally binding (Swedish EPA, 2009), they play an important role in environmental risk assessment methodology, both in Sweden and in an international context.

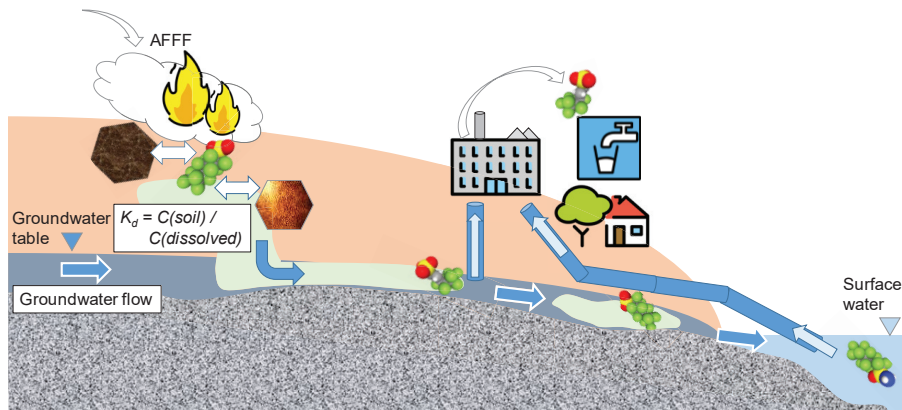


Figure 2. A schematic conceptual model describing human PFAS exposure via the drinking water pathway from an AFFF-impacted site. Drinking water is, for the general public, one of the principal routes of PFAS exposure. Credit subfigures: Openmoji (CC BY-SA 4.0 license): <https://emojipedia.org/openmoji/>.

Table 1. The so-called PFAS₁₁ substances that are included in the current guidelines of the Swedish Food Agency. The guidelines state that the sum of these 11 PFASs should not exceed a concentration of 90 ng L⁻¹ in the finished drinking water (Ankarberg & Lindberg 2016).

Acronym		Molecular formula	CAS number
PFBA	Perfluorobutanoate	C ₃ F ₇ COO ⁻	375-22-4 ^a
PFPeA	Perfluoropentanoate	C ₄ F ₉ COO ⁻	2706-90-3 ^a
PFHxA	Perfluorohexanoate	C ₅ F ₁₁ COO ⁻	307-24-4 ^a
PFHpA	Perfluoroheptanoate	C ₆ F ₁₃ COO ⁻	375-85-9 ^a
PFOA	Perfluorooctanoate	C ₇ F ₁₅ COO ⁻	335-67-1 ^a
PFNA	Perfluorononanoate	C ₈ F ₁₇ COO ⁻	375-95-1 ^a
PFDA	Perfluorodecanoate	C ₉ F ₁₉ COO ⁻	335-76-2 ^a
PFBS	Perfluorobutane sulfonate	C ₄ F ₉ SO ₃ ⁻	45187-15-3
PFHxS	Perfluorohexane sulfonate	C ₆ F ₁₃ SO ₃ ⁻	108427-53-8
PFOS	Perfluorooctane sulfonate	C ₈ F ₁₇ SO ₃ ⁻	45298-90-6
6:2 FTSA	6:2 fluorotelomer sulfonate	C ₆ F ₁₃ C ₂ H ₄ SO ₃ ⁻	27619-97-2 ^a

^aThe CAS number is given for the undissociated species of the chemical.

The sorption coefficient (Brusseau & Chorover 2019) is central in environmental risk assessment methodology (Leeuwen & Hermens 2012; Jensen & Mesman 2006; Swedish EPA 2009). Not only does it in a direct way describe the partitioning of a substance between the solid phase and the dissolved (solution) phase, but this partitioning also has important implications on several other fate and transport processes. For example, it is mainly the dissolved species of a substance that is available for biological uptake. Furthermore, with the exception of any colloidal association, a substance needs to be dissolved in the soil solution to be leached, i.e. to be available for transport in the soil profile and onwards to ground- and surface waters. In other words, usually, it is not the total soil concentration of a harmful substance that relates in a direct way to the posed risk, but rather it is the dissolved fraction that is more closely related to the risk. Moreover, robust long-term risk assessment requires understanding of how this dissolved fraction may change with geochemical conditions (e.g. the pH value) and over time, why it is crucial to have knowledge on the underlying mechanisms and processes that control the soil solubility of the substance in question.

For PFASs, the retention mechanisms in soil are still far from fully understood, and thus, there is to date no standard tool or protocol available for authorities, consultants or problem owners to use when risk assessing a site contaminated with PFASs. Previous research on PFAS environmental behavior and the uniqueness of their chemistry indicates that their binding behavior in soil is of a complex nature and may involve several mechanisms/contributions, such as hydrophobic and electrostatic interactions, ion exchange mechanisms (Guelfo et al., 2021; Nguyen et al. 2020; Guelfo & Higgins 2013), formation of inner- and outer-sphere surface complexes (Gao & Chorover 2012), and air–water interfacial adsorption in the unsaturated zone (Lyu et al. 2018; Lyu & Brusseau 2020). The large environmental mobility of PFASs relates to their charged (often anionic) molecular features and unique organofluorine chemistry: the van der Waals forces exerted by PFAS molecules towards their environment are much weaker as compared to other substances of similar size (Goss & Bronner 2006). Thus, an accurate prediction of the binding behavior of PFASs in soil across a wider range of geochemical conditions cannot likely be achieved through a simple normalization against soil organic carbon, as commonly has been done for other legacy hydrophobic organic contaminants (Swedish EPA, 2009).

2. Aim, objectives and hypotheses

2.1 Overall aim

The overall aim of this thesis was to advance the knowledge on how poly- and perfluoroalkyl substances (PFASs) are bound in soil and to soil components.

2.2 Specific objectives

The specific objectives were to:

O1) Determine the pH-, charge- and concentration-dependent binding behavior of PFASs onto soil organic matter of different quality.

O2) Determine the pH-, charge- and concentration-dependent binding behavior of PFASs onto poorly crystalline iron (hydr)oxide (ferrihydrite).

O3) Determine the pH-dependent binding of PFASs in a wide range of soils of varying characteristics, and relate the findings to the results obtained from the experiments associated with objective O1) and O2).

2.3 Hypotheses

Connected to the objectives O1–O3 were the following hypotheses:

H1) Binding of PFASs to soil organic matter occurs primarily through hydrophobic interactions. The binding of PFASs to organic matter is therefore related to its net charge, i.e., the lower the net charge, the stronger the PFAS binding.

H2) The interaction between PFASs and Fe (hydr)oxide surfaces involves mainly electrostatic contributions, and the binding is related to the charge of the surface as affected by solution chemistry (i.e. pH, $[\text{PO}_4^{3-}]$, ...).

H3) The overall binding of PFASs to soil and soil components increases with the perfluorocarbon chain length within each PFAS subclass, and the sorption is further influenced by the functional group of the respective subclass.

H4) PFASs are bound to soils primarily by hydrophobic interactions with organic matter, although electrostatic interactions and surface complexation, involving also metal (hydr)oxides, could be important in some mineral soils at low pH.

H5) A component additivity approach, building on the findings on the binding to isolated phases of soil organic matter and mineral surfaces, is able to predict the binding of PFASs in a wide range of soils of different characteristics.

3. Materials and Methods

3.1 Background for the structure of the experimental work

The structure of the work presented in this thesis took a bottom-up (additive) approach, where the initial investigations (Paper **I–III**) focused on the binding of PFASs to “isolated” soil components (i.e., soil organic matter, iron (hydr)oxides), whereas the latter work (Paper **IV**) investigated the binding behavior in more complex soil systems that simultaneously contained a multitude of components, including soil organic matter and iron (hydr)oxides (c.f. approaches described by Groenenberg & Lofts (2014) and Arp et al. (2014) for prediction of the binding of metal(loid)s and polycyclic aromatic compounds in soil). The basic idea was, that in order to better understand the binding behavior of PFASs in soils, one needs to understand the binding to its respective components.

3.2 Overview of the experimental work

The additive approach was reflected in the structure of the thesis work (Figure 3). The initial investigations focused on the binding of PFASs onto isolated soil components, i.e., soil organic matter (Paper **I–II**) and the poorly crystalline iron (hydr)oxide ferrihydrite (Paper **III**), whereas the latter work investigated the binding behavior of PFASs across a wide range of soils of different characteristics (Paper **IV**). An overview of the materials is given in Table 2.

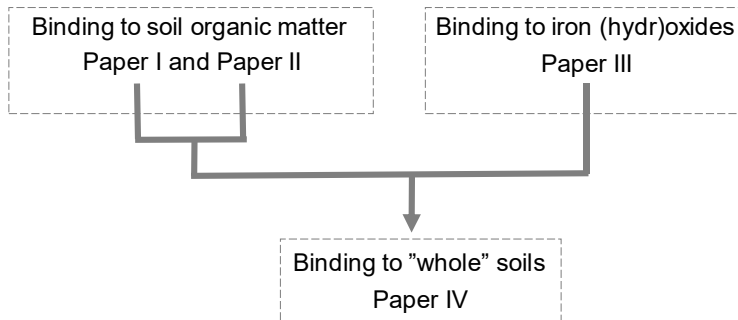


Figure 3. Workflow and schematic relationship between Papers I–IV included in this thesis.

Table 2. Overview of the materials for which the binding of PFASs was investigated.

	Soils/sorbent	Comment
Paper I	$n = 1$ temperate organic soil (<i>Spodosol</i> Oe)	Surface horizon
Paper II	$n = 3$ temperate organic soils, of which $n = 1$ <i>Spodosol</i> Oe soil $n = 2$ peat soils (Oi and Oe)	Surface horizons
Paper III	2-line ferrihydrite	Synthesized in the laboratory ^c
Paper IV	$n = 10$ temperate mineral soils	$n = 6$ surface horizons, $n = 4$ subsoils

^cSynthesized according to the procedure of Schwertmann & Cornell (2000).

Table 3 presents an overview of the different experimental methods employed. pH-/charge-dependent binding experiments were included in all four works (I–IV, Table 4), as this was considered a powerful tool to, for instance, gain increased mechanistic understanding of the binding of various PFAS chemistries onto the different materials. Related to the extensive use of pH-/charge-dependent binding tests was also the application of methods to quantify the surface net charge of the sorbents at different pH values and solution chemistries (e.g., upon additions of Al^{3+} or Ca^{2+} to a suspension). This was performed through two main methods: geochemical modeling of the solid species present at the sorbent surface at equilibrium (Paper I–II, section 3.3.4 below), and by measuring the electrical ζ (zeta)-potential of the suspended

particles (Paper **III**). Additional methods that were employed to increase the understanding of the nature of PFAS binding in soil and to soil components included spectroscopic methods (Paper **II** and **III**), and derivation of sorption and desorption isotherms (Paper **II** and **III**, Table 4).

Apart from where explicitly noted, all experiments and analyzes were performed at the Swedish University of Agricultural Sciences (SLU).

Table 3. Overview of methods employed in Paper **I–IV**.

	Paper I	Paper II	Paper III	Paper IV
pH-dependent binding experiments	✓	✓	✓	✓
Sorption isotherms		✓	✓	
Desorption isotherms		✓		
Calculation/measurement of sorbent charge	✓	✓	✓	✓
¹³ C NMR spectroscopy		✓		
S K-edge XANES spectroscopy			✓	

3.3 Batch mode partitioning experiments

The partitioning of PFASs between the solid phase (i.e. soils (Paper **I**, **II** and **IV**), or 2-line ferrihydrite (Paper **III**)) and the aqueous phase was determined in batch experiments, as summarized in Table 4 and 5. The PFASs were added to suspensions of organic soils (**I** and **II**) or iron (hydr)oxides (**III**), or, as in Paper **IV**, spiked to a selection of mineral soils prior to suspending the aged soils in solution. Suspensions were equilibrated by end-over-end shaking for 7 days (**I–II**, **IV**) or 24 hours (**III**) prior to phase-separation and analysis (section 3.4).

3.3.1 pH-dependent binding experiments

pH-dependent binding experiments, as summarized in Table 4, were conducted as a part of the work of all four papers (**I–IV**). By studying how the binding changes with the pH value, and thus with the charge of the sorbent, valuable quantitative and qualitative (mechanistic) understanding of the binding may be obtained. Nitric acid (HNO₃) and sodium hydroxide (NaOH)

were used to add acid and base, respectively, in all experiments that tested the pH-dependent binding. To distinguish the effect of pH/sorbent charge on binding from any effects that could arise by changing the ionic strength of the solution, the latter was kept at a similar level over the entire investigated pH range. This was performed by keeping the total concentration of nitrate (NO_3^-) ions constant at (or close to) 10 mmol L^{-1} by additional addition of NaNO_3 to some of the suspensions. The solution compositions were further varied through addition of nitrate salts of Ca^{2+} (3 and 5 mmol L^{-1}) or Al^{3+} (2 mmol L^{-1}) (Paper **I** and **II**), or through the addition of phosphate in the form of NaH_2PO_4 (**III**). These treatments were applied to investigate in detail the role of sorbent surface charge on the binding of PFASs.

Table 4. pH-dependent binding experiments (Paper **I–IV**). Time of equilibration: 7 days for each experiment, with exception for those that included ferrihydrite (24 hours). Background electrolyte for all batch experiments: $10 \text{ mmol L}^{-1} \text{NO}_3^-$.

Paper	Analytes	pH	Batch test, treatments
I	PFCAAs $\text{C}_3\text{--C}_{11}$, C_{13} ; PFSAAs C_4 , C_6 and C_8 ; FOSA	3–6	Initial additions of individual PFASs to suspension: 2.8 nmol L^{-1} , on average Solution–soil ratio: 90 mL g^{-1} dw soil Series: a) $2 \text{ mmol L}^{-1} \text{Al}(\text{NO}_3)_3$ b) $3 \text{ mmol L}^{-1} \text{Ca}(\text{NO}_3)_2$ c) $5 \text{ mmol L}^{-1} \text{Ca}(\text{NO}_3)_2$ d) $\sim 10 \text{ mmol L}^{-1} \text{Na}^+$
II	PFCAAs C_7 , C_{10} , C_{11} and C_{13} ; PFSAAs C_4 , C_6 and C_8 ; FOSA and EtFOSA; 6:2 and 8:2 FTSA	3–6	Initial additions of individual PFASs to suspension: $2.6\text{--}69 \text{ nmol L}^{-1}$ Solution–soil ratio: $41\text{--}54 \text{ mL g}^{-1}$ dw depending on soil Series: a) $2 \text{ mmol L}^{-1} \text{Al}(\text{NO}_3)_3$ b) $5 \text{ mmol L}^{-1} \text{Ca}(\text{NO}_3)_2$ c) $\sim 10 \text{ mmol L}^{-1} \text{Na}^+$

Paper	Analytes	pH	Batch test, treatments
III	PFCAs C ₃ –C ₅ and C ₇ –C ₉ ; PFASs C ₄ , C ₆ and C ₈ ; FOSA; 6:2 and 8:2 FTSA	4–8	Initial additions of individual PFASs to suspension: 1.6–5.5 nmol L ⁻¹ Series: a) 3.2 mmol L ⁻¹ Fe as Fh b) 3.2 mmol L ⁻¹ Fe as Fh + 200 μmol L ⁻¹ phosphate
IV	PFCAs C ₇ , C ₉ , C ₁₀ PFASs C ₆ and C ₈ ; FOSA	3–9	Initial soil concentrations of individual PFASs: 66–340 nmol kg ⁻¹ dw spiked soil, and 18 and 140 nmol PFHxS and PFOS, respectively, per kg dw field-contaminated soil Solution–soil ratio: 10 mL g ⁻¹ dw

3.3.2 Sorption isotherms

Concentration-dependent binding experiments (sorption isotherms) were performed by adding PFASs at varying concentrations to soil or ferrihydrite suspensions (Paper II and III, as summarized in Table 5). The shape of a sorption isotherm may provide insight into the binding mode of a substance onto a sorbent (Schwarzenbach et al. 2016). For example, a linear isotherm indicates that the partitioning is independent of the concentration in solution (over a given range of concentrations at equilibrium conditions). This means that no significant interactions between the sorbate molecules are thought to occur on the sorbent. Many environmental fate and transport models assume such a linear sorption behavior, including the model of the Swedish EPA that is often used as a tool for deriving general and site-specific guideline values (Swedish EPA, 2009). Two other types of sorption isotherms are those of “concave-down” and “concave-up” type, which may be observed when the sorbate molecules are interacting with each other in some way on the sorbent.

3.3.3 Desorption isotherms

The process of retention or leaching of contaminants in a soil profile involves not only the process of their sorption but also that of their desorption rate. Knowledge on the nature of the desorption process (isotherm) is essential when assessing numerous aspects related to the fate and transport of a substance (Pignatello & Xing 1996; Pan et al. 2009), such as for example plant uptake, or the rapid or retarded flush-out of an aquifer system. Retarded long-term leaching may be associated with factors such as desorption hysteresis and rate-limited desorption. Such retardation processes likely play an important role in that PFAS soil/groundwater contamination may persist for timescales of years up to decades after the ceasing of the emission-causing activities (Adamson et al., 2020; Backe et al., 2013; Barzen-Hanson et al., 2017a; Filipovic et al., 2015; Moody et al., 2003; Wilhelm et al., 2010; Xiao et al., 2015).

A desorption experiment (Table 5) was performed in connection to the derivation of the sorption isotherms of Paper II. Two desorption branches were constructed according to the method of successive dilution, for which the solution volume and concentrations of background electrolyte (10 mmol L⁻¹ NaNO₃) were kept constant. The dilution and re-equilibration step was repeated in total four times to yield desorption isotherms.

Table 5. The concentration-dependent sorption and desorption experiments (sorption and desorption isotherms) presented in Paper II and III. Time of equilibration: 7 days for each experiment or re-equilibration step, with exception for those that included ferrihydrite (24 hours).

Paper	Analytes	Soils/sorbent	pH	Experimental conditions
II	PFCA _s C ₆ –C ₁₁ ; PFSA _s C ₆ and C ₈ ; FOSA and EtFOSA; 6:2 and 8:2 FTSA _s (multi-solute experiments)	Temperate organic soils (<i>n</i> = 2)	3.5– 3.7	<i>C_w</i> after eq. = 2.8–87 nmol L ⁻¹ of individual PFAS _s , on average Solution–soil ratio: 41–54 mL g ⁻¹ dw depending on soil Background electrolyte for both series: 10 mmol L ⁻¹ NO ₃ ⁻
II			3.6– 4.0	Desorption tests (<i>n</i> = 2 de- sorption branches from the sorption isotherms described above). <i>n</i> = 4 re-equilibration steps. Solution–soil ratio: 41–54 mL g ⁻¹ dw depending on soil Background electrolyte for both series: 10 mmol L ⁻¹ NO ₃ ⁻
III	PFSA C ₈ (i.e. PFOS) PFCA C ₇ (i.e. PFOA) FOSA (single-solute experiments)	Ferrihydrite	4.4– 4.6	<i>C_w</i> after eq. = 1–700 nmol L ⁻¹ PFOS; 1–2000 nmol L ⁻¹ PFOA; 0.3–1000 nmol L ⁻¹ FOSA; Sorbent concentration: 10 mmol L ⁻¹ Fe as ferrihydrite Background electrolyte for all isotherms: 30 mmol L ⁻¹ NO ₃ ⁻

3.3.4 Quantification of sorbent surface net charge

Geochemical modeling

In Paper **I**, **II** and **IV**, geochemical modeling was applied to calculate the surface net charge of soil organic matter for various solution chemistries (Table 4). Due to the charged molecular features of PFASs, it may be expected that the surface net charge of the sorbent will affect their binding, similarly as for many other ionic organic chemicals (e.g., Jafvert 1990). The modeling software employed was Visual MINTEQ (Gustafsson 2020), incorporating the sub-model Stockholm Humic Model (SHM) (Gustafsson 2001) which was used to model the surface net charge of SOM.

Measurement of ζ -potential

As part of the sorbent characterization in Paper **III**, the charge of the suspended ferrihydrite particles was determined by measurements of their ζ -potential (Zetasizer Nano-ZS, Malvern). The measurements encompassed the same solution chemistries (i.e. pH values, additions of phosphate anions) and experimental conditions, excluding addition of PFASs, as in the pH-dependent sorption experiment with ferrihydrite. The ζ -potential of a surface is strongly related to its surface charge (Poisson-Boltzmann equation).

3.4 Chemical analysis

3.4.1 Studied PFASs and their quantification

Analysis of aqueous-phase PFAS concentrations was conducted at SLU on high- (Paper **I**) or ultra-performance (Paper **II-IV**) liquid chromatography – tandem mass spectrometers (HPLC-MS/MS, UPLC-MS/MS (Dionex Ultimate 3000, Thermo Fisher Scientific, MA; TSQ Quantiva, Thermo Fisher Scientific, MA). The analytes included C₃–C₁₁ and C₁₃ perfluorocarboxylates (PFCAs), C₄, C₆ and C₈ perfluorosulfonates (PFSAs), C₆ and C₈ fluorotelomer sulfonates (C_x:2 FTSAs), perfluorooctane sulfonamide (FOSA), and *N*-ethyl perfluorooctane sulfonamide (EtFOSA), with C_x indicating the number of perfluorinated carbons in the molecular structure. To quantify the PFASs, a mixture of 14 mass-labeled internal standards (ISs) was added to the samples. Target analytes and ISs were matched according to structural

similarity. For information on analyte–IS pairs and limits of quantification (LoQs), the reader is referred to the respective paper of the thesis.

3.4.2 Analysis of aqueous PFAS concentrations

Samples were analyzed through direct injection into the instrument (Paper II–IV), or as extracts prepared by offline solid-phase extraction (SPE, method ISO/DIS 25101:2009 (ISO, 2009) (Paper I). The solid-phase extraction method has been described in detail by for example Ahrens et al. (2015). For analysis with direct injection, the soil suspensions were first phase-separated by centrifugation (2000–2500g). Subsequently, 500 μL of aqueous sample was fortified with an aliquot, generally 50 μL , of ISs dissolved in MeOH (0.05 $\mu\text{g mL}^{-1}$ of each IS). In addition, 450 μL MeOH was added with the purpose of improving chromatographic peak shape in the instrument. Samples were filtered through an 0.45 μm Sartorius Minisart hydrophilic regenerated cellulose syringe filter. PFAS recoveries for these filters have been evaluated by Lath et al. (2019) and Sörengård et al. (2020).

3.4.3 Analysis of total PFAS concentrations in soil

For determination of total concentrations of PFASs in soil (Paper IV), samples were analyzed at SLU according the method described by Gobelius et al. (2017). In brief, an aliquot of freeze-dried homogenized soil was extracted with a IS-fortified mixture of 80% MeOH and 20% 1 M NaOH. Prior to injection into the instrument, pH-adjusted extracts (50/50 methanol/H₂O v/v) were filtered at 0.45 μm (Sartorius Minisart hydrophilic regenerated cellulose syringe filter). The results from the soil extractions conducted at SLU were further compared and in agreement with those of two commercial laboratories who analyzed aliquots of the same samples (ALS Scandinavia, accredited method; Eurofins).

3.4.4 PFAS instrumental analysis

The analytes (10 μL) were separated on a BEH (ethylene bridged hybrid)-C18 analytical column (1.7 μL , 50 mm, Waters, UK), using an eluent gradient of 12 min and Milli-Q (LC-PAK) water and 5 mM ammonium acetate in 2% acetonitrile as mobile phases. A nine-point calibration curve (50/50

MeOH/H₂O) ranging from 0.01 to 100 ng mL⁻¹ was used for quantification (all r^2 values ≥ 0.99). The limits of quantification (LoQs) were defined as the lowest calibration point for which the response factor of the instrument was within $\pm 30\%$ of the average response factor of the calibration curve (Higgins et al. 2005). All peak integrations were manually checked using the Trace-Finder™ software (Thermo Fisher Scientific). In the UPLC system, all Teflon® parts were removed in order to avoid background contamination. Furthermore, to avoid effects from possible mobile phase contamination, trapping columns were installed after the mixing chamber of the system.

3.4.5 Quality assurance and quality control

Fluorinated materials (labware, instrument parts as described above) were avoided throughout all studies in order to minimize contamination. In addition, the Milli-Q water used in the experimental work (Milli-Q® IQ 7000 lab water system) was filtered through cartridges of powdered activated carbon (Milli-Q LC-PAK, Merck, Darmstadt, Germany) prior to use, with the purpose of removing PFAS background concentrations. For all analytical applications, all solvent products were of analytical grade (for example methanol; LiChrosolv® hypergrade, Merck, Darmstadt, Germany). Negative controls (blanks) were included in all batch experiments in order to further control for any background contamination. The use of mass-labeled internal standards corrected for any losses onto analysis vials, syringes, filters, *et cetera*, across the analytical chain. To assess sorption losses onto reactor walls, positive controls were included in the work reported in Paper I–III. Reactor–solution partitioning coefficients were derived from the positive controls of Paper III and were used to correct the sorbent–solution partitioning for reactor sorption losses (see details in III).

In all experiments, the amount of methanol that was co-spiked with the added PFASs was less than 0.45% (v/v) in the equilibrated suspensions, i.e. the addition of co-solvent could be considered to have a negligible effect on the PFAS partitioning behavior (Schwarzenbach et al., 2016, Environmental Organic Chemistry, 3rd Edition, page 302). All samples analyzed for PFASs were produced as duplicates or as higher-order replicates. Replicate errors for measured aqueous PFAS concentrations were typically in the range of 5–

15%. Recoveries of the internal standards were determined as the ratio between their measured intensities in the analyzed samples and those of the calibration curve, and were typically in the range of 76–102%.

3.4.6 Supporting analyses

Supporting analyses and soil extractions were conducted at SLU, KTH (Royal Institute of Technology), and by the commercial laboratories ALS Scandinavia and Eurofins. Soil organic carbon content (Paper **I**, **II** and **IV**) was measured at SLU using a TruMac CN analyzer (LECO, MI) (ISO10694, 1995; ISO 13878 (1998), and/or at ALS Scandinavia (method SS-EN 13137, accredited). Metals were quantified at SLU (dissolved concentrations) using inductively coupled plasma optical emission spectrometry (ICP-OES, PerkinElmer Avio 200) and at KTH (soil extracts) using a Thermo ICAP 6300 ICP-OES. Dissolved concentrations of iron and phosphorus (Paper **III**) were determined at SLU using an ICP-OES instrument. Parts of the soil properties needed for Paper **IV** were assessed at ALS Scandinavia, such as particle size distribution and cation exchange capacity (accredited and not accredited analysis, respectively). Dissolved organic carbon (DOC) was determined at SLU using a Shimadzu TOC-V CPH analyzer (**II**), or by ALS Scandinavia (**I**).

For further details on supporting analyses and soil extractions, the reader is referred to the respective studies included in this thesis.

3.5 Data treatment

PFAS binding to the solid phases was calculated as the difference between added and dissolved PFASs upon equilibration. The solid–water partitioning coefficient K_d [mL g^{-1}] was calculated as the ratio between the concentration of the individual PFAS bound to the sorbent (C_s [ng g^{-1} dw]) and its concentration in the aqueous phase upon equilibration (C_w [ng mL^{-1}]) (Eq. 1):

$$K_d = \frac{c_s}{c_w} \quad \text{Eq. 1}$$

In Paper **I** and **II** where the binding to organic soils was investigated, the partitioning coefficient K_d was for comparative purposes normalized to the fraction of organic carbon in the soil (f_{oc}), yielding the so-called K_{oc} value [$\text{mL g}^{-1} \text{OC}$] (Eq. 2):

$$K_{oc} = \frac{K_d}{f_{oc}} = \frac{c_s}{c_w \cdot f_{oc}} \quad \text{Eq. 2)}$$

In Paper **III**, where the work focused on the binding behavior onto the poorly crystalline iron (hydr)oxide ferrihydrite, the partitioning coefficients [$\text{mL g}^{-1} \text{Fe}$] were determined on the basis of the amount of Fe in the ferrihydrite (Eq. 3):

$$K_d = \frac{c_s [\text{ng g}^{-1} \text{Fe}]}{c_w} \quad \text{Eq. 3)}$$

The logarithms of the partitioning coefficients were normally distributed ($\alpha = 0.05$) for the experiments described in this thesis (Shapiro-Wilk test; Shapiro and Wilk, 1965), as is generally the case for quantities that are formed from ratios (e.g., partitioning coefficients) according to the central limit theorem. Hence, when the average of several measured partitioning coefficients was evaluated in the work described in this thesis, for example those of a specific PFAS over a certain pH range, the arithmetic mean of the logarithmic partitioning coefficients (i.e., $\log K_d$ or $\log K_{oc}$) was employed.

3.6 ^{13}C NMR spectroscopy

3.6.1 Background

Solid-state cross-polarization magic angle spinning carbon-13 (^{13}C) nuclear magnetic resonance (CP/MAS ^{13}C -NMR) spectroscopy was employed to characterize the soils used for the sorption experiments in Paper **II**. The method allows characterization of the chemical environment of the ^{13}C isotope in a sample. This is done by exploiting the magnetically active properties of the ^{13}C atom that arise from its quantum spin number (1/2) which makes it resonate in a magnetic field. The resonance (i.e. the chemical shift) will look different depending on the chemical environment of the ^{13}C atom.

This makes it possible to assess the carbon chemistry of a sample (e.g., the content of aliphatic and aromatic carbon) both from a qualitative and a quantitative standpoint (Baldock et al. 1997).

3.6.2 Experiment and data treatment

A Bruker DSX 200 spectrometer (Billerica/USA) at the Technical University of Munich was employed to measure CP/MAS ^{13}C NMR spectra for the three organic soils used in Paper II (Figure 4). The chemical shift of tetramethylsilane was equated with 0 ppm as a reference for the soil spectra. Phase-adjustment and baseline-correction of the spectra was performed prior to integration over the C regions given in Figure 4 and in Table 1 in Paper II. Furthermore, the spectra were converted into the compound classes of carbohydrates, proteins, lignins, lipids and carbonyls. This was performed by integrating the spectra according to Baldock et al. (2004) and Nelson & Baldock (2005) to allow their molecular mixing model to be applied. For further details, see Paper II and its Supporting Information.

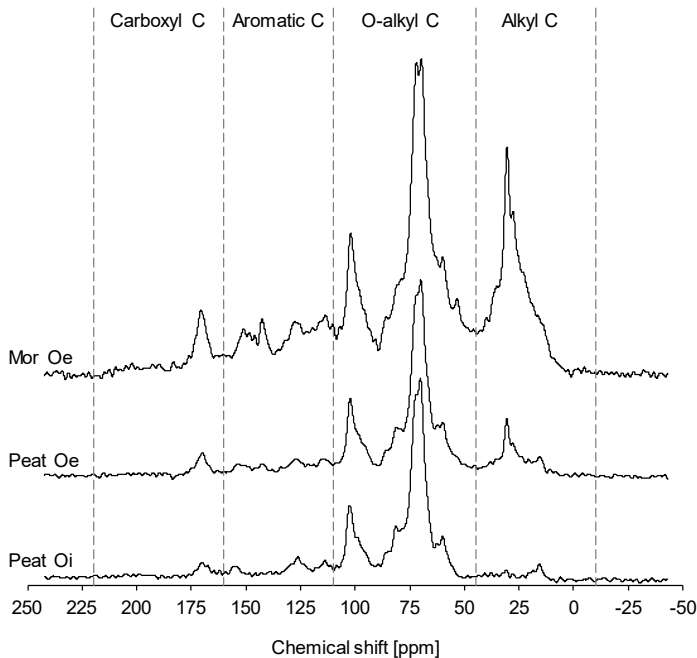


Figure 4. The CP-MAS ^{13}C NMR spectra acquired for the three organic soil used in the experiments of Paper II.

3.7 X-ray absorption spectroscopy

3.7.1 Background

Sulfur X-ray absorption spectroscopy (XAS) was employed to acquire information about the oxidation state and local binding environment of sulfonated PFASs onto the mineral ferrihydrite (Paper III). X-ray absorption spectra are acquired by irradiating samples with high-energy X-rays at synchrotron radiation facilities, which are available to the research community at various locations around the world. For example, the oxidation state of an element increases with the so-called white-line position relative to that of the element in its elementary form (oxidation state 0) (Xia et al. 1998; Vairavamurthy et al. 1993; Waldo et al. 1991). By this relationship, conclusions can be drawn as to whether the oxidation state of the element changes upon adsorption or not, which may provide direct information about the binding mechanism. Below (Figure 5) is shown an example of two S K-edge X-ray absorption near-edge structure (XANES) spectra: those of PFOS and sulfate (SO_4^{2-}) adsorbed to ferrihydrite. The difference in the white-line position for ferrihydrite-adsorbed PFOS and sulfate (2480.7 electron volts (eV) and 2482.5 eV, respectively) reflects the difference in oxidation state of its respective sulfur atom (S(V) and S(VI), respectively).

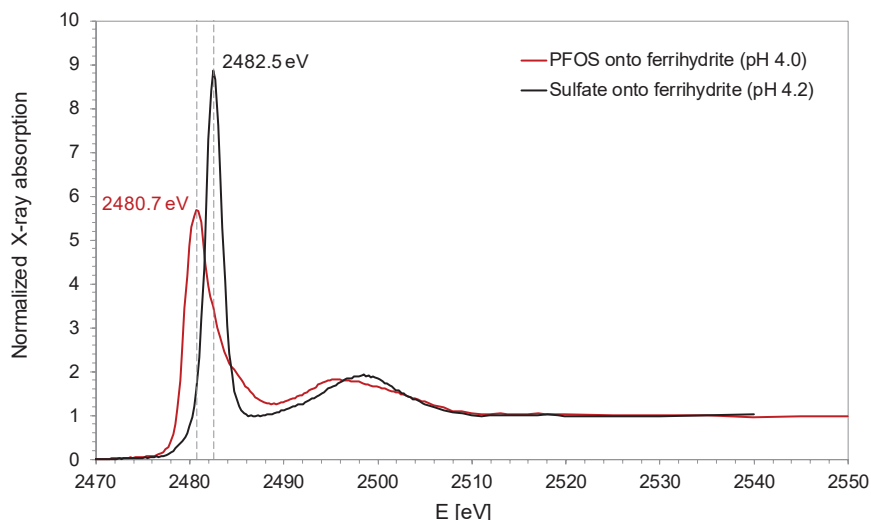


Figure 5. Sulfur K-edge X-ray absorption near-edge structure (XANES) spectra for PFOS and sulfate (SO_4^{2-}) adsorbed to ferrihydrite. Spectra were acquired at the Synchrotron Light Research Institute (SLRI), Nakhon Ratchasima, Thailand. The pH values indicate those of the equilibrated suspensions prior to phase-separation.

3.7.2 Experiment and data treatment

Sulfur K-edge X-ray absorption near-edge structure (XANES) spectra for sulfonated PFASs (PFHxS, PFOS, FOSA) onto ferrihydrite were acquired at beamline BL8 at the Synchrotron Light Research Institute (SLRI), Nakhon Ratchasima, Thailand, in May 2017. In addition, various reference spectra were acquired (see Paper **III**), including those of the pure PFAS standards in their solid state, and that of sulfate (SO_4^{2-}) adsorbed to ferrihydrite. The purpose of including spectra for sulfate was that the inner-sphere complex formed by sulfate onto ferrihydrite gives rise to a so-called pre-edge peak due to orbital hybridization, and thus, this feature could be compared with those of the PFAS–ferrihydrite spectra to examine the nature of the binding mechanism. The sulfate white-line of FeSO_4 (2482.5 eV, Prietzel et al. (2013)) was used for energy calibration. The Athena software (Ravel & Newville 2005) was used for energy shift correction and normalization of all XANES spectra. For additional details on the experiment and the data treatment, see Paper **III**.

4. Results and Discussion

4.1 pH- and charge-dependent binding of PFASs

The pH-/charge-dependent binding of all PFAS subclasses was more or less pronounced onto all types of soils and sorbents for which their binding was investigated. That is, the overall binding was inversely related (confidence level 95%, i.e., $p < 0.05$) to solution pH (Paper **I-IV**), and to the surface net charge or ζ -potential of the solid phases (**I-III**). The relationship between the binding and the pH value, and the binding and the sorbent charge, is illustrated in Figure 6 and 7, respectively, for PFOS and PFOA. However, for the (overall weak) binding of some of the short-chained PFCAs and PFSAAs (i.e., PFBA, PFPeA, PFBS) onto organic soils and ferrihydrite, changes in the pH value and/or the sorbent charge had no or limited effect (Paper **I-III**, significance level $\alpha = 0.05$).

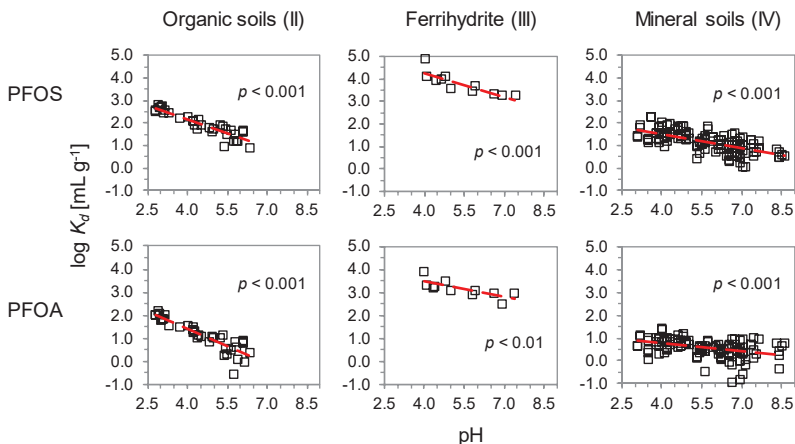


Figure 6. pH-dependent binding of PFOS (upper row) and PFOA (lower row) to temperate organic soils (Paper II, unit [mL g^{-1} soil]), the iron (hydr)oxide ferrihydrite (III, [mL g^{-1} Fe]) and temperate mineral soils (IV, [mL g^{-1} soil]).

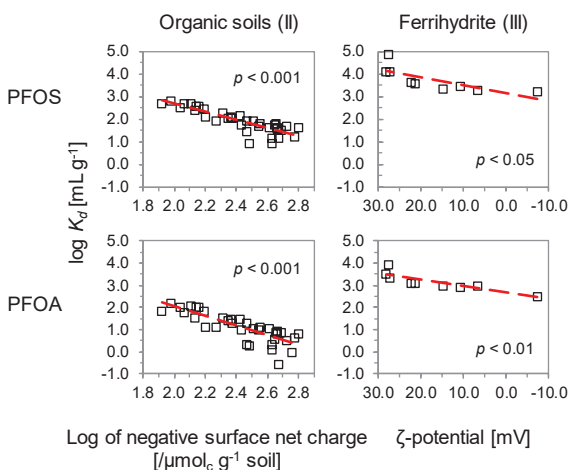


Figure 7. Charge-dependent binding of PFOS (upper row) and PFOA (lower row) to temperate organic soils (Paper II, unit [mL g^{-1} soil]) and to the iron (hydr)oxide ferrihydrite (III, [mL g^{-1} Fe]).

As a rule, the PFASs analyzed in this thesis are not expected to change their aqueous speciation (protonation) over the studied pH range (~ 3 – 9) according to the acid constants derived by Moroi et al. (2001), Rayne & Forest (2009b, 2010) and Barzen-Hanson et al. (2017a). Thus, the effect of a change in the

pH value on binding was interpreted as an effect of a change in the charge present on the sorbent or the soil. A more acidic pH value decreases the net negative charge present on the soil, or increases the positive charge present on the ferrihydrite particles (Figure 8), which enhances the binding of PFASs due to more favorable electrostatic conditions on the solid phase. Not only was the effect of pH/sorbent net charge evident for the binding of PFASs that were present as negatively charged anions (i.e., PFCAs, PFSAAs and FTSAAs), but it was also observed for the binding of the fluoroalkyl sulfonamides FOSA and EtFOSA that were both present as non-ionic species (for pH < ~6.4 in the case of FOSA (Rayne & Forest 2009a; Steinle-Darling & Reinhard 2008)).

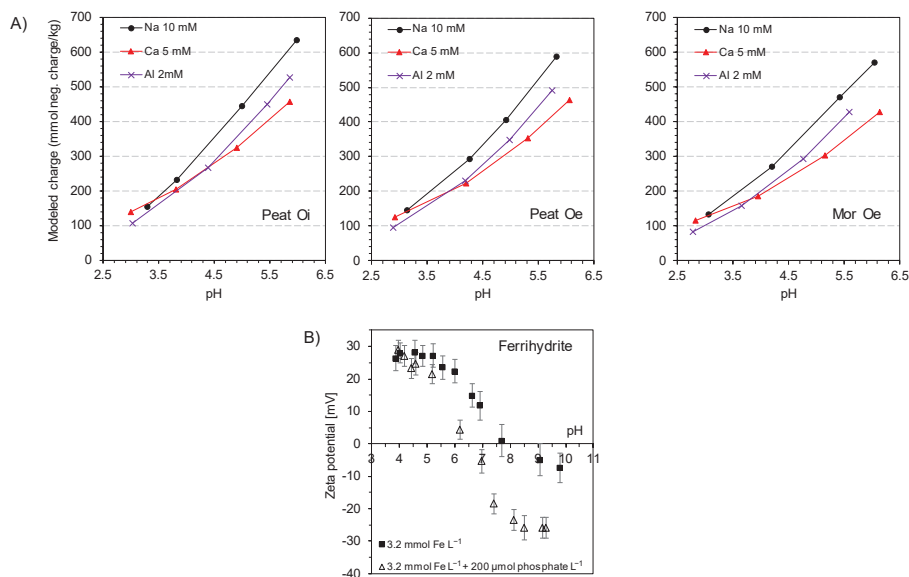


Figure 8. A) Calculated surface net charge of temperate organic soils (Paper II), and B) ferrihydrite ζ -potential (III), as affected by solution pH and additions of inorganic multivalent ions. Subplot B) has, with minor modifications, previously been published in Campos-Pereira et al., *Environmental Science and Technology* 54 (2020), pp 15722–15730. DOI: 10.1021/acs.est.0c01646

The ζ -potential of the iron (hydr)oxide ferrihydrite was able to predict the binding of many of the long-chained PFASs (Paper III) with good accuracy when the two treatments of the experiment (i.e., 0 and 200 $\mu\text{mol L}^{-1}$ of added phosphate, respectively) were considered jointly. When only the pH value

was considered, the binding was, for many substances, somewhat weaker in the presence of phosphate as compared to that measured in the absence of the anion. Adding to the line of evidence from X-ray absorption spectroscopy of ferrihydrite-adsorbed sulfonated PFASs (detailed below and in Paper III), the results of the pH-/charge-dependent batch sorption tests emphasize the primarily electrostatic nature of the adsorption onto ferrihydrite.

For the overall binding to organic matter (Paper I–II), it was, however, difficult to distinguish the effect of the surface net charge from that of the pH value alone. For example, both variables generally exhibited similar and often high correlations with the binding both within and across the organic soils (e.g., Figure 6 and 7). This maybe due to that the cation additions (i.e., 3 and 5 mmol L⁻¹ Ca²⁺, 2 mmol L⁻¹ Al³⁺), which were employed to further alter the charge of the organic soils, were kept relatively low, i.e., their concentrations were at the lower end of those previously employed in similar sorption studies (c.f. Higgins & Luthy 2006; Chen et al. 2009; Zhang et al. 2013).

4.2 Effect of PFAS structure on binding

4.2.1 Overall binding as affected by PFAS structure

Effect of perfluorocarbon chain length

The overall binding, i.e., the binding strength normalized against the pH value or the sorbent surface charge, increased with the number of perfluorinated carbons, and with the molecular weight, within each PFAS subclass in all works (I–IV) of this thesis (examples in Figure 9). For example, the binding ($\log K_{OC}$) to temperate organic soils (Paper II) increased with, on average (\pm stdev), 0.13(\pm 0.12), 0.30(\pm 0.06), and 0.49(\pm 0.13) log units for the subclasses of PFCAs, PFASAs and FTASAs, respectively, for each additional CF₂ moiety that was added to the tail of the molecule. As for the binding to temperate mineral soils (IV), the corresponding increase in binding strength ($\log K_d$) was, on average, 0.41 and 0.26 log units for the PFCA and PFSA homologues, respectively, per additional CF₂ moiety. Thus, the main mechanism that was driving the overall binding of PFASs to soil and to isolated phases of SOM was concluded to be hydrophobic interactions.

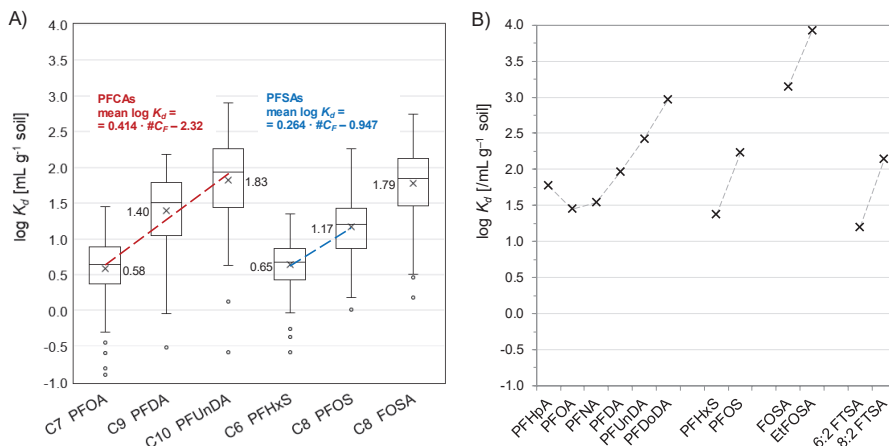


Figure 9. Examples of the chain length-dependent binding behavior of PFASs in soil. Subplot A) shows means (crosses) and boxplots for the pH-dependent binding in up to 10 mineral soils (Paper IV, pH 2.8–8.6), and B) shows the partitioning to the organic soil Peat Oi (II) (pH = 3.7). $C_W \leq 10$ nmol L⁻¹ for individual PFAS concentrations, and concentration of background electrolyte (NO₃⁻) = 10 mmol L⁻¹, for both data sets of A) and B).

Effect of functional head group type

As for the effect of head group type on the overall binding strength, a complete analysis across all sorbents and soils studied within the thesis work was not possible, since not all subclasses (i.e. PFCAs, PFSAs, FTSAs, FASAs) were analyzed within the work of each paper. For the PFASs with 8 perfluorinated carbons in their tail (“C₈”), for which the largest amount of data was available for comparisons, the presence of a uncharged sulfonamide functionality (i.e., that of FOSA, given pH < ~6.4) increased the overall binding in organic and mineral soils as compared to the presence of a negatively charged sulfonate moiety (i.e., that of PFOS (Paper I, II, IV) and 8:2 FTSA (II)). In turn, the sulfonate functionality of 8:2 FTSA and PFOS favored binding as compared to a carboxylate functionality (i.e., PFNA; I, II). Moreover, the binding of the neutral substance *N*-ethyl perfluorooctane sulfonamide (i.e. EtFOSA/Sulfluramid) onto organic soils was stronger by, on average (±stdev), 0.41 (±0.49) log units as compared to that of FOSA (Paper II), which was attributed to the greater hydrophobicity associated with the larger

head group of EtFOSA ($-\text{SO}_2\text{NHC}_2\text{H}_5$) as compared to that of FOSA ($-\text{SO}_2\text{NH}_2$). The stronger binding of neutral PFASs onto soil as compared to that of anionic PFASs is in agreement with the observations of e.g. Nguyen et al. (2020). However, as for the adsorption onto the positively charged iron(hydr)oxide ferrihydrite, for which the main sorption driving force was identified to be of an electrostatic nature, the binding of PFOS was stronger as compared to that of FOSA (pH 4.4–4.6, $C_w < 0.75 \mu\text{mol L}^{-1}$). This exemplifies the manner in which the binding strength is a result of an interplay between the properties of the sorbate and those of the sorbent.

4.2.2 pH- and charge-dependent binding as affected by PFAS structure

Effect of perfluorocarbon chain length

The effect of solution pH and soil/sorbent surface net charge on binding (i.e., $\log K_d$ or $\log K_{OC}$) was quantified as the regressed slope of the relationship between the two quantities (Figure 10) given statistical significance (i.e. $p < 0.05$). The binding of longer-chain PFASs was, as a rule, affected to a larger degree by changes in the pH value (Paper I–IV) and by changes of the sorbent charge (I–III) as compared to that of shorter-chained PFASs, within as well as across the various subclasses. This observation is in agreement with that of Nguyen et al. (2020) who studied the pH-dependent sorption onto ten soils and described an increased sensitivity of binding to solution pH with respect to longer-chained PFCAs, PFASs, FTSAAs and FASAAs as compared to that of their shorter-chained homologues and analogs. The authors suggested the reason to be the overall lower affinity of shorter-chained PFASs for the solid soil-phase, which would make their binding less sensitive to solution pH and thus to the soil surface chemistry (i.e., in particular its charge) as compared to that of longer-chained PFASs that overall were more strongly bound.

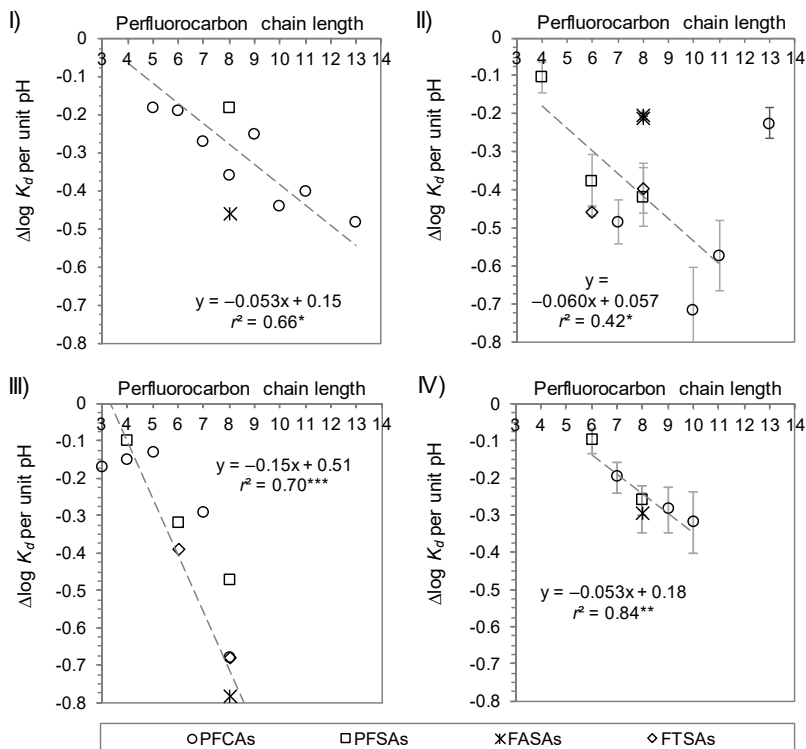


Figure 10. Binding pH-dependency, expressed as the regressed slopes $\Delta \log K_d$ per pH unit, as affected by the length of the perfluorinated carbon chain. The roman numerals by each subplot indicate the respective paper for which data is shown. For Paper **II** and **IV**, where multiple soils were included, the data points show the average \pm standard error of the mean of the individual regressed slopes $\Delta \log K_d$ unit pH^{-1} . For Paper **I** and **II**, K_d values are expressed in the unit mL g^{-1} dry weight soil, and their subplots reflect the binding pH-dependency for all treatments aggregated (i.e., including additions of 3 and 5 mmol L^{-1} Ca^{2+} and 2 mM Al^{3+}). For Paper **III**, the unit of the K_d value is mL g^{-1} Fe, and the subplot represents the pH-dependence without any addition of phosphate. The very large pH-dependence of the binding of PFCA C_9 PFDA in Paper **III** (-1.32 log units per unit pH) is not shown since it is out of scale, but is included in the total regression. For Paper **II**, C_{13} PFTeDA was excluded from the regression. pH 2.8–8.6 for the data as a whole. $^*p < 0.05$, $^{**}p < 0.01$, $^{***}p < 0.001$.

However, because the effect of solution pH on binding is an effect of charge, one should also consider the electronic (i.e. charge) distribution of the PFAS molecules themselves as a possible explanation for the larger soil/sorbent charge effect observed for the binding of longer-chained PFASs as compared

to that of shorter-chained substances. Johnson et al. (2007), Xiao et al. (2011) and Erkoç & Erkoç (2001) performed calculations of atomic partial charges of the PFOS molecule, and found each fluorine atom to carry an excess charge δ^- of, on average, -0.27 ± 0.014 , -0.2 and -0.11 ± 0.021 elementary charge units, respectively (schematically illustrated in Figure 11). Consequently, the authors proposed that the PFOS molecule as a whole, due to the strong electronegative (electron-withdrawing) properties of the fluorine, is negatively charged towards its surrounding environment. The carbon atoms consequently form a positively charged core within a shell of negative charge. Thus, electrostatic interactions are not exclusively limited to the negatively charged head group but may also involve the partially negatively charged hydrophobic chain (Johnson et al., 2007; Xiao et al., 2011). The increasingly larger effect of solution pH and of soil/sorbent net charge on binding of longer-chained PFASs is thus consistent with an important additional electrostatic repulsion or attraction involving the perfluorocarbon chain, in addition to the effect of the head group. In the case of the adsorption onto the more or less positively charged ferrihydrite, electrostatic interactions involving the tail are expected to enhance the binding; the longer the tail and the more acidic the pH, the more so. As regards the binding onto more or less negatively charged SOM, however, the electrostatic component of the tail (along with that of the head group, in the case of an anionic PFAS) needs to be overcome in order for hydrophobic interactions to take place and result in the binding of the molecule.

The hypothesized reason, as described above, to why the binding of longer-chained PFASs to soil and soil components is more sensitive to changes in solution pH/sorbent charge as compared to that of shorter-chained PFASs relies on the assumption that the cited results on the atomic charge distribution of the PFOS molecule also can be extended, or are at least similar, to other PFASs with similar structures (i.e. PFCAs, other PFASs, x:2 FTSAAs, FASAs). This is considered likely, due to the similar high degree of fluorination of all PFAS subclasses analyzed within the work of this thesis.

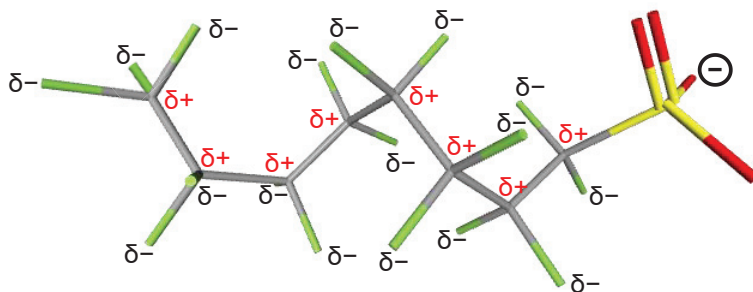


Figure 11. Schematic representation of the charge distribution on the perfluorooctane sulfonate (PFOS) molecule, according to data of Johnson et al. (2007), Xiao et al. (2014) and Erkoç & Erkoç (2001). The cited studies calculated the excess negative charge δ^- of each fluorine atom to be about -0.27 ± 0.014 (Johnson et al., 2007; gas-phase molecular geometry), -0.2 (Xiao et al. 2014), or -0.11 ± 0.021 elementary charges (Erkoç and Erkoç (2001). Due to the strong electronegative properties of the fluorine atoms, it was calculated that each carbon atom correspondingly carries an excess positive charge of, on average, $+0.54 \pm 0.12$ (Johnson et al., 2007), $+0.4$ (Xiao et al., 2014), or $+0.23 \pm 0.090$ (Erkoç and Erkoç (2001). The negative charge of the dissociated head group (SO_3^-) is indicated with a minus sign to the right in the figure.

Effect of head group type

Clues on the effect of head group type on the pH/-charge-dependency of the binding may be obtained by comparing the binding behavior of PFASs that have equal perfluorocarbon chain length but different head group functionalities. For the binding of the PFAS subclasses with completely ionized functionalities (i.e., PFCAs, PFSAs, FTSAs), it was difficult to discern a consistent pattern, over Paper I–IV, in the magnitude of the pH-dependency with respect to the type of head group. However, the binding of the neutral species ($\text{pH} < \sim 6.4$) of perfluorooctane sulfonamide (FOSA) was less affected by solution pH and soil net charge as compared to its anionic analog PFOS in 11 out of 12 organic and mineral soils, in agreement with previous research on the environmental binding behavior of neutral and anionic organic chemicals (e.g., Jafvert 1990). In addition, the binding of the neutral C_8 analog EtFOSA (Sulfluramid) showed a moderate dependency on solution pH and soil net charge in temperate organic soils similar to that of FOSA (Paper II). However, at pH values above the pK_a value of FOSA, where its speciation is dominated by its anionic species, the binding strength of FOSA decreased

with solution pH (Figure 12), with a similar magnitude as was observed for the PFOS anion of equal chain length (Paper IV).

To conclude, the results suggest that the pH-/charge-dependency of the binding of PFASs in soil is influenced both by the head group type (i.e., anionic or uncharged) and by the number of perfluorinated carbons that make up the tail of the molecule.

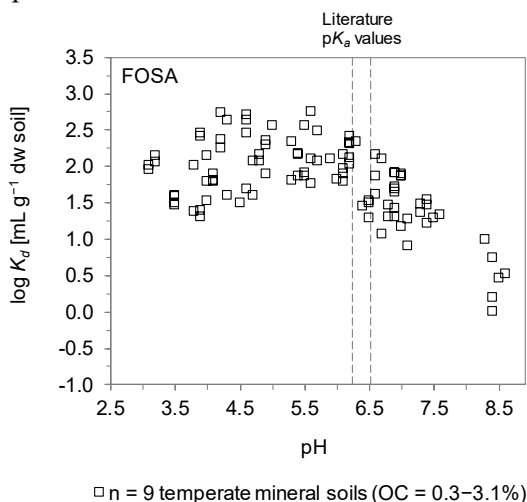


Figure 12. pH-dependent binding of perfluorooctane sulfonamide (FOSA) to $n = 9$ temperate mineral soils (Paper IV). Literature estimations of the pK_a value are indicated as vertical dashed lines ($pK_a = 6.24$ and 6.52 ; Rayne & Forest 2009a; Steinle-Darling & Reinhard 2008, respectively). At pH values below and above the pK_a value, the speciation of FOSA is dominated by its neutral and anionic species, respectively.

4.3 Binding of PFASs to isolated soil components

4.3.1 Binding to soil organic matter

Binding of all analyzed subclasses of PFASs to organic soils materials (Paper I and II) was influenced by solution pH, i.e., by the pH-induced change in soil organic matter net charge, as described above. When considering the data of Paper I and II together, any consistent effects on binding induced by cation treatments were however difficult to discern from that of solution pH. Binding onto two *Sphagnum* peat materials with a low (Oi) and moderate

(Oe) degree of decomposition were 4 times stronger, on average, as compared to that onto soil organic matter from a Spodosol Oe horizon (Figure 13). In particular, longer-chained PFASs were more strongly bound by the two peat materials. The difference in binding strength was however not likely to be caused primarily by a difference in the net charge present on the different SOMs, as acid/base titrations as well as geochemical modeling indicated that the charge properties of the sorbents were similar (Figure 8A above). This suggests, instead, that the overall quality of SOM caused the difference in sorption behavior. The combined results of batch sorption experiments and ^{13}C NMR spectroscopy (Figure 13) suggested the sorption to be positively related to the content of carbohydrates (i.e., O-alkyl carbon), in particular as regards the binding of C_8 – C_{11} and C_{13} PFCAs and EtFOSA.

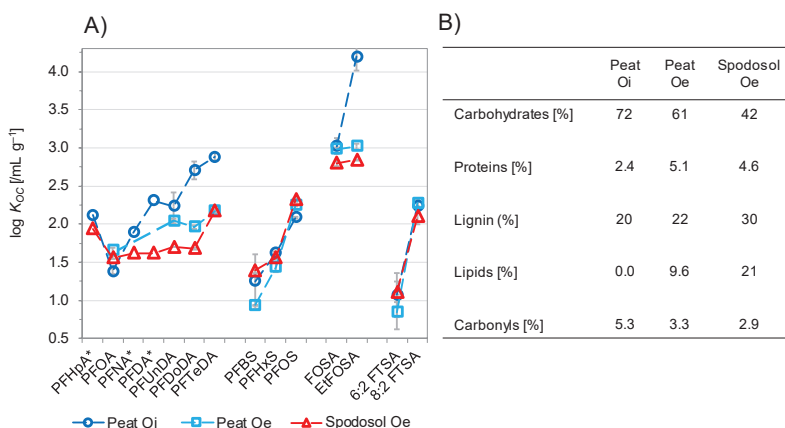


Figure 13. A) Organic carbon-normalized partitioning coefficients $\log K_{OC}$ for the temperate organic soils used for the work of Paper II. Binding data from pH-dependent sorption tests at $\text{pH} = 4.2 \pm 0.2$. An asterisk (*) indicates that the partitioning coefficients were calculated from the respective sorption isotherm at a C_w of 10 nmol L^{-1} ($\text{pH} = 3.5\text{--}3.7$). Background electrolyte: $0.01 \text{ mol L}^{-1} \text{ NO}_3^-$ for all data. Error bars represent the standard deviation ($n = 2$). B) Distribution of carbon compound classes of the respective soil as derived from CP-MAS ^{13}C NMR measurements. Molecular mixing model and associated integrations of chemical shifts: Baldock et al. (2004) and Nelson and Baldock (2005).

Concentration-dependent sorption

Sorption isotherms (Figure 14) onto the peat material with a low degree of decomposition (Peat Oi) were closer to ideal linearity (average Freundlich

exponent $n = 0.85$) as compared to that of the Spodosol Oe sample (denoted as Mor Oe in Paper II) (average Freundlich exponent $n = 0.75$). This suggests that the energetic distribution of possible “binding sites” for PFASs was more homogeneous on the Peat Oi material as compared to that of the Spodosol Oe SOM. The Peat Oi sample was made up entirely of *Sphagnum fuscum* material and exhibited a low degree of alteration through decomposition, while the SOM of the Spodosol Oe sample originated from a mix of different litter qualities (Scots Pine-dominated vegetation) and its SOM was in addition altered to a larger degree by decomposition processes (humification).

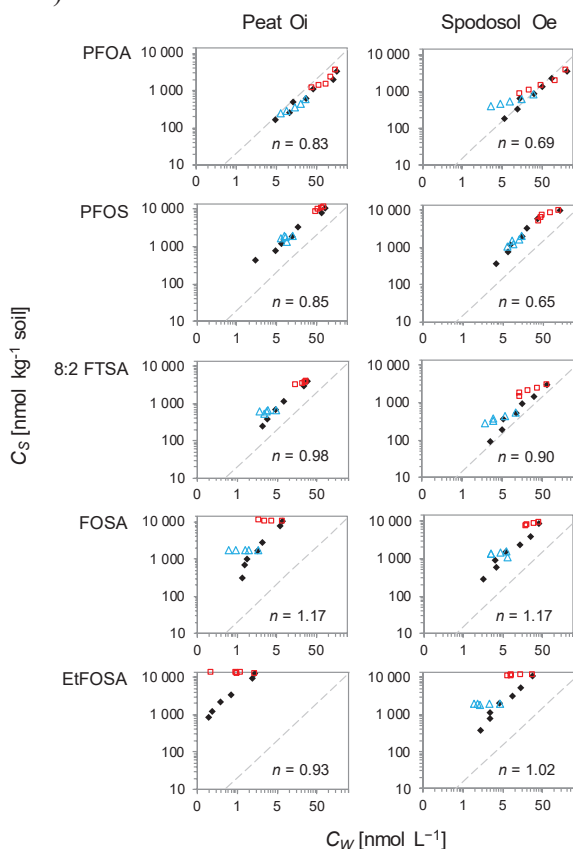


Figure 14. Sorption and desorption isotherms of selected PFASs as indicated by closed and open symbols, respectively, onto the temperate organic soils Peat Oi and Spodosol Oe (Mor Oe) (Paper II). n is the fitted exponent of the Freundlich sorption isotherm. The dashed line indicates 50% binding. Each data point corresponds to duplicate samples. Experimental conditions: background electrolyte 10 mmol L⁻¹ NaNO₃, pH 3.5–4.0.

Desorption – effects of PFAS structure and concentration

In general, sorption of PFASs was more or less irreversible to at least one of the organic soils Peat Oi and/or Spodosol Oe (Figure 14). The results suggested that all of the analyzed subclasses (i.e. PFASs, FTSA, FASA, and long- as well as short-chained PFCAs) have the potential to undergo retarded long-term leaching from organic-rich surface horizons. In particular, the neutral substances FOSA and EtFOSA as well as the shorter-chained, anionic, PFHpA showed pronounced sorption irreversibility (hysteresis) across both soils in the desorption experiment. The sorption irreversibility of the respective subclasses followed their order of affinity for the organic soils, i.e., sorption irreversibility decreased in the order of EtFOSA > FOSA > PFOS \approx 8:2 FTSA > PFNA among the C₈ analogs. The cumulative desorption yields of PFASs decreased with increasing length of the perfluorinated carbon chain (PFCAs), and with increasing molecular weight/size of the head group (FOSA, EtFOSA). A similar dependency on chain length has been reported for the desorption of PFASs (i.e., PFBS and PFOS) for soils with lower OC contents of 0.2–9.4% (Milinovic et al. 2015).

The relative desorption yields for both soil Peat Oi and Spodosol Oe tended to be positively related ($p < 0.05$) to initial aqueous additions of PFASs and consequently to initial sorbed PFAS concentrations (*t*-test, paired two samples for means). When the initial aqueous additions of individual PFASs increased by a factor of 6, the cumulative desorption yield of individual PFASs increased by, on average (\pm stdev), 58% (\pm 59%) and 25% (\pm 19%) in soils Peat Oi and Spodosol Oe, respectively. This suggests that more effective sorption sites/environments of SOM to a larger extent get occupied upon larger loadings of PFASs, which, if so, further suggests that organic surface horizons could leach PFASs to a relatively larger extent upon larger loadings (emissions) as compared to if contamination was lower.

4.3.2 Binding to ferrihydrite

X-ray absorption spectroscopy

As shown in Figure 15, the sulfur K-edge XANES spectra of sulfonated PFASs (i.e., PFHxS, FOSA and PFOS) adsorbed onto ferrihydrite were similar, with respect to their white-line positions, to that of dissolved dilute sodium methylsulfonate (S(+V)). Hence, it could be concluded that when the PFASs adsorbed from solution to the ferrihydrite surface, the sulfur atom of the head group functionality retained an oxidation state of +V. The same observation was made for the adsorption onto poorly crystalline aluminum hydroxide (Alhox). The spectrum of ferrihydrite-adsorbed sulfate (K_2SO_4) showed a so-called pre-edge on the low-energy side of the main absorption peak, a feature that indicates the involvement of inner-sphere complexes in the adsorption mechanism (Okude et al. 1999; Majzlan & Myneni 2005; Majzlan et al. 2011; Gu et al. 2016). This feature was not observed for any of the spectra of the ferrihydrite-adsorbed sulfonated PFASs. To conclude, these results rule out a significant involvement of inner-sphere complexation in the adsorption mechanism of sulfonated PFASs onto ferrihydrite. Weaker, electrostatically-dominated, outer-sphere complexation that involves the S-containing head group is still however likely to occur, as also was suggested by the results of the sorption batch experiments with ferrihydrite.

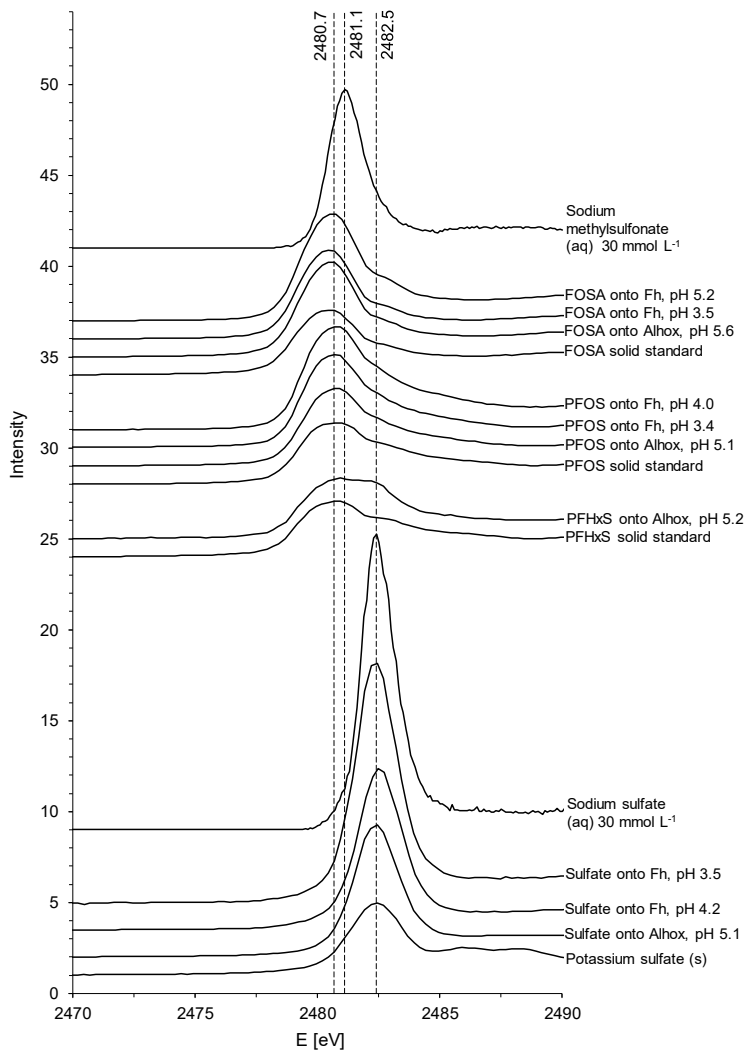


Figure 15. Stacked normalized S K-edge XANES spectra for sulfonated PFASs adsorbed to ferrihydrite (Fh) and poorly crystalline aluminum hydroxide (Alhox). Dashed white-line positions are, from lower to higher energies, those of PFOS onto Fh and Alhox, of dissolved dilute sodium methylsulfonate (NaCH_3SO_3), and of sulfate onto Fh and Alhox. Spectra for sodium sulfate (Na_2SO_4) (aq) and sodium methylsulfonate (aq) were provided by Almkvist et al. (2011) and their intensities were set to unity at 2490 eV for the purpose of comparison. Figure from Campos-Pereira et al., *Environmental Science and Technology* 54 (2020), pages 15722–15730. DOI: 10.1021/acs.est.0c01646

Binding mechanisms and concentration-dependent binding

The results of the pH- and concentration-dependent sorption batch tests lended further support to the hypothesis that the adsorption to ferrihydrite is dominated by electrostatic contributions, i.e., interactions between the more or less positively charged ferrihydrite particles and the head group as well as the partially negatively charged tail group (section 4.2.2 above). In particular, the results from single-solute sorption isotherm experiments (Figure 16) supported the presence of an electrostatic contribution involving the head group, as the negatively charged sulfonate functionality of PFOS favored the binding onto ferrihydrite over the neutrally charged sulfonamide head group of FOSA. The overall sorption affinity decreased in the order of PFOS > PFOA \approx FOSA ($C_W < 0.75 \mu\text{mol L}^{-1}$, pH = 4.4–4.6). All three PFASs exhibited concave-down isotherms for aqueous concentrations C_W less than $\sim 0.5 \mu\text{mol L}^{-1}$ (FOSA), $\sim 0.75 \mu\text{mol L}^{-1}$ (PFOS) and $\sim 2 \mu\text{mol L}^{-1}$ (PFOA), of which the isotherms of PFOS and PFOA exhibited pronounced nonlinearities. Their suggested monolayer adsorption modes were best described by the Langmuir equation, with fitted (predicted) maximum adsorption capacities Q_{max} of 180 and 160 $\mu\text{mol mol}^{-1}$ Fe for PFOS and PFOA, respectively.

However, at high aqueous concentrations C_W ($> 1 \mu\text{mol L}^{-1}$), the binding of FOSA was significantly greater than that of both PFOS and PFOA. The change from concave-down to a seemingly concave-up shape of the FOSA isotherm at a C_W of $\sim 0.5 \mu\text{mol L}^{-1}$ suggests a sorption-enhancing formation of hemi-micelles at the ferrihydrite–solution interface (c.f. (Schwarzenbach et al. 2016)).

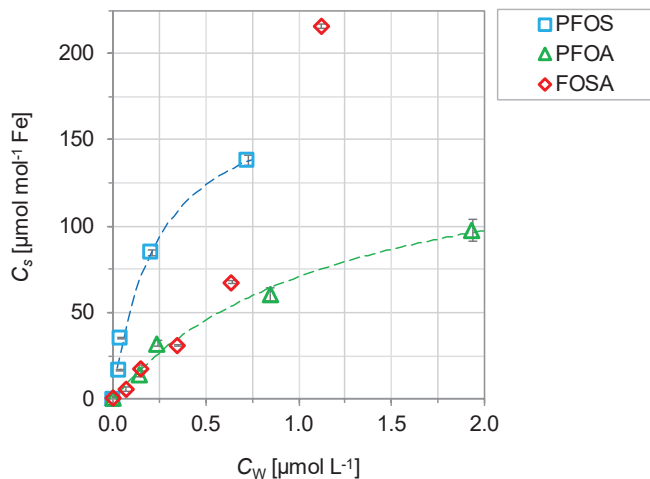


Figure 16. Sorption isotherms for PFOS, PFOA, and FOSA, onto ferrihydrite (10 mmol Fe L⁻¹) at pH 4.4–4.6. The dashed lines represent the fitted Langmuir isotherms. Error bars represent the standard deviation of the calculated sorbed concentration C_s . Modified figure from Campos-Pereira et al., *Environmental Science and Technology* 54 (2020), pages 15722–15730. DOI: 10.1021/acs.est.0c01646.

4.4 Binding of PFASs to soils

4.4.1 Overview

For the work of Paper IV, ten temperate mineral soils (S1–S10) were chosen to represent a wide range of soil properties as detailed in Table 6. Thus, whereas the work described in Paper I–III focused on the binding behavior to isolated soil components, in the soils of Paper IV, a multitude of possible sorbent phases were present simultaneously to varying degree (c.f. hypothesis H5). The work aimed to i) investigate the role of soil properties on the pH-dependent binding behavior of PFASs across a wide array of soils, and ii), by drawing knowledge from the work of Paper I–III, to investigate how a bottom-up or component additivity approach may further progress or complement the understanding of the pH-dependent binding behavior in soil.

The soils were assigned labels (S1, S2, ... , S10) in order of decreasing OC content, i.e., soil S1 corresponded to the material with the highest OC content. Collected in south and central Sweden, $n = 6$ soils were sampled

from surface horizons (i.e. from the top 10 or 20 centimeters) and $n = 4$ soils were subsurface materials.

Table 6. Selected properties of the temperate mineral soils S1–S10 that were used for the pH-dependent desorption experiments of Paper IV. Additional soil properties are provided in the manuscript.

Soil	Collection site ^a	OC [%]	C/N	pH (H ₂ O)	Fe _{ox} ^b + Al _{ox-Pyp} ^c [mmol kg ⁻¹]	Silt + clay [%] ^d	Textural class
S1	Kungsängen (0–10 cm)	3.1	10	5.9 ^e	230	96	Clay
S2	Paskalampa Bs	2.2	42	5.5	630	46	Sandy loam
S3	Arboga (field-contaminated)	1.7	11	6.9	170	76	Clay
S4	Fors	1.6	11	8.2 ^e	62	72	Silt loam
S5	Arboga	1.3	11	5.5	140	73	Clay
S6	Nåntuna	1.2	11	8.3 ^e	64	19	Sandy loam
S7	Krusenberg	1.2	13	5.5	36	14	Loamy sand
S8	Paskalampa E	1.1	40	4.6	4.4	47	Sandy loam
S9	Kungsängen (70–80 cm)	0.91	8.0	6.6	250	100	Clay
S10	Högåsa (sub-soil)	0.30	17	5.8	58	11	Loamy sand

^aAll soils were sampled from their surface horizons (i.e. from the top 10 or 20 cm) with the exception of soils S2, S8, S9 and S10. ^bFe_{ox}: oxalate-extractable iron (0.2 M oxalate, pH 3.0). ^cAl_{ox-Pyp}: The difference between oxalate-extractable aluminum (0.2 M oxalate, pH 3.0) and 0.1 M pyrophosphate-extractable aluminum. n.a.: not available. ^dDetermined according to ISO 11277:2020 by the means of laser diffraction. ^eSoil contained inorganic carbon, i.e., carbonates.

4.4.2 Overall binding behavior

As mentioned in previous sections, the overall binding to the temperate minerals soils was positively related to the length of the perfluorinated carbon chain and to the molecular weight (C_7 , C_9 and C_{10} PFCAs, and C_6 and C_8 PFSAAs) (Figure 9). C_8 FOSA was overall bound more strongly than its completely ionized analog PFOS, which again highlighted the role of head group type for the binding behavior in addition to that of the chain length of the molecule. Similar to the binding onto isolated sorbent phases (Paper I–III), the binding of all six analyzed PFASs was inversely related to solution pH ($p < 0.001$, Figure 17), and the magnitude of the pH-dependency increased with the length of the perfluorinated carbon chain of the molecule (Figure 10). To conclude, the pH-dependent binding behavior in a wide range of soils was indicated to be a combination of hydrophobic interactions, in which the fluorinated carbon chain plays an important role, and electrostatic interactions, in which both the head group and the fluorinated carbon chain were indicated to be involved.

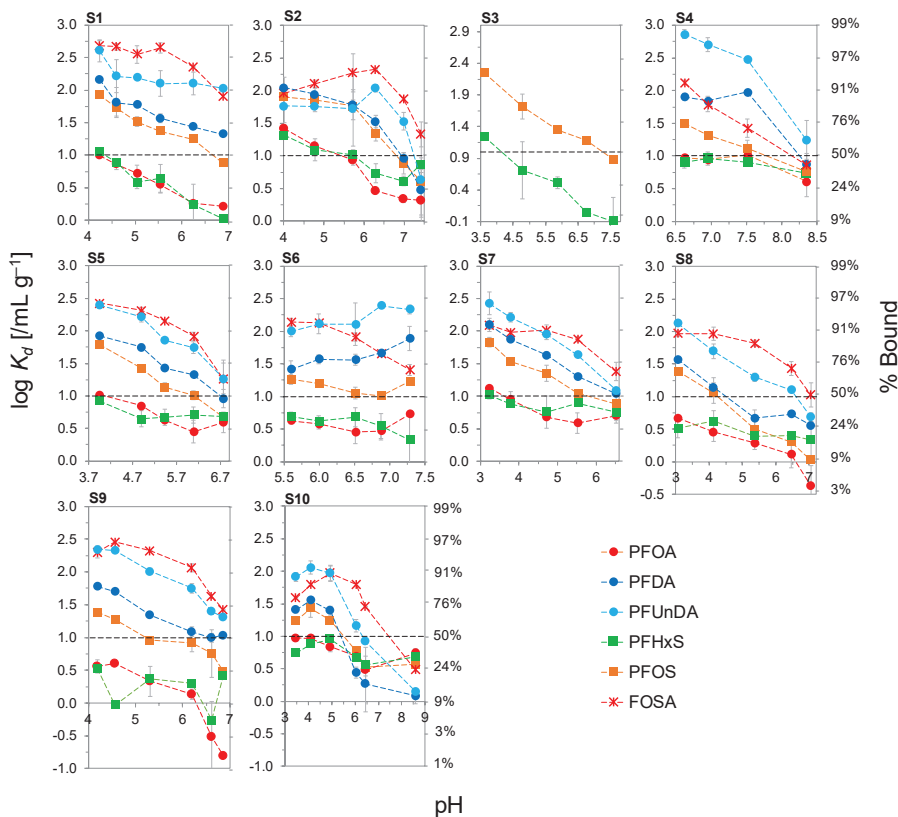


Figure 17. pH-dependent soil–water partitioning coefficients $\log K_d$ for the desorption of $n = 6$ PFASs from 10 temperate mineral soils (S1–S10) at $10 \text{ mL g}^{-1} \text{ dw}$. $\log K_d$ values [mL g^{-1}] of 0, 1, 2 and 3 correspond to 9%, 50% (horizontal dashed line), 91% and 99% binding, respectively, as indicated on the right axes. Note that the vertical axis extends to negative $\log K_d$ values for soils S3 and S8–S10. The time of aging of the soils prior to the desorption experiment was nine months. $\sum \text{NO}_3^- = 10 \text{ mmol L}^{-1}$ and liquid-to-solid ratio $10 \text{ mL g}^{-1} \text{ dw soil}$ for all data points.

4.4.3 The role of soil properties

While there were important patterns in the binding behavior to the temperate mineral soils of Paper IV that were well recognized from that onto isolated sorbent phases (I–III), at the same time, the aggregated data for the mineral soils exhibited more complexity (e.g., Figure 18), likely due to the wider span of sorbent properties. For example, using single linear regression, several soil properties exhibited significant ($p \leq 0.05$) positive correlations with the binding of one or more PFASs at a selected fixed pH value of 5.6 ± 0.1

(c.f. $\text{pH}(\text{H}_2\text{O}) = 6.1$, on average, for $n = 10$ soils). These soil properties included OC (PFOS, FOSA), oxalate-extractable Fe (FOSA), estimated allophane and imogolite (PFOS, PFDA), cation exchange capacity (FOSA), and the summed content of silt and clay particles (*silt+clay*, FOSA), all for which low to moderate predictive strength was observed (average $r^2 = 0.58$). A corresponding multiple linear regression analysis similarly suggested multiple contributions to the binding of PFOS and FOSA, where OC together with Fe and Al mineral phases explained 80% and 85% of the variation in the K_d values, respectively (Figure 19). In the case of PFOS, these findings are similar to those of Nguyen et al. (2020) and Li et al. (2018) who found that its binding to soils and sediments was better predicted by a combination of sorbent properties than by any single property. However, for three of the six analyzed PFASs (i.e., PFOA, PFUnDA, PFHxS) in Paper IV, no significant correlation with any of the soil properties OC, oxalate-extractable Fe, estimated allophane and imogolite, or silt+clay was identified, irrespectively of whether single or multiple linear regression analysis was employed.

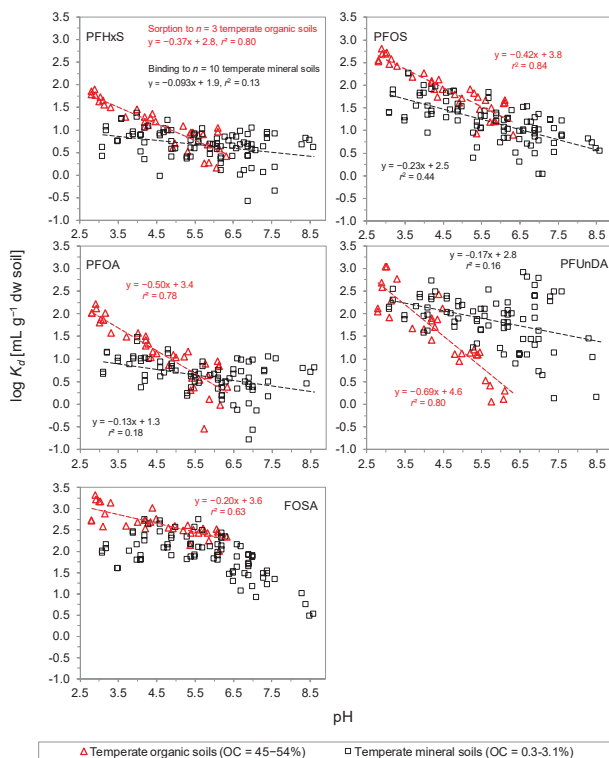


Figure 18. Soil–solution partitioning $\log K_d$ values for temperate organic soils (red triangles, Paper II) and mineral soils (black squares, IV). Data is shown for all substances that were analyzed both in Paper II and IV. The binding of all substances was correlated with the pH value ($p < 0.001$) within each of the groups of organic and mineral soils.

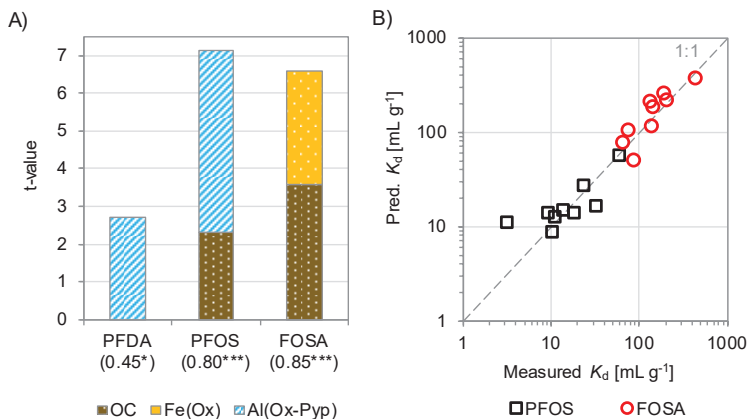


Figure 19. A) t -values of soil properties of significant ($F \leq 0.05$) multiple linear regression models describing the K_d values at pH 5.6 ± 0.1 in $n = 9$ laboratory-spiked soils (Paper IV). Adjusted r^2 values for the MLR models are given in parenthesis after the name of the substance on the horizontal axis. All the partial slopes of the MLR models were significantly different from zero ($p \leq 0.05$). The binding of PFDA was better described by regression with single soil properties (SLR) as compared to by a combination of multiple properties, why this substance is presented with its single correlation r^2 value within parenthesis. * $p \leq 0.05$, *** $p \leq 0.001$. B) Measured versus predicted K_d values for PFOS and FOSA plotted on a log–log scale. MLR model for PFOS: predicted K_d [mL g⁻¹] = $5.97 \cdot \%OC + 0.0796 \cdot Al_{Ox-Pyp}$ [mmol kg⁻¹]. MLR model for FOSA: predicted K_d [mL g⁻¹] = $71.8 \cdot \%OC + 0.751 \cdot Fe_{Ox}$ [mmol kg⁻¹].

In line with the weak to moderate (PFOS, FOSA) or absent (PFOA, PFDA, PFUnDA, PFHxS) correlation between binding and soil OC content, normalization of the binding strength against OC content ($\log K_{OC}$) did not successfully explain the differences in the binding across the mineral soils of Paper IV (Figure 20). Moreover, the binding strength per unit organic carbon was significantly greater for the mineral soils (i.e., most often >1 log unit greater for PFHxS, PFOS, PFOA and FOSA) as compared to the corresponding partitioning coefficients measured for the organic soils (II). This indicates that extrapolation of $\log K_{OC}$ values from organic soils to soils with lower organic content is likely to underestimate the binding of PFASs.

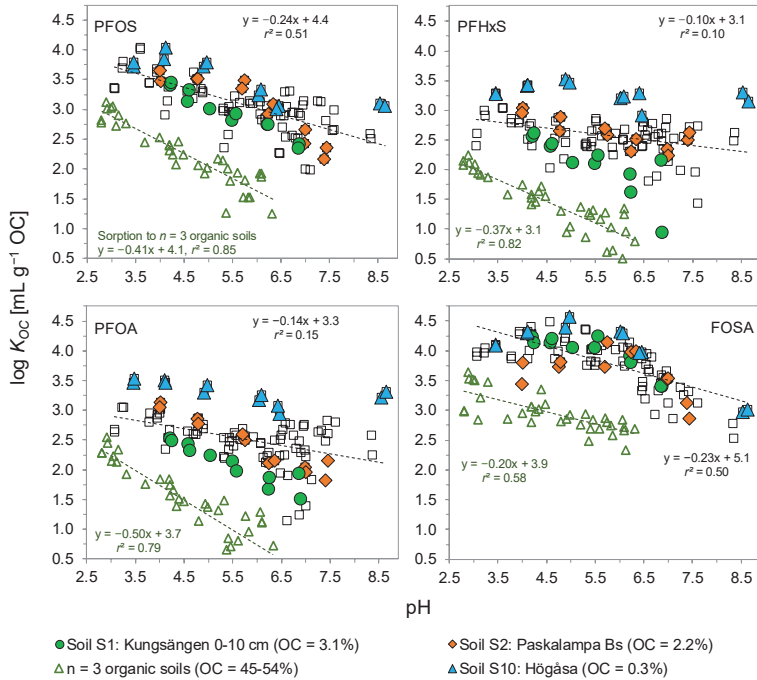


Figure 20. Organic carbon-normalized soil–water partitioning coefficients $\log K_{OC}$ [mL g⁻¹ OC] for the organic soils of Paper II (green open triangles) and the mineral soils of Paper IV (open squares). For the latter group, a subset of soils with higher (2.2–3.1%) and lower (0.3%) content of organic carbon is highlighted by closed symbols.

4.4.4 Binding as related to the calculated net charge of SOM

Because a straightforward normalization against OC content did not predict the binding to the mineral soils of Paper IV satisfactorily, an attempt was made to explain the binding behavior based on the net charge present on the SOM of the soils. The pH-dependent net charge of the SOM of the materials was modeled using the Stockholm Humic Model (Gustafsson 2001). Assumptions that underlie the calculations are described in Paper IV. Subsequently, the calculated net charge of SOM was related to the charge-dependent binding strength (i.e. K_{OC}) of organic soil material that was derived in Paper II. For the latter step, the binding data for the Peat Oe material was chosen. Lastly, the predicted K_d values ($K_{d, \text{pred}}$) for the soils of Paper IV were obtained from the predicted K_{OC} values ($K_{OC, \text{pred}}$) as $K_{d, \text{pred}} = K_{OC, \text{pred}} \cdot f_{OC}$, where f_{OC} is the fraction of organic carbon of the soil.

For all soils, this model underestimated the binding strength (Figure 21). The smallest deviation from the measured partitioning was observed for soil S2 (Paskalampa Bs horizon), for which the model performed fairly well for most PFASs. The largest deviations from the modeled partitioning were observed for the clay soils S3 and S5 (i.e., Arboga field-contaminated and Arboga, respectively), which had been collected from an AFFF-impacted former fire-fighting training site (S3) or from its direct vicinity (S5). For these two soils, the model underestimated the partitioning with, on average(\pm stdev), 1.6(\pm 0.4) log units.

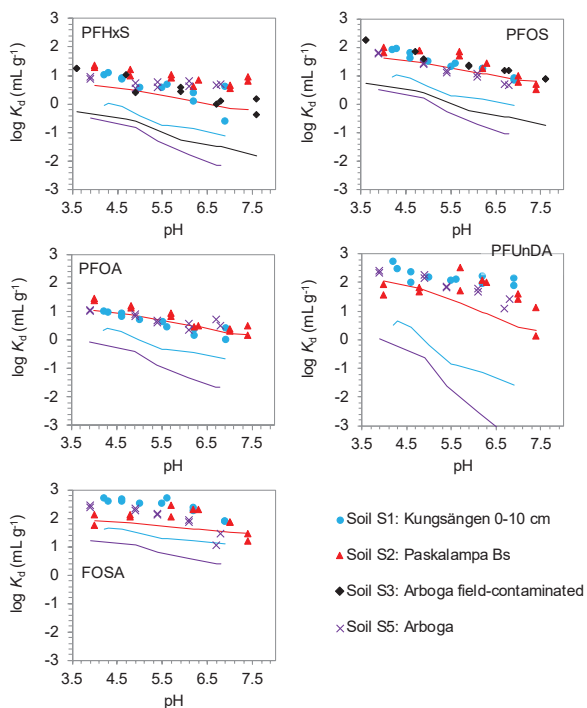


Figure 21. Measured (points) and modeled (lines) soil–water partitioning for selected soils of Paper IV.

4.4.5 A binding component not related to pH/charge?

On the basis of the observations and modeling described above (section 4.4.1–4.4.4), it can be hypothesized that the binding of PFASs in soil is the sum of three components: a) binding to SOM (depends on a combination of

hydrophobic and electrostatic interactions), b) binding to metal (hydr)oxides (predominately electrostatic interactions), and c) binding to other soil components (unknown interactions). While a) and b) are strongly pH-dependent, which in both cases has to do with charge, c) may or may not be dependent on the pH value/sorbent charge, depending on the exact mechanism involved.

The binding to “pure” (isolated) SOM becomes strong at low pH (strong hydrophobic interaction, small net negative charge), but low at high pH (large net negative charge present on the SOM). In a mineral soil, with the above reasoning, the binding of PFASs should generally be stronger per unit SOM, since the net negative charge present on the SOM of the mineral soil is smaller due to interaction with ions such as Al^{3+} and Ca^{2+} , which are ubiquitous in mineral soil. The difference in binding as compared to “pure” SOM becomes particularly large at higher pH values as the SOM net charge is decreased due to strong interactions with cations such as Ca^{2+} .

Conversely, the binding to oxides (ferrihydrite, allophane, imogolite, *et cetera*) is expected to be significantly weaker in a soil than to the pure oxides, because the oxides, due to adsorption of phosphate and SOM, have a small positive net charge in the soil. This means that the oxides might not contribute to the binding of PFASs to any appreciable extent in any of the soils in Paper IV, except possibly to a minor part in some soils that are either rich in metal (hydr)oxides, such as soil S2 (Paskalampa Bs), or very low in SOM content. Judging from pH-dependent binding data (Figure 17–18, 20–21) and the modeling of the net charge of SOM (Figure 8 and Figure 21), there appears to be some soil component (e.g., black carbon, clay minerals, or other particle surfaces) that contributes to the overall binding with a flatter, less pronounced pH-dependency, especially as regards the binding of the shorter-chained substances PFOA and PFHxS. Thus, it can be hypothesized that there is a component c) that contributes to a binding of PFASs that is more or less constant over the pH range.

The fact that the model underestimated the measured partitioning the most for the two materials that were collected from an AFFF-impacted site suggests the presence of some kind of high-affinity sorbent component, possibly black carbon/pyrogenic carbonaceous material (PCM), i.e., soot/char (Zhi & Liu 2018), or oil/oil-derived black carbon (Chen et al. 2009). Zhi and Liu (2018) reported a substantially stronger binding of PFAS to PCMs as

compared to that onto peat SOM, and identified PCMs as potentially significant sinks for PFASs at AFFF-impacted sites. However, at present there is no analytical data to confirm (nor dismiss) any presence of such high-affinity pyrogenic carbonaceous materials at the Arboga or indeed any other site. Hence the current data only allow the author to hypothesize that all mineral soil samples except Paskalampa Bs contained some high-affinity binding sites that were not present (or only present at low concentration) in the SOM of the organic samples studied in Paper II.

5. Conclusions

The main conclusions of this thesis can be summarized as follows:

1. Entropy-driven hydrophobic interaction is the main process that drives the overall binding of PFASs to soil organic matter. The binding is inversely related to the net negative surface charge of the organic matter, i.e., the lower the net negative charge, the stronger the PFAS binding. *Corroboration of hypothesis H1.*
2. The binding of PFASs onto the iron (hydr)oxide ferrihydrite is governed mainly by electrostatic attraction, which is dependent both on the length of the perfluorinated carbon chain and on the type of head group functionality (i.e., anionic or neutral). Thus, the binding is related to the charge of the ferrihydrite surface, which is affected by factors such as solution pH and the bound concentrations of phosphate. *Corroboration of hypothesis H2.*
3. The overall binding of PFASs to soil and soil components increases with the perfluorocarbon chain length within each PFAS subclass, and is further influenced by the functional head group type of the respective subclass. *Corroboration of hypothesis H3.*
4. Although PFAS binding to pure ferrihydrite is substantial, at least at low pH, there is no evidence for a major role of Fe and Al (hydr)oxides as major PFAS sorbents in mineral soils. Instead, for Paskalampa Bs (the soil with the largest amount of such sorbent phases), the observed $\log K_{OC}$ values were in reasonable agreement with those predicted from the charge– $\log K_{OC}$ relationships of the

organic samples, suggesting organic matter to be the dominant PFAS sorbent also in this soil. *Thus, hypothesis H4 could not be corroborated.*

5. The pH-dependency of PFAS binding to mineral soil was weaker than that observed for organic soil samples. Moreover, for all mineral soils except Paskalampa Bs, the overall sorption was considerably stronger than that expected from the relationship between K_{OC} and net charge as observed for the organic soil samples. This suggests that, at present, a simple component additivity method cannot be used successfully for predicting PFAS sorption in mineral soil, because of the possible presence of high-affinity binding sites of an unknown nature. *Thus, hypothesis H5 could not be corroborated.*

Implications and future research

The binding of PFASs to soil and soil components was substantially influenced by the pH value. Thus, if one is to make predictions of the soil retention of PFASs at a contaminated site, the pH value(s) of the soil profile is an essential variable to consider, in particular as regards the binding of longer-chained PFASs, and/or PFASs that may change their aqueous speciation at environmentally relevant pH values (e.g., FOSA). Although the soil organic carbon content plays an important role in determining the retention behavior of PFASs in soil, the results of this thesis indicate that other soil components (organic or mineral) are at play too. Thus, for derivation of generic environmental guideline values, or for soil retention predictions with respect to a specific contaminated site (tier 1 and 2 or corresponding), the author advises not to rely on extrapolations from organic carbon-normalized partitioning coefficients (i.e. K_{OC} values [mL g^{-1} organic carbon]) from the literature. One may instead, for the above purposes, employ literature K_d values [mL g^{-1} soil] values, as relevant as possible for the soil type(s) and conditions in question, to relate the soil-bound concentration of the substance directly to that in solution. For environmental risk assessments of tier 3 type, i.e., when more detailed site-specific investigations are undertaken, site-specific leaching tests of batch- and/or column type along with lysimeter (soil water-) sampling (c.f. Anderson 2021) and ground water sampling have the potential to provide a more complete picture of the mechanisms that govern the site-specific binding and leaching of PFASs.

In this thesis, the larger part of the work concerned the binding behavior of long-chained PFASs (i.e., C_7 or longer PFCAs, C_6 or longer PFSA, among others). However, along with the ongoing industrial transition from longer-chained PFASs to shorter-chained substances comes an increasing

need to more in depth study the binding behavior of low-molecular, short-chained PFASs in soil to better assess their environmental transport, fate and risks. This is underlined not least by the poor removal of short-chained PFASs by the large majority of techniques in drinking water treatment plants.

To progress the development of geochemical models to describe the binding of PFASs in soils of diverse properties, there is a need for more data that do not only encompass the binding data itself (i.e., K_d values, information on soil properties), but also information on the underlying sample recipes (e.g., acid/base additions, additions of metal ions, *et cetera*) and data on the solution chemistry at equilibrium (i.e., pH values, concentrations of metals, DOC, *et cetera*). In addition, more research on the influence of SOM quality, and on the binding of PFASs to high-affinity soil components such as black carbon, is needed. For example, soil material from AFFF-impacted sites could be analyzed for pyrogenic carbonaceous materials in order to better understand their possible role in the retention of PFASs.

References

- 3M Company. *History of PFAS and 3M*. https://www.3m.com/3M/en_US/pfas-stewardship-us/pfas-history/ [Accessed 2021-08-16]
- Adamson, D.T., Nickerson, A., Kulkarni, P.R., Higgins, C.P., Popovic, J., Field, J., Rodowa, A., Newell, C., DeBlanc, P. & Kornuc, J.J. (2020). Mass-Based, Field-Scale Demonstration of PFAS Retention within AFFF-Associated Source Areas. *Environmental Science & Technology*, 54 (24), 15768–15777. <https://doi.org/10.1021/acs.est.0c04472>
- Ahrens, L., Norström, K., Viktor, T., Cousins, A.P. & Josefsson, S. (2015). Stockholm Arlanda Airport as a source of per- and polyfluoroalkyl substances to water, sediment and fish. *Chemosphere*, 129, 33–38. <https://doi.org/10.1016/j.chemosphere.2014.03.136>
- Anderson, R.H. (2021). The Case for Direct Measures of Soil-to-Groundwater Contaminant Mass Discharge at AFFF-Impacted Sites. *Environmental Science & Technology*, 55 (10), 6580–6583. <https://doi.org/10.1021/acs.est.1c01543>
- Andersson, E.M., Scott, K., Xu, Y., Li, Y., Olsson, D.S., Fletcher, T. & Jakobsson, K. (2019). High exposure to perfluorinated compounds in drinking water and thyroid disease. A cohort study from Ronneby, Sweden. *Environmental Research*, 176, 108540. <https://doi.org/10.1016/j.envres.2019.108540>
- Ankarberg, E.H. & Lindberg, T. (2016). *Riskhanteringsrapport- Risker vid förorening av dricksvatten med PFAS*. Uppsala: Livsmedelverket.
- Arp, H.P.H., Lundstedt, S., Josefsson, S., Cornelissen, G., Enell, A., Allard, A.-S. & Kleja, D.B. (2014). Native Oxy-PAHs, N-PACs, and PAHs in Historically Contaminated Soils from Sweden, Belgium, and France: Their Soil-Porewater Partitioning Behavior, Bioaccumulation in *Enchytraeus crypticus*, and Bioavailability. *Environmental Science & Technology*, 48 (19), 11187–11195. <https://doi.org/10.1021/es5034469>
- Backe, W.J., Day, T.C. & Field, J.A. (2013). Zwitterionic, cationic, and anionic fluorinated chemicals in aqueous film forming foam formulations and groundwater from u.s. Military bases by nonaqueous large-volume injection hplc-ms/ms. *Environmental Science & Technology*, 47 (10), 5226–5234. <https://doi.org/10.1021/es3034999>
- Baldock, J.A., Oades, J.M., Nelson, P.N., Skene, T.M., Golchin, A., Clarke, P., 1997. Assessing the extent of decomposition of natural organic materials using solid-state ¹³C NMR spectroscopy. *Austr. J. Soil Res.* 35, 1061–1084. <https://doi.org/10.1071/S97004>

- Baldock, J.A., Masiello, C.A., Gélinas, Y. & Hedges, J.I. (2004). Cycling and composition of organic matter in terrestrial and marine ecosystems. *Marine Chemistry*, 92 (1), 39–64. <https://doi.org/10.1016/j.marchem.2004.06.016>
- Bartell, S.M. & Vieira, V.M. (2021). Critical review on PFOA, kidney cancer, and testicular cancer. *Journal of the Air & Waste Management Association*, 71 (6), 663–679. <https://doi.org/10.1080/10962247.2021.1909668>
- Barzen-Hanson, K.A., Davis, S.E., Kleber, M. & Field, J.A. (2017a). Sorption of Fluorotelomer Sulfonates, Fluorotelomer Sulfonamido Betaines, and a Fluorotelomer Sulfonamido Amine in National Foam Aqueous Film-Forming Foam to Soil. *Environmental Science & Technology*, 51 (21), 12394–12404. <https://doi.org/10.1021/acs.est.7b03452>
- Barzen-Hanson, K.A., Roberts, S.C., Choyke, S., Oetjen, K., McAlees, A., Riddell, N., McCrindle, R., Ferguson, P.L., Higgins, C.P. & Field, J.A. (2017b). Discovery of 40 Classes of Per- and Polyfluoroalkyl Substances in Historical Aqueous Film-Forming Foams (AFFFs) and AFFF-Impacted Groundwater. *Environmental Science and Technology*, 51 (4), 2047–2057. <https://doi.org/10.1021/acs.est.6b05843>
- Blake, B.E., Pinney, S.M., Hines, E.P., Fenton, S.E. & Ferguson, K.K. (2018). Associations between longitudinal serum perfluoroalkyl substance (PFAS) levels and measures of thyroid hormone, kidney function, and body mass index in the Fernald Community Cohort. *Environmental Pollution*, 242, 894–904. <https://doi.org/10.1016/j.envpol.2018.07.042>
- Borg, D., Lund, B.-O., Lindquist, N.-G. & Håkansson, H. (2013). Cumulative health risk assessment of 17 perfluoroalkylated and polyfluoroalkylated substances (PFASs) in the Swedish population. *Environment International*, 59, 112–123. <https://doi.org/10.1016/j.envint.2013.05.009>
- Brusseau, M.L. & Chorover, J. (2019). Chapter 8 - Chemical Processes Affecting Contaminant Transport and Fate. I: Brusseau, M.L., Pepper, I.L., & Gerba, C.P. (red.) *Environmental and Pollution Science (Third Edition)*. Academic Press, 113–130. <https://doi.org/10.1016/B978-0-12-814719-1.00008-2>
- Buck, R.C., Franklin, J., Berger, U., Conder, J.M., Cousins, I.T., Voogt, P.D., Jensen, A.A., Kannan, K., Mabury, S.A. & van, L. (2011). Perfluoroalkyl and polyfluoroalkyl substances in the environment: Terminology, classification, and origins. *Integrated Environmental Assessment and Management*, 7 (4), 513–541. <https://doi.org/10.1002/ieam.258>
- Chen, H., Chen, S., Quan, X., Zhao, Y. & Zhao, H. (2009). Sorption of perfluorooctane sulfonate (PFOS) on oil and oil-derived black carbon: Influence of solution pH and $[Ca^{2+}]$. *Chemosphere*, 77 (10), 1406–1411. <https://doi.org/10.1016/j.chemosphere.2009.09.008>
- ECHA (2021). Perfluoroalkyl chemicals (PFAS). <https://echa.europa.eu/hot-topics/perfluoroalkyl-chemicals-pfas> [Accessed 2021-09-10]

- Erkoç, Ş. & Erkoç, F. (2001). Structural and electronic properties of PFOS and LiPFOS. *Journal of Molecular Structure: Theochem*, 549 (3), 289–293. [https://doi.org/10.1016/S0166-1280\(01\)00553-X](https://doi.org/10.1016/S0166-1280(01)00553-X)
- Filipovic, M., Woldegiorgis, A., Norström, K., Bibi, M., Lindberg, M. & Österås, A.-H. (2015). Historical usage of aqueous film forming foam: A case study of the widespread distribution of perfluoroalkyl acids from a military airport to groundwater, lakes, soils and fish. *Chemosphere*, 129, 39–45. <https://doi.org/10.1016/j.chemosphere.2014.09.005>
- Gao, X. & Chorover, J. (2012). Adsorption of perfluorooctanoic acid and perfluorooctanesulfonic acid to iron oxide surfaces as studied by flow-through ATR-FTIR spectroscopy. *Environmental Chemistry*, 9 (2), 148–157
- Gobelius, L., Lewis, J. & Ahrens, L. (2017). Plant Uptake of Per- and Polyfluoroalkyl Substances at a Contaminated Fire Training Facility to Evaluate the Phytoremediation Potential of Various Plant Species. *Environmental Science & Technology*, 51 (21), 12602–12610. <https://doi.org/10.1021/acs.est.7b02926>
- Goldenman, G., Fernandes, M., Holland, M., Tugran, T., Nordin, A., Schoumacher, C. & McNeill, A. (2019). The cost of inaction: A socioeconomic analysis of environmental and health impacts linked to exposure to PFAS., 2019. <https://doi.org/10.6027/TN2019-516>
- Goss, K.-U. & Bronner, G. (2006). What is so special about the sorption behavior of highly fluorinated compounds? *The Journal of Physical Chemistry. A*, 110 (30), 9518–9522. <https://doi.org/10.1021/jp062684o>
- Groenenberg, J.E. & Lofts, S. (2014). The use of assemblage models to describe trace element partitioning, speciation, and fate: A review. *Environmental Toxicology and Chemistry*, 33 (10), 2181–2196. <https://doi.org/10.1002/etc.2642>
- Gu, C., Wang, Z., Kubicki, J.D., Wang, X. & Zhu, M. (2016). X-ray Absorption Spectroscopic Quantification and Speciation Modeling of Sulfate Adsorption on Ferrihydrite Surfaces. *Environmental Science & Technology*, 50 (15), 8067–8076. <https://doi.org/10.1021/acs.est.6b00753>
- Guelfo, J.L. & Higgins, C.P. (2013). Subsurface Transport Potential of Perfluoroalkyl Acids at Aqueous Film-Forming Foam (AFFF)-Impacted Sites. *Environ. Sci. Technol.* 47 (9), 4164–4171. <https://doi.org/10.1021/es3048043>
- Guelfo, J.L., Korzeniowski, S., Mills, M.A., Anderson, J., Anderson, R.H., Arblaster, J.A., Conder, J.M., Cousins, I.T., Dasu, K., Henry, B.J., Lee, L.S., Liu, J., McKenzie, E.R. & Willey, J. (2021). Environmental Sources, Chemistry, Fate and Transport of Per- and Polyfluoroalkyl Substances: State of the Science, Key Knowledge Gaps, and Recommendations Presented at the August 2019 SETAC Focus Topic Meeting. *Environmental Toxicology and Chemistry*, 00 (00), 1–27. <https://doi.org/10.1002/etc.5182>

- Gustafsson, J.P. (2001). Modeling the Acid–Base Properties and Metal Complexation of Humic Substances with the Stockholm Humic Model. *Journal of Colloid and Interface Science*, 244 (1), 102–112. <https://doi.org/10.1006/jcis.2001.7871>
- Gustafsson, J.P., Pechová, P. & Berggren, D. (2003). Modeling Metal Binding to Soils: The Role of Natural Organic Matter. *Environmental Science & Technology*, 37 (12), 2767–2774. <https://doi.org/10.1021/es026249t>
- Gustafsson, J.P. (2020). Visual MINTEQ – Visual MINTEQ – a free equilibrium speciation model. <https://vminteq.lwr.kth.se/> [2021-03-18]
- Herzke, D., Olsson, E. & Posner, S. (2012). Perfluoroalkyl and polyfluoroalkyl substances (PFASs) in consumer products in Norway - a pilot study. *Chemosphere*, 88 (8), 980–987. <https://doi.org/10.1016/j.chemosphere.2012.03.035>
- Higgins, C.P., Field, J.A., Criddle, C.S. & Luthy, R.G. (2005). Quantitative Determination of Perfluorochemicals in Sediments and Domestic Sludge. *Environmental Science & Technology*, 39 (11), 3946–3956. <https://doi.org/10.1021/es048245p>
- Higgins, C.P. & Luthy, R.G. (2006). Sorption of Perfluorinated Surfactants on Sediments. *Environmental Science & Technology*, 40 (23), 7251–7256. <https://doi.org/10.1021/es061000n>
- ISO (2009). *ISO 25101:2009*. <https://www.iso.org/> [2021-09-11]
- Jafvert, C. (1990). Sorption of organic acid compounds to sediments: Initial model development. *Environmental Toxicology and Chemistry*, 9, 1259–1268.
- Jensen, J. & Mesman, M. (2006). Ecological risk assessment of contaminated land: decision support for site specific investigations. Bilthoven: RIVM. <http://www.rivm.nl/bibliotheek/rapporten/711701047.pdf> [Accessed 2021-09-11]
- Johansson, N., Fredriksson, A. & Eriksson, P. (2008). Neonatal exposure to perfluorooctane sulfonate (PFOS) and perfluorooctanoic acid (PFOA) causes neurobehavioural defects in adult mice. *NeuroToxicology*, 29 (1), 160–169. <https://doi.org/10.1016/j.neuro.2007.10.008>
- Johnson, R.L., Anschutz, A.J., Smolen, J.M., Simcik, M.F. & Penn, R.L. (2007). The Adsorption of Perfluorooctane Sulfonate onto Sand, Clay, and Iron Oxide Surfaces. *Journal of Chemical & Engineering Data*, 52 (4), 1165–1170. <https://doi.org/10.1021/jc060285g>
- Kim, S., Thapar, I. & Brooks, B.W. (2021). Epigenetic changes by per- and polyfluoroalkyl substances (PFAS). *Environmental Pollution*, 279, 116929. <https://doi.org/10.1016/j.envpol.2021.116929>
- Kissa, E. (2001). *Fluorinated Surfactants and Repellents, Second Edition*,. CRC Press.
- Lath, S., Knight, E.R., Navarro, D.A., Kookana, R.S. & McLaughlin, M.J. (2019). Sorption of PFOA onto different laboratory materials: Filter membranes

- and centrifuge tubes. *Chemosphere*, 222, 671–678.
<https://doi.org/10.1016/j.chemosphere.2019.01.096>
- Leeuwen, C.J. van & Hermens, J.L.M. (2012). *Risk Assessment of Chemicals: An Introduction*. Springer Science & Business Media.
- Li, Y., Oliver, D.P. & Kookana, R.S. (2018). A critical analysis of published data to discern the role of soil and sediment properties in determining sorption of per and polyfluoroalkyl substances (PFASs). *The Science of the Total Environment*, 628–629, 110–120. <https://doi.org/10.1016/j.scitotenv.2018.01.167>
- Linde, M., Öborn, I. & Gustafsson, J.P. (2007). Effects of Changed Soil Conditions on the Mobility of Trace Metals in Moderately Contaminated Urban Soils. *Water, Air, and Soil Pollution*, 183 (1–4), 69–83.
<https://doi.org/10.1007/s11270-007-9357-5>
- Lindstrom, A.B., Strynar, M.J. & Libelo, E.L. (2011). Polyfluorinated compounds: Past, present, and future. *Environmental Science and Technology*, 45 (19), 7954–7961. <https://doi.org/10.1021/es2011622>
- Ludwicki, J.K., Góralczyk, K., Struciński, P., Wojtyniak, B., Rabczenko, D., Toft, G., Lindh, C.H., Jönsson, B.A.G., Lenters, V., Heederik, D., Czaja, K., Her-
 nik, A., Pedersen, H.S., Zvyezday, V. & Bonde, J.P. (2015). Hazard quotient profiles used as a risk assessment tool for PFOS and PFOA serum levels in three distinctive European populations. *Environment International*, 74, 112–118. <https://doi.org/10.1016/j.envint.2014.10.001>
- Lyu, Y. & Brusseau, M.L. (2020). The influence of solution chemistry on air-water interfacial adsorption and transport of PFOA in unsaturated porous media. *Science of The Total Environment*, 713, 136744.
<https://doi.org/10.1016/j.scitotenv.2020.136744>
- Lyu, Y., Brusseau, M.L., Chen, W., Yan, N., Fu, X. & Lin, X. (2018). Adsorption of PFOA at the Air–Water Interface during Transport in Unsaturated Porous Media. *Environmental Science & Technology*, 52 (14), 7745–7753.
<https://doi.org/10.1021/acs.est.8b02348>
- Majzlan, J., Alpers, C.N., Koch, C.B., McCleskey, R.B., Myneni, S.C.B. & Neil, J.M. (2011). Vibrational, X-ray absorption, and Mössbauer spectra of sulfate minerals from the weathered massive sulfide deposit at Iron Mountain, California. *Chemical Geology*, 284 (3), 296–305.
<https://doi.org/10.1016/j.chemgeo.2011.03.008>
- Majzlan, J. & Myneni, S.C.B. (2005). Speciation of Iron and Sulfate in Acid Waters: Aqueous Clusters to Mineral Precipitates. *Environmental Science & Technology*, 39 (1), 188–194. <https://doi.org/10.1021/es049664p>
- Milinovic, J., Lacorte, S., Vidal, M. & Rigol, A. (2015). Sorption behaviour of perfluoroalkyl substances in soils. *Science of The Total Environment*, 511, 63–71. <https://doi.org/10.1016/j.scitotenv.2014.12.017>

- Moody, C.A., Hebert, G.N., Strauss, S.H. & Field, J.A. (2003). Occurrence and persistence of perfluorooctanesulfonate and other perfluorinated surfactants in groundwater at a fire-training area at Wurtsmith Air Force Base, Michigan, USA. *Journal of Environmental Monitoring*, 5 (2), 341–345. <https://doi.org/10.1039/B212497A>
- Moroi, Y., Yano, H., Shibata, O. & Yonemitsu, T. (2001). Determination of Acidity Constants of Perfluoroalkanoic Acids. *Bulletin of the Chemical Society of Japan*, 74 (4), 667–672. <https://doi.org/10.1246/bcsj.74.667>
- Muir, D., Bossi, R., Carlsson, P., Evans, M., De Silva, A., Halsall, C., Rauert, C., Herzke, D., Hung, H., Letcher, R., Rigét, F. & Roos, A. (2019). Levels and trends of poly- and perfluoroalkyl substances in the Arctic environment – An update. *Emerging Contaminants*, 5, 240–271. <https://doi.org/10.1016/j.emcon.2019.06.002>
- Nelson, P. & Baldock, J. (2005). Estimating the molecular composition of a diverse range of natural organic materials from solid-state ¹³C NMR and elemental analyses. *Biogeochemistry*, 72, 1–34. <https://doi.org/10.1007/s10533-004-0076-3>
- NC Policy Watch. New research confirms presence of toxic "forever chemicals" in scores of NC water supplies (2020-07-01). <http://www.ncpolicy-watch.com/2020/07/01/new-research-confirms-presence-of-toxic-forever-chemicals-in-scores-of-nc-water-supplies/> [Accessed 2021-09-09]
- Newburgh - NYS Dept. of Environmental Conservation (2020). <https://www.dec.ny.gov/chemical/108825.html> [Accessed 2021-09-09]
- Nguyen, T.M.H., Bräunig, J., Thompson, K., Thompson, J., Kabiri, S., Navarro, D.A., Kookana, R.S., Grimison, C., Barnes, C.M., Higgins, C.P., McLaughlin, M.J. & Mueller, J.F. (2020). Influences of Chemical Properties, Soil Properties, and Solution pH on Soil–Water Partitioning Coefficients of Per- and Polyfluoroalkyl Substances (PFASs). *Environmental Science & Technology*, 54 (24), 15883–15892. <https://doi.org/10.1021/acs.est.0c05705>
- O'Hagan, D. (2008). Understanding organofluorine chemistry. An introduction to the C–F bond. *Chem. Soc. Rev.*, 37 (2), 308–319. <https://doi.org/10.1039/B711844A>
- Okude, N., Nagoshi, M., Noro, H., Baba, Y., Yamamoto, H. & Sasaki, T.A. (1999). P and S K-edge XANES of transition-metal phosphates and sulfates. *Journal of Electron Spectroscopy and Related Phenomena*, 101–103, 607–610. [https://doi.org/10.1016/S0368-2048\(98\)00341-7](https://doi.org/10.1016/S0368-2048(98)00341-7)
- Pan, G., Jia, C., Zhao, D., You, C., Chen, H. & Jiang, G. (2009). Effect of cationic and anionic surfactants on the sorption and desorption of perfluorooctane sulfonate (PFOS) on natural sediments. *Environmental Pollution*, 157 (1), 325–330. <https://doi.org/10.1016/j.envpol.2008.06.035>

- Paul, A.G., Jones, K.C. & Sweetman, A.J. (2009). A First Global Production, Emission, And Environmental Inventory For Perfluorooctane Sulfonate. *Environmental Science & Technology*, 43 (2), 386–392. <https://doi.org/10.1021/es802216n>
- Pettersson, M., Ländell, M., Ohlsson, Y., Kleja, D.B. & Tiberg, C. (u.å.). Preliminära riktvärden för högfluorerade ämnen (PFAS) i mark och grundvatten. 146
- Pignatello, J.J. & Xing, B. (1996). Mechanisms of Slow Sorption of Organic Chemicals to Natural Particles. *Environmental Science & Technology*, 30 (1), 1–11. <https://doi.org/10.1021/es940683g>
- Prietzl, J., Wu, Y., Dümig, A., Zhou, J. & Klysubun, W. (2013). Soil sulphur speciation in two glacier forefield soil chronosequences assessed by S K-edge XANES spectroscopy. *European Journal of Soil Science*, 64 (2), 260–272. <https://doi.org/10.1111/ejss.12032>
- Ravel, B. & Newville, M. (2005). ATHENA, ARTEMIS, HEPHAESTUS: data analysis for X-ray absorption spectroscopy using IFEFFIT. *Journal of Synchrotron Radiation*, 12 (4), 537–541. <https://doi.org/10.1107/S0909049505012719>
- Rayne, S. & Forest, K. (2009a). A new class of perfluorinated acid contaminants: primary and secondary substituted perfluoroalkyl sulfonamides are acidic at environmentally and toxicologically relevant pH values. *Journal of Environmental Science and Health. Part A, Toxic/Hazardous Substances & Environmental Engineering*, 44 (13), 1388–1399. <https://doi.org/10.1080/10934520903217278>
- Rayne, S. & Forest, K. (2009b). Perfluoroalkyl sulfonic and carboxylic acids: A critical review of physicochemical properties, levels and patterns in waters and wastewaters, and treatment methods. *Journal of Environmental Science and Health - Part A Toxic/Hazardous Substances and Environmental Engineering*, 44 (12), 1145–1199. <https://doi.org/10.1080/10934520903139811>
- Rayne, S. & Forest, K. (2010). Theoretical studies on the pK_{a} values of perfluoroalkyl carboxylic acids. *Nature Precedings*, 1–1. <https://doi.org/10.1038/npre.2010.3829.2>
- Schultes, L., Vestergren, R., Volkova, K., Westberg, E., Jacobson, T. & Benskin, J.P. (2018). Per- and polyfluoroalkyl substances and fluorine mass balance in cosmetic products from the Swedish market: implications for environmental emissions and human exposure. *Environmental Science: Processes & Impacts*, 20 (12), 1680–1690. <https://doi.org/10.1039/C8EM00368H>
- Schwarzenbach, R.P., Gschwend, P.M. & Imboden, D.M. (2016). *Environmental Organic Chemistry*. 3rd Edition. John Wiley & Sons.
- Schwertmann, U. & Cornell, R.M. (2000). *Iron Oxides in the Laboratory*. Wiley Books. <https://onlinelibrary.wiley.com/doi/book/10.1002/9783527613229> [2019-11-14]

- Shapiro, S.S. & Wilk, M.B. (1965). An Analysis of Variance Test for Normality (Complete Samples). *Biometrika*, 52 (3/4), 591–611. <https://doi.org/10.2307/2333709>
- Steenland, K. & Winquist, A. (2021). PFAS and cancer, a scoping review of the epidemiologic evidence. *Environmental Research*, 194, 110690. <https://doi.org/10.1016/j.envres.2020.110690>
- Steinle-Darling, E. & Reinhard, M. (2008). Nanofiltration for Trace Organic Contaminant Removal: Structure, Solution, and Membrane Fouling Effects on the Rejection of Perfluorochemicals. *Environmental Science & Technology*, 42 (14), 5292–5297. <https://doi.org/10.1021/es703207s>
- Stockholm Convention. Chemicals listed in Annex B. <http://chm.pops.int/Implementation/Alternatives/AlternativestoPOPs/ChemicalslistedinAnnexB/tabid/5850/Default.aspx> [Accessed 2021-09-09]
- Stockholm Convention. Chemicals proposed for listing under the Convention. <http://www.pops.int/TheConvention/ThePOPs/ChemicalsProposedforListing/tabid/2510/Default.aspx> [Accessed 2021-09-20]
- Sunderland, E.M., Hu, X.C., Dassuncao, C., Tokranov, A.K., Wagner, C.C. & Allen, J.G. (2019). A Review of the Pathways of Human Exposure to Poly- and Perfluoroalkyl Substances (PFASs) and Present Understanding of Health Effects. *Journal of exposure science & environmental epidemiology*, 29 (2), 131–147. <https://doi.org/10.1038/s41370-018-0094-1>
- Swedish Environmental Protection Agency (Naturvårdsverket) (2009). Riktvärden för förorenad mark - Modellbeskrivning och vägledning. (In Swedish.) <https://www.naturvardsverket.se/Om-Naturvardsverket/Publikationer/ISBN/5900/978-91-620-5976-7/> [2021-08-18]
- Söregård, M., Franke, V., Tröger, R. & Ahrens, L. (2020). Losses of poly- and perfluoroalkyl substances to syringe filter materials. *Journal of Chromatography A*, 1609, 460430. <https://doi.org/10.1016/j.chroma.2019.460430>
- Tiberg, C., Sjöstedt, C. & Gustafsson, J.P. (2018). Metal sorption to Spodosol Bs horizons: Organic matter complexes predominate. *Chemosphere*, 196, 556–565. <https://doi.org/10.1016/j.chemosphere.2018.01.004>
- UN-Water Human Rights. *UN-Water*. <https://www.unwater.org/water-facts/human-rights/> [2021-09-09]
- Vairavamurthy, A., Manowitz, B., Luther, G.W. & Jeon, Y. (1993). Oxidation state of sulfur in thiosulfate and implications for anaerobic energy metabolism. *Geochimica et Cosmochimica Acta*, 57 (7), 1619–1623. [https://doi.org/10.1016/0016-7037\(93\)90020-W](https://doi.org/10.1016/0016-7037(93)90020-W)
- Waldo, G., Carlson, R.M.K., Moldowan, J.M., Peters, K.E. & Penner-Hahn, J.E. (1991). Sulfur speciation in heavy petroleum: Information from X-ray absorption near-edge structure., 1991. [https://doi.org/10.1016/0016-7037\(91\)90343-4](https://doi.org/10.1016/0016-7037(91)90343-4)

- Wilhelm, M., Bergmann, S. & Dieter, H.H. (2010). Occurrence of perfluorinated compounds (PFCs) in drinking water of North Rhine-Westphalia, Germany and new approach to assess drinking water contamination by shorter-chained C4–C7 PFCs. *International Journal of Hygiene and Environmental Health*, 213 (3), 224–232. <https://doi.org/10.1016/j.ijheh.2010.05.004>
- Xia, K., Weesner, F., Bleam, W.F., Helmke, P.A., Bloom, P.R. & Skyllberg, U.L. (1998). XANES Studies of Oxidation States of Sulfur in Aquatic and Soil Humic Substances. *Soil Science Society of America Journal*, 62 (5), 1240–1246. <https://doi.org/10.2136/sssaj1998.03615995006200050014x>
- Xiao, F., Simcik, M.F., Halbach, T.R. & Gulliver, J.S. (2015). Perfluorooctane sulfonate (PFOS) and perfluorooctanoate (PFOA) in soils and groundwater of a U.S. metropolitan area: Migration and implications for human exposure. *Water Research*, 72, 64–74. <https://doi.org/10.1016/j.watres.2014.09.052>
- Xiao, F., Zhang, X., Penn, L., Gulliver, J.S. & Simcik, M.F. (2011). Effects of Monovalent Cations on the Competitive Adsorption of Perfluoroalkyl Acids by Kaolinite: Experimental Studies and Modeling. *Environmental Science & Technology*, 45 (23), 10028–10035. <https://doi.org/10.1021/es202524y>
- Zhang, C., Yan, H., Li, F., Hu, X. & Zhou, Q. (2013). Sorption of short- and long-chain perfluoroalkyl surfactants on sewage sludges. *Journal of Hazardous Materials*, 260, 689–699. <https://doi.org/10.1016/j.jhazmat.2013.06.022>
- Zhi, Y. & Liu, J. (2018). Sorption and desorption of anionic, cationic and zwitterionic polyfluoroalkyl substances by soil organic matter and pyrogenic carbonaceous materials. *Chemical Engineering Journal*, 346, 682–691. <https://doi.org/10.1016/j.cej.2018.04.042>

Popular science summary

So-called highly fluorinated substances (PFAS substances) are a group of chemicals that in recent years have come to be regarded as environmental contaminants of global concern. Large emissions to the environment have occurred at fire-fighting training sites through the use of PFAS-containing fire-fighting foam. The substances are found almost everywhere in the environment, including in the drinking water we drink every day, albeit usually in small amounts. As these substances are persistent to degradation, and are (confirmed or suspected to be) associated with adverse health effects in humans and other organisms, the use of some of them is now being phased out. However, the legacy of global and long-standing emissions will remain to be dealt with for a long time to come.

This work has investigated how strongly or weakly PFAS substances are bound in soil, and which chemical binding mechanisms come into play, in order to contribute to improved environmental risk assessment of PFAS-contaminated sites.

The methods used in this thesis included batch experiments with soil samples and with components (organic matter, iron minerals) that are often found in soil. Since PFAS substances are often negatively charged, factors that may affect the charge of the soil particles, including the pH value (acidity) of the soil solution, were investigated in connection with the batch experiments. Spectroscopic methods (X-ray absorption, nuclear magnetic resonance from carbon atoms) were used to gain a better understanding of the substances' binding to iron minerals and to organic matter.

The overall binding of PFAS substances to soil and to samples of isolated organic material was found to be determined by how hydrophobic the PFAS substance in question is, i.e., how much a certain substance wants to "escape" the water phase present in the pores (the solution) of the soil. However, in

the case of the iron mineral ferrihydrite, which is more or less positively charged, the binding strength of the PFASs was determined by how much positive charge the mineral held in the experiment. The more acidic the pH value, the greater the positive charge of the mineral, and hence the stronger the binding of the negatively charged PFAS substances. In addition, for PFASs with more fluorine atoms in their molecule, it was found that the binding strength was affected to a larger extent by the charge present both on the soil particles and on the pure organic material and iron minerals, as compared to that of PFASs with less fluorine atoms. This indicates that the fluorine atoms of the molecule's "tail" contribute to the overall charge-dependency of the binding, together with the (often negatively charged) so-called head group of the molecule.

An attempt to predict how strongly PFAS substances are bound in mineral soils, based on the soils' content of organic material and on how strongly the substances were bound in previous experiments with isolated ("pure") organic material, was shown to underestimate the binding strength. Modeling of the charge present on the organic material of the mineral soils also underestimated the binding of the substances. It could not be ruled out that there were chemical binding sites in the mineral soils, for example on specific types of organic material or clay minerals, to which the PFAS substances were bound strongly. Hence, modeling methods involving simultaneous binding contributions from several soil components (i.e., those from organic matter and iron oxides) could not be tested properly. This highlights the need for more experimental data on the binding of PFASs to soil: data of the type that can be used to develop more accurate models to simulate and predict the binding and mobility of PFAS substances in the terrestrial environment.

Populärvetenskaplig sammanfattning

Så kallade högfluorerade ämnen (PFAS-ämnen) är en grupp kemikalier som på senare år har kommit att betraktas som viktiga globala miljöföroreningar att hantera och riskbedöma. Större utsläpp till miljön har skett bland annat vid brandövningsplatser genom användning av brandskum som har innehållit PFAS. Ämnena finns i stort sett överallt i miljön, inklusive i det dricksvatten vi till vardags dricker, om än oftast i låga mängder. På grund av att dessa ämnen är väldigt svåra att bryta ner, och har (eller misstänks ha) negativa hälsoeffekter gentemot människor och andra organismer, faras deras användning nu ut alltmer. Men arvet av globala och mångåriga utsläpp finns kvar att hantera för lång tid framöver.

Det här arbetet har syftat till att kartlägga hur starkt eller svagt PFAS-ämnen binds (fastläggs) i mark, och vilka kemiska bindningsmekanismer som är i verksamma. Detta har gjorts för att i förlängningen kunna hitta metoder för att bättre kunna förutsäga miljörisker kopplade till PFAS-förorenade områden.

Metoderna som användes i denna avhandling inkluderade skakförsök med jordprov och med komponenter (organiskt material, järnoxider) som ofta återfinns i mark. Eftersom PFAS-ämnen ofta är negativt laddade undersöktes faktorer som kan påverka markpartiklarnas egen laddning, bland annat marklösningens pH (surhet), i anslutning till skakförsöken. Spektroskopiska metoder (röntgenabsorption, kärnmagnetisk resonans från kolatomer) användes för att få ökad förståelse för ämnens bindning till järnoxider och till organiskt material.

Den övergripande bindningen av PFAS-ämnen till mark och till prover av isolerat organiskt material bestämdes av hur hydrofobt PFAS-ämnet i fråga är, det vill säga hur gärna ett visst ämne vill "undkomma" vattnet som finns i markens porer (marklösningen). Däremot, i fallet med järnoxiden

ferrihydrit, som är mer eller mindre positivt laddad, bestämdes PFAS-ämnenas bindningsstyrka av hur stark positiv laddning som mineralet hade i experimentet. Ju större positiv laddning som fanns på mineralet (till exempel, alltså ju surare lösning som mineralet slammades upp i), desto starkare band de negativt laddade PFAS-ämnena. Dessutom visade det sig, för PFAS-ämnena med många fluoratomer i molekylen, att bindningsstyrkan påverkades mer av laddningen på markpartiklarna och på organiskt material/järnoxider än vad som var fallet med PFAS-ämnena som hade färre fluoratomer. Detta tyder på att de elektrontäta fluoratomerna i molekylen ”svans” bidrar till att bestämma bindningens övergripande laddningsberoende, tillsammans med molekylen (ofta negativt laddade) så kallade huvudgrupp.

Ett försök att förutsäga hur starkt PFAS-ämnena binds i mineraljordar, baserat på jordarnas innehåll av organiskt material och ämnenas bindningsstyrka till isolerat (”rent”) organiskt material, visade sig underskatta bindningens omfattning. Också en modellering av laddningen på mineraljordarnas organiska material underskattade hur starkt ämnena bands till jordarna. Baserat på resultaten kunde det inte uteslutas att det fanns kemiska bindningsställen i mineraljordarna, till exempel på specifika typer av organiskt material eller lermineral, till vilka PFAS-ämnena skulle kunna bindas extra starkt. Därför kunde inte heller en modelleringsmetod som omfattar olika markkomponenters samtida bindningsbidrag (organiskt material, järnoxider) testas fullt ut. Detta belyser att det behövs mer experimentella data för PFAS-ämnens bindning i mark: data som kan användas för att utveckla bättre (mer precisa) modeller för att förutsäga ämnens bindning, rörlighet och ytterst deras risker i miljön.

Acknowledgments

I am grateful to the **Swedish Research Council** (Vetenskapsrådet) for funding this project (grant number 2015-03938) and making it possible. Furthermore, I wish to thank the **Swedish Geotechnical Institute** (Statens geotekniska institut, SGI) who contributed with parts of the funding for Paper IV. Moreover, I am thankful to the staff at Beamline 8 (BL8), **Synchrotron Light Research Institute** (Nakhon Ratchasima, Thailand), and to Dr. **Sabina Braun**, for their valuable support during the collection of XANES data. In addition, I wish to thank the staff at the **Technische Universität München** who helped to measure the ^{13}C NMR spectra for Paper II.

I wish to thank my supervisors at the Swedish University of Agricultural Sciences (SLU) – Prof. Jon Petter Gustafsson, Prof. Dan Berggren Kleja, Dr. Carin Sjöstedt, and Dr Lutz Ahrens. **Jon Petter**, thank you for your valuable advice, guidance and help, on this sometimes winding path that was my journey as a PhD student. **Dan**, thank you for our good discussions, for your critical eye and feedback, and for sparking my interest as a student in the field of environmental contaminants some nine(?) years ago. **Carin**, thank you for your valuable feedback on the manuscripts, and for listening and discussing with me. **Karin Blombäck**, and also **Anke Herrmann**, at SLU; thank you for your support, for listening, and understanding. It helped me more than you perhaps think.

The “PFAS guys” – **George, Mattias, Vera, and Winnie** – for great support, help, and friendship; thank you! Jennifer (**Jenny**) Maksiel, it was a pleasure to have you as a Master student in the project. Thank you for your hard work, our good discussions, and cheerful company. To all the nice **colleagues**, both PhD students and non-students, that I got to work or cross paths with during my project; you lit up my time at SLU and made me feel good about coming in to work.

Last but not least, a big and humble Thank you to my family; **António, Carin, and Hannes**, for your never-ending support during the ups and the downs. I love you guys.



Sorption of perfluoroalkyl substances (PFASs) to an organic soil horizon – Effect of cation composition and pH

Hugo Campos Pereira ^{a,*}, Malin Ullberg ^a, Dan Berggren Kleja ^{a,c},
Jon Petter Gustafsson ^{a,d}, Lutz Ahrens ^b

^a Department of Soil and Environment, Swedish University of Agricultural Sciences, Box 7014, SE-75007 Uppsala, Sweden

^b Department of Aquatic Sciences and Assessment, Swedish University of Agricultural Sciences, Box 7050, SE-75007 Uppsala, Sweden

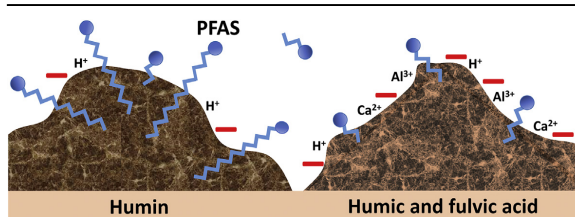
^c Swedish Geotechnical Institute, Kornhamnstorg 61, SE-11127 Stockholm, Sweden

^d Department of Sustainable Development, Environmental Science and Engineering, KTH Royal Institute of Technology, Teknikringen 10B, 10044 Stockholm, Sweden

HIGHLIGHTS

- Sorption of PFASs of C₅ or longer depends on the pH or on the SOM bulk net charge.
- For C₅–C₈ PFCAs, SOM bulk net charge is strongly related to sorption.
- For longer-chained PFASs, pH is a better predictor of sorption.
- Cation effects are evident only for shorter-chained PFASs.
- Longer-chained PFASs probably bind preferentially to the humin fraction of SOM.

GRAPHICAL ABSTRACT



ARTICLE INFO

Article history:

Received 30 January 2018

Received in revised form

1 May 2018

Accepted 2 May 2018

Available online 4 May 2018

Handling Editor: J. de Boer

Keywords:

Soil–water partitioning

PFOs

PFOA

Surface net charge

Geochemical modeling

Visual MINTEQ

ABSTRACT

Accurate prediction of the sorption of perfluoroalkyl substances (PFASs) in soils is essential for environmental risk assessment. We investigated the effect of solution pH and calculated soil organic matter (SOM) net charge on the sorption of 14 PFASs onto an organic soil as a function of pH and added concentrations of Al³⁺, Ca²⁺ and Na⁺. Often, the organic C-normalized partitioning coefficients (*K*_{OC}) showed a negative relationship to both pH ($\Delta \log K_{OC} / \Delta \text{pH} = -0.32 \pm 0.11$ log units) and the SOM bulk net negative charge ($\Delta \log K_{OC} = -1.41 \pm 0.40$ per log unit mol_c g⁻¹). Moreover, perfluorosulfonic acids (PFSAs) sorbed more strongly than perfluorocarboxylic acids (PFCAs) and the PFAS sorption increased with increasing perfluorocarbon chain length with 0.60 and 0.83 log *K*_{OC} units per CF₂ moiety for C₃–C₁₀ PFCAs and C₄, C₆, and C₈ PFSAs, respectively. The effects of cation treatment and SOM bulk net charge were evident for many PFASs with low to moderate sorption (C₅–C₈ PFCAs and C₆ PFSA). However for the most strongly sorbing and most long-chained PFASs (C₉–C₁₁ and C₁₃ PFCAs, C₈ PFSA and perfluorooctane sulfonamide (FOA)), smaller effects of cations were seen, and instead sorption was more strongly related to the pH value. This suggests that the most long-chained PFASs, similar to other hydrophobic organic compounds, are preferentially sorbed to the highly condensed domains of the humin fraction, while shorter-chained PFASs are bound to a larger extent to humic and fulvic acid, where cation effects are significant.

© 2018 The Authors. Published by Elsevier Ltd. This is an open access article under the CC BY-NC-ND license (<http://creativecommons.org/licenses/by-nc-nd/4.0/>).

* Corresponding author.

E-mail address: hugo.pereira@slu.se (H. Campos Pereira).

1. Introduction

Perfluoroalkyl substances (PFASs) have been produced in large quantities for use in a variety of consumer products and industrial applications since the 1950s (Cousins et al., 2016). However, in recent years they have been recognized as environmental contaminants of global concern due to their persistency (Houtz et al., 2013), bioaccumulative potential (Conder et al., 2008) and toxicity (Giesy et al., 2010; Apelberg et al., 2007). PFASs have been found ubiquitously in the environment (Zareitalabad et al., 2013; Ahrens, 2011), and are taken up by organisms including humans (Giesy and Kannan, 2001; Yeung et al., 2006). The environmental behavior of PFASs differs from other persistent organic pollutants (POPs) due to their extreme surface-active properties (Goss and Bronner, 2006) characterized by their hydrophobic (oleophobic) poly- or perfluorinated carbon chain (tail) in combination with the hydrophilic, usually anionic, functional head group. Thus, in contrast to other, non-ionic, POPs, for which the environmental behavior is well predicted solely by their hydrophobic or lipophilic properties, the behavior of the PFASs is governed not only by hydrophobic (oleophobic) but also by electrostatic interactions (Higgins and Luthy, 2007). Due to this complexity of PFAS chemistry, sorption of these substances cannot be predicted from a single sorbent bulk property such as for example organic carbon (OC) content (Barzen-Hanson et al., 2017; Li et al., 2018) and there are still significant uncertainties as regards how various sorbent-specific properties, such as for example pH and surface-bound cations, interact to determine the binding of PFASs to soils (Li et al., 2018). Accordingly, up to date there is a lack of standard protocols to assess the soil chemical properties of PFASs.

Organic matter is known to be an important sorbent for PFASs in soils (Milinovic et al., 2015) and sediments (Higgins and Luthy, 2006). However, the number of studies on PFAS sorption to “pure” phases of soil organic matter (SOM) is scarce. Moreover, studies on sorption in soils have usually included only a limited number of PFASs (e.g. Milinovic et al., 2015). Furthermore, there is still a lack of knowledge as for what fractions of SOM may be important for binding of PFASs. Zhang et al. (2015) reported that the humin fraction accounted for most of the sorption by comparing perfluorooctane sulfonate (PFOS) sorption to untreated soils with that of sodium hydroxide (NaOH)-treated soils. Humic (HA) and fulvic acids (FA) were found to be less important, presumably because of their higher charge, hydrophilicity and polarity (Zhang et al., 2015). However, this contrasts with the results of Zhao et al. (2014), who found that both the humin and the HA/FA fractions may be important for the sorption of PFOS and perfluorohexane sulfonate (PFHxS). Humin has been shown to be an important sorbent also for other hydrophobic organic compounds (HOCs) (Kohl and Rice, 1998; Han et al., 2013). For polycyclic aromatic hydrocarbons (PAHs) the humin fraction contributed more to binding than the HA/FA fraction (e.g. Gunasekara and Xing, 2003; Chen et al., 2017; Kang and Xing, 2005).

In general, the sorption of ionizable, anionic, organic contaminants is promoted by a decrease in pH and by an increase in solution cation concentration (Järfvert, 1990). For PFASs this has been confirmed by e.g. Higgins and Luthy (2006), Chen et al. (2009) and Zhang et al. (2013) concerning the effect of pH and Ca^{2+} , and by Wang et al. (2015) concerning the positive impact of Mg^{2+} , Fe^{3+} and Al^{3+} . However, no significant effect on sorption has been observed for monovalent cations such as Na^+ and K^+ (e.g. Higgins and Luthy, 2006; Wang et al., 2015). Under environmental pH values, natural organic matter (NOM) carries a negative net charge due to the presence of dissociated carboxylic and phenolic acid groups (Kinniburgh et al., 1999). Thus, in systems where NOM is present, the increased sorption of anionic organic compounds after adding

multivalent cations can be understood in terms of a reduced negative electrostatic potential of NOM caused by cation complexation (Higgins and Luthy, 2006, 2007). The modeling work by Higgins and Luthy (2007) on sorption of PFASs to sediment in the presence of Ca^{2+} and Na^+ suggested a strong relationship with the electrostatic Donnan potential for sediment organic matter.

The main objective of this study was to assess the effect of solution cation composition on the sorption of 14 PFASs onto SOM. The effect of the modeled bulk net charge of SOM was compared to that of pH, with the hypothesis that the bulk net charge would be the better predictor of PFAS sorption in the presence of variable concentrations of divalent and trivalent ions. In particular we examined the effect of Al^{3+} on PFAS sorption to an organic soil sample and compared it to the effects of Ca^{2+} and Na^+ , as Al^{3+} has a high charge density (a high valence in combination with small ionic radius) and therefore a high propensity to form complexes with organic functionalities. Accordingly, we hypothesized that the effect of Al^{3+} on PFAS sorption would exceed those of Ca^{2+} and Na^+ .

2. Materials and methods

2.1. Standards

Fourteen target PFASs (purchased from Sigma Aldrich) were analyzed including C_3 – C_{11} and C_{13} perfluoroalkyl carboxylates (PFCAs), C_4 , C_6 , C_8 perfluoroalkyl sulfonates (PFASs) and perfluorooctane sulfonamide (FOSA) (Table 1). For quality control, 10 mass-labelled internal standards (ISs) (i.e., $^{13}\text{C}_4$ -PFBA, $^{13}\text{C}_2$ -PFHxA, $^{13}\text{C}_4$ -PFOA, $^{13}\text{C}_5$ -PFNA, $^{13}\text{C}_2$ -PFDA, $^{13}\text{C}_2$ -PFUnDA, $^{13}\text{C}_2$ -PFDoDA, $^{18}\text{O}_2$ -PFHxS, $^{13}\text{C}_4$ -PFOS, $^{13}\text{C}_8$ -FOSA, purity >99%, Wellington Laboratories, Guelph, ON) and one recovery standard ($^{13}\text{C}_8$ -PFOA, purity >98%, Wellington Laboratories, Guelph, ON) were included.

2.2. Sample characteristics

A mor layer soil sample with $\text{pH}(\text{H}_2\text{O})$ of 4.8, containing 45% C, 1.3% N and 3.4% ash content on a dry weight (dw) basis, was used for the experiment. The sample (Risbergshöjden Oe) was collected in 2011 from a Spodosol in central Sweden (Risbergshöjden, 59°43'00"N 15°01'59"E), a site dominated by Scots Pine (*Pinus sylvestris*) vegetation. Soil from this site has been used in several previous studies on metal binding to SOM (Gustafsson and van Schaik, 2003; Gustafsson et al., 2007; Gustafsson et al., 2014), and was selected for our experiment as it is representative for northern latitude organic surface horizons, especially for those of coniferous forest. The sample was sieved (<2 mm) prior to homogenization, and then stored at +5 °C in its field-moist state with 69% water content until further use. The geochemically active concentrations of humic and fulvic acid, Al, Ca, Fe, K, Mg, Mn, Cr and Cu were determined by Gustafsson et al. (2014) and are shown in Table S1 in the Supporting Information.

2.3. Sorption batch experiment

Four batch sorption experiments were conducted using 50 mL polypropylene (PP) tubes (Corning®, nonpyrogenic) with 0.45 g sample (dry weight) to which nitrate (NO_3^-) salts of 10 mM Na^+ , 3.0 and 5.0 mM Ca^{2+} or 2.0 mM Al^{3+} were added to obtain environmentally relevant ionic compositions within the range of previous studies (Chen et al., 2009; Higgins and Luthy, 2006). Additional sodium nitrate (NaNO_3) salt was added to the Ca^{2+} and Al^{3+} series to keep the NO_3^- concentration similar (~10 mM) in all series (for details see Table S2, Supporting Information). In addition, each batch experiment was carried out at four different pH values (3, 4, 5 and 6), which were reached using variable volumes of 20 mM nitric

Table 1Target PFASs and field- and laboratory-derived soil/sediment organic carbon-normalized partitioning coefficients (log K_{OC}).

Substance	Acronym	Chemical formula (dissociated)	log K_{OC} [mL g ⁻¹]
Perfluorobutanoate	PFBA	C ₃ F ₇ COO ⁻	1.88 ^f
Perfluoropentanoate	PFPeA	C ₄ F ₉ COO ⁻	1.37 ^f
Perfluorohexanoate	PFHxA	C ₅ F ₁₁ COO ⁻	1.31 ^f , 2.1 ^a
Perfluoroheptanoate	PFHpA	C ₆ F ₁₃ COO ⁻	1.63 ^f , 2.1 ^a
Perfluorooctanoate	PFOA	C ₇ F ₁₅ COO ⁻	1.89–3.5 ^{b,c,d,e,f}
Perfluorononanoate	PFNA	C ₈ F ₁₇ COO ⁻	2.36–4.0 ^{b,d,f}
Perfluorodecanoate	PFDA	C ₉ F ₁₉ COO ⁻	2.96–4.6 ^{b,d,f}
Perfluoroundecanoate	PFUnDA	C ₁₀ F ₂₁ COO ⁻	3.3–5.1 ^{b,d,f}
Perfluorododecanoate	PFDoDA	C ₁₁ F ₂₃ COO ⁻	5.6 ± 0.2 ^a
Perfluorotetradecanoate	PFTeDA	C ₁₃ F ₂₇ COO ⁻	na
Perfluorobutane sulfonate	PFBS	C ₄ F ₉ SO ₃ ⁻	1.22 ^e , 1.79 ^f
Perfluorohexane sulfonate	PFHxS	C ₆ F ₁₃ SO ₃ ⁻	2.05–3.7 ^{a,d,f}
Perfluorooctane sulfonate	PFOS	C ₈ F ₁₇ SO ₃ ⁻	2.6–3.8 ^{a,b,c,d,e,f}
Perfluorooctane sulfonamide	FOSA	C ₈ F ₁₇ SO ₂ NH ₂ ^g	4.2–4.5 ^{c,d}

na = not available.

^a Labadie and Chevreuil (2011).^b Higgins and Luthy (2006).^c Ahrens et al. (2011).^d Ahrens et al. (2010).^e Milinovic et al. (2015).^f Guelfo and Higgins (2013).^g Non-ionic species predominates within the investigated pH range (pK_a = 6.52 (Steinle-Darling and Reinhard, 2008)).

acid (HNO₃) or NaOH. The equilibrium solution chemistries of all soil suspensions were checked to ensure undersaturation with respect to Al(OH)₃ soil phases. The suspensions (40 mL) were spiked with 10 μL of a standard stock mixture of 14 PFASs dissolved in methanol (5 μg mL⁻¹ of each substance), resulting in 111 ng of each substance per gram dry sample. All four samples in the four cation series were prepared in duplicate yielding in total 31 samples after removing one outlier from the subsequent data treatment. A horizontal 1D-shaker (Gerhardt) was used to equilibrate the suspensions for 7 days (168 h), which has been shown to be sufficient to reach equilibrium (Higgins and Luthy, 2006; Ahrens et al., 2011). After 7 days, the samples were centrifuged for 20 min at 3000 rpm, and the pH was measured in the supernatant using a GK2401C combined pH electrode (Radiometer Analytical).

The aqueous phase was analyzed for PFASs using high-performance liquid chromatography coupled to tandem mass spectrometry (HPLC-MS/MS) and the validated method is described elsewhere (Ahrens et al., 2015) and in the Supporting Information. The sorbed amount of each compound was calculated with the method of aqueous loss. Furthermore, all PFAS sorption was attributed to the organic carbon content of the soil (f_{OC} = 45%) and sorption to mineral phases was thus assumed to be negligible.

2.4. Quality assurance and control

The method detection limits (MDLs) ranged from 0.07 ng L⁻¹ (PFHpA, PFDA) to 1.01 ng L⁻¹ (PFHxA) using a signal-to-noise ratio of 3. To minimize contamination, no fluorinated material (e.g. tetrafluoroethylene) was used in the experiments. All PFASs in the negative blank samples ($n = 2$) were below the respective MDLs. The recovery of the ISs (mean ± standard deviation) was on average 89 ± 12% and the relative errors between duplicates were generally <20%. Positive control blanks were prepared in duplicate using similar pH values, background ionic strength (10 mM NaNO₃) and dissolved organic carbon (DOC) levels (DOC from the same soil sample as used throughout the study) as obtained in the main sorption experiment. With the exception of the C₈–C₁₁ and C₁₃ PFCAs, recoveries in the positive control blanks ranged from 79% (PFBS) to 103% (PFHxA, PFOA), on average, where a recovery of 100%

corresponded to a reference spike in Milli-Q water ($n = 2$) (Table S4 in the Supporting Information). As for the C₈–C₁₁ PFCAs, average positive blank recoveries were higher than 100%, i.e. 130% (PFNA)–166% (PFDA), which is likely attributed to smaller losses to PP tube walls in the DOC-containing blanks as compared to the reference spikes prepared with only Milli-Q water. As for the most long-chained PFAS (i.e. C₁₃ PFTeDA) however, blank recoveries were low (on average, 15%), most likely due to analytical uncertainties. Applying a three-compartment equilibrium mass-balance (soil–water–PP tube) on the basis of the positive DOC-containing blanks indicated nevertheless that PP tube losses should not have influenced the results for PFTeDA in the sorption experiment to any significant extent, nor the results for any of the other compounds (data not shown). Thus, losses to PP tubes were assumed to be negligible in the sorption experiment.

2.5. Modeling of organic matter bulk net charge

Visual MINTEQ ver. 3.1 (Gustafsson, 2013), with the Stockholm Humic Model (SHM) (Gustafsson, 2001), was used to model the bulk net charge of SOM (Z⁻, mmol_c L⁻¹) in the sorption experiment. Good performance of SHM for cation sorption has been demonstrated in previous modeling studies for soil from the same area (e.g. Gustafsson et al., 2014). A basic model assumption is that the sum of humic and fulvic acid constitute the proton and metal binding component of SOM, thus any contribution from the humin fraction is not explicitly accounted for. Thus, the bulk net charge of SOM is a function of the cation concentrations, solution pH, and the fraction of active humic and fulvic acid (Tipping and Woolf, 1991; Löfgren et al., 2010). As an example, the net charge Z⁻ of humic and fulvic acids in a system with Ca²⁺ and Al³⁺ can be obtained from Eq. (1)

$$[Z^-] = [RO^-] - [ROCa^+] - [(RO)_2Al^+] \quad (1)$$

where RO⁻ is a deprotonated functional group (mainly carboxylic or phenolic), ROCa⁺ represents a Ca²⁺ ion monodentately complexed by one functional group and (RO)₂Al⁺ represents bidentate binding of an Al³⁺ ion by two functional groups. If additional cations are present, the surface net charge is still given as the sum of

charge contributions from various species of SOM. Detailed information on the assumed complex configurations in the Stockholm Humic Model is discussed elsewhere (Gustafsson, 2001; Gustafsson and Kleja, 2005). Since $[RO^-]$ is usually greater than the sum of positive charge contributions, $[Z^-]$ will be a positive number as seen from Eq. (1). This number is henceforth referred to as the net (negative) charge.

The input to Visual MINTEQ was given as the geochemically active concentrations (Table S1 in the Supporting Information) (Gustafsson et al., 2014) along with measured pH, DOC and added concentrations of cations and NO_3^- , and simulated equilibrium concentrations of solid-phase organic complexes were obtained as output. Visual MINTEQ input and output data (Table S3 in the Supporting Information) along with modeling assumptions are described in the Supporting Information.

3. Results and discussion

3.1. Solid–liquid partitioning

Increasing binding strength with increasing perfluorocarbon chain length was observed for both PFASs (C_4 , C_6 and C_8) and PFCAs (C_3 – C_{10}) (Figs. 1 and 2, Table 1) when accounting for the effect of pH and net charge on sorption. For the PFASs and PFCAs, the increase in $\log K_{OC}$ per additional CF_2 moiety were 0.83 and 0.60 log units, respectively. Short-chained PFASs such as PFBA, PFPeA and PFBS were weakly sorbed (less than 10% on average), whereas long-chained PFASs (PFOS, FOSA, C_9 – C_{11} and C_{13} PFCAs) were sorbed strongly (on average, 99–100%). The increased sorption with increased PFCA chain length is in agreement with previous results of Ahrens et al. (2010) and Higgins and Luthy (2006), who found suspended particulate matter and sediment partitioning coefficients to increase with 0.50–0.75 log units per CF_2 moiety. For the PFASs, however, previous studies found an increase of 0.40–0.60 log units per CF_2 moiety, which is lower as compared to this study (Milinovic et al., 2015; Higgins and Luthy, 2006). The increased sorption upon increasing chain length is attributed to an increase in PFAS hydrophobicity with each CF_2 moiety. For the most long-chained PFASs (i.e. PFDoDA and PFTeDA), however, no increased sorption was observed upon increasing perfluorocarbon chain length (Fig. 2), which is in agreement with what was observed by Zhang et al. (2013). This observation might be explained by possible strong binding of the most long-chained PFCAs to DOC, which would decrease their observed K_{OC} values. Such an effect of DOC on sorption has for example been shown by Enell et al. (2016) with regard to high-molecular polycyclic aromatic compounds (PACs). Alternatively, the more or less equal average sorption among the C_9 – C_{11} and C_{13} PFCAs could be attributed to steric hindrances originating from the increased rigidity reported for PFCA perfluorocarbon chains longer than C_{10} (Ellis et al., 2004).

PFASs of a given perfluorocarbon chain length were sorbed more strongly than the corresponding PFCAs, with the exception of the analogs PFPeA and PFBS (Fig. 2), meaning that the presence of a sulfonate functional head group led to stronger sorption (by 0.72 log units, on average) than the presence of a carboxylic head group. This is in agreement with what was found in earlier research (Higgins and Luthy, 2006; Ahrens et al., 2009, 2010). Furthermore, the presence of an uncharged sulfonamide head group appeared to favor sorption, as FOSA was sorbed more strongly than its anionic analogs PFNA and PFOS, by, on average, 1.91 and 0.53 log units, respectively. This agrees with the order of sediment sorption observed by Ahrens et al. (2010, 2011).

3.2. Impact of pH and cations on sorption

Sorption increased with decreasing pH ($p < 0.05$) for 10 of 14 PFASs, i.e. for PFHxA, PFHpA, PFOA, PFNA, PFDA, PFUnDA, PFDoDA, PFTeDA, FOSA and PFOS (Fig. 1). For these 10 PFASs, the mean decrease in $\log K_{OC}$ value per unit pH ($\Delta \log K_{OC}/\Delta pH$) was 0.32 ± 0.11 log units (Fig. S4a and Table S7 in the Supporting Information), which again is similar to that of 0.37 log units found by Higgins and Luthy (2006). Furthermore, the regressed $\log K_{OC}$ –pH slopes became somewhat steeper with increasing perfluorocarbon chain length and were calculated to decrease 0.04 log units per unit pH per CF_2 moiety ($p < 0.05$) (Fig. S4a, Supporting Information). Within the PFCA class, the Pearson r^2 values for the $\log K_{OC}$ –pH relationship increased consistently with perfluorocarbon chain length from C_3 PFBA ($r^2 = 0$) to C_8 PFNA ($r^2 = 0.68$). After a lower r^2 value for C_9 PFDA ($r^2 = 0.44$) the r^2 values for the C_{10} – C_{11} and C_{13} PFCAs were again higher ($r^2 = 0.76$ – 0.83) (Fig. 4). As for the PFASs, however, sorption was poorly predicted by the pH value (Fig. 1, Fig. S3 and Table S8 in the Supporting Information).

For PFASs with intermediate chain length (i.e. C_5 – C_8 PFCAs and PFHxS) the $\log K_{OC}$ increased with the addition of cations to the soil in the following order: Al^{3+} (2 mM) > Ca^{2+} (5 mM) > Ca^{2+} (3 mM) = Na^+ (10 mM) (paired Student's t -test, Fig. 1, Table S9 in the Supporting Information). Moreover, for the C_5 – C_8 PFCAs, the effects on sorption due to different cation treatments were more pronounced at higher pH as compared to lower pH values. These effects are consistent with the observations of Higgins and Luthy (2006) and Zhang et al. (2013) (effect of $Ca^{2+} > Na^+$), and Wang et al. (2015) ($Al^{3+} > Ca^{2+} > Na^+$). Except for stronger sorption in the Al^{3+} treatment, there was no clear effect of either the pH value or added cations for two of the three shortest PFASs, i.e. PFBA (C_3) and PFBS (C_4). By contrast, for the most long-chained PFASs (i.e. C_9 – C_{11} and C_{13} PFCAs, PFOS and FOSA), there were few statistically significant effects of the added cations on the observed sorption (Table S9, Supporting Information). In other words, the strong effects of added cations that were seen for the PFASs of intermediate length were not seen for the substances with the longest chain lengths.

3.3. Impact of modeled SOM bulk net charge on sorption

The calculated SOM bulk net charge increased with increasing pH (Fig. 3), with the largest relative increase for the Na^+ (10 mM) treatment and the smallest for the Ca^{2+} (5 mM) treatment, while the Ca^{2+} (3 mM) treatment showed intermediate behavior. The Al^{3+} (2 mM) treatment yielded the lowest bulk net charge at pH < 5 due to strong complexation with humic and fulvic acid.

For 11 of the 14 investigated PFASs (i.e. PFHxA, PFHpA, PFOA, PFNA, PFDA, PFUnDA, PFDoDA, PFTeDA, FOSA, PFHxS and PFOS) sorption increased with decreased SOM net negative charge ($p < 0.05$) (Fig. 1), with a mean decrease of 1.41 ± 0.40 log units for $\log K_{OC}$ per log unit $mole_c g^{-1}$ (Fig. S4b and Table S8 in the Supporting Information). For the three most short-chained PFASs (i.e. PFBA, PFPeA and PFBS), however, no significant relationship was found (Fig. 1). For PFHxS, addition of Al^{3+} resulted in an increase of sorption of ≥ 1 log unit as compared to the other cation treatments (Fig. 1), which was larger than expected with respect to the simulated net charge (Fig. 1). The reason for this is not known. For example, it is not likely that sorption increased as a result of Al^{3+} bridging between the sulfonate head group and the sorbent, due to the significant electron-withdrawing properties (low nucleophilicity) of organofluorine sulfonate groups (Lawrance, 1986).

The relationship between PFAS sorption and the SOM bulk net charge can be compared to the relationship with the pH value (Fig. 4, Fig. S3 in the Supporting Information). For short-chained

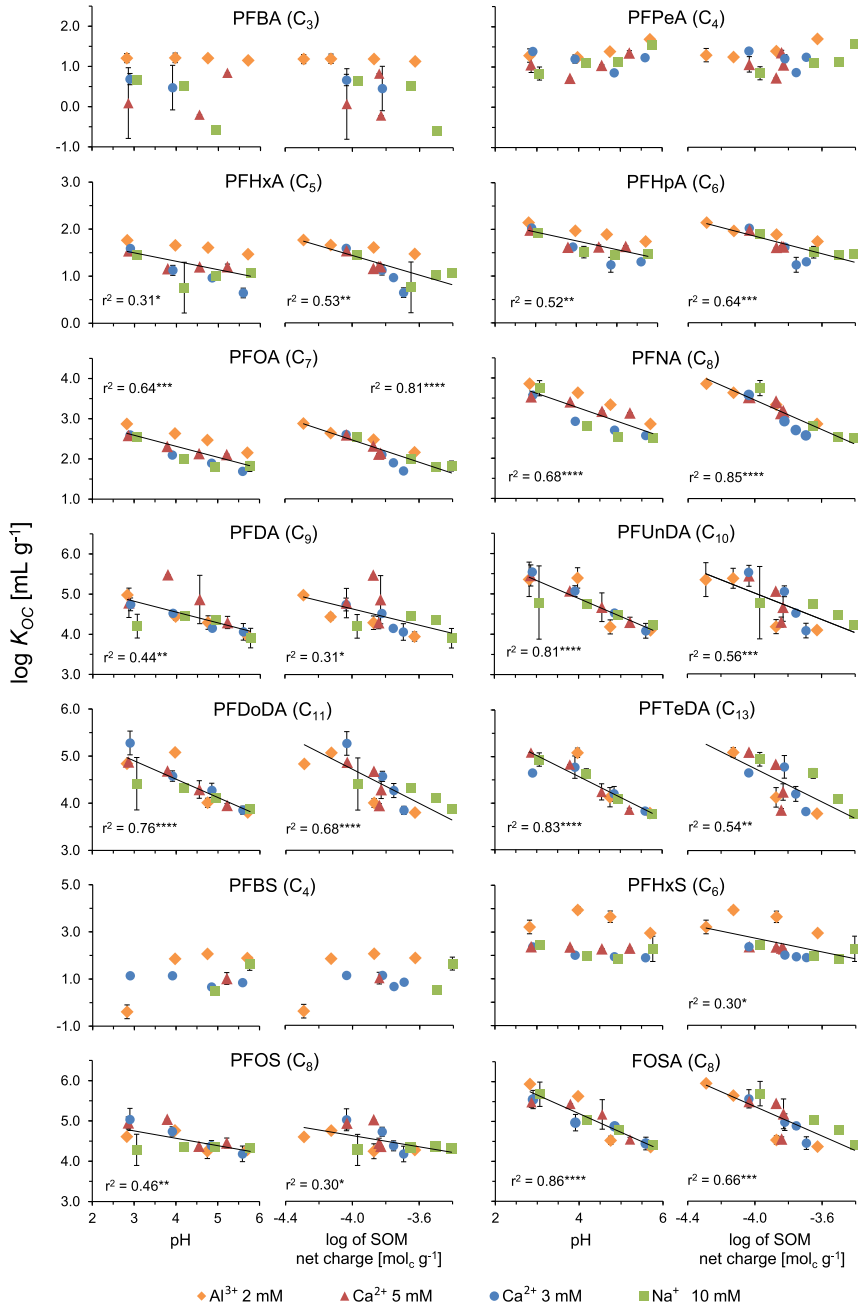


Fig. 1. Effect of pH and simulated SOM bulk net charge on $\log K_{OC}$ for the 14 target PFASs in the treatments with Al³⁺ (2 mM), Ca²⁺ (5 mM), Ca²⁺ (3 mM) and Na⁺ (10 mM) in the soil sorption experiment. Each data point represents the average of duplicates. $\log K_{OC}$ values of 0, 1, 2, 3, 4 and 5 correspond to sorbed fractions of 0.5, 4.5, 33.1, 83.6, 98.1 and 99.8%, respectively. * $p \leq 0.5$, ** $p \leq 0.01$, *** $p \leq 0.001$, **** $p \leq 0.0001$.

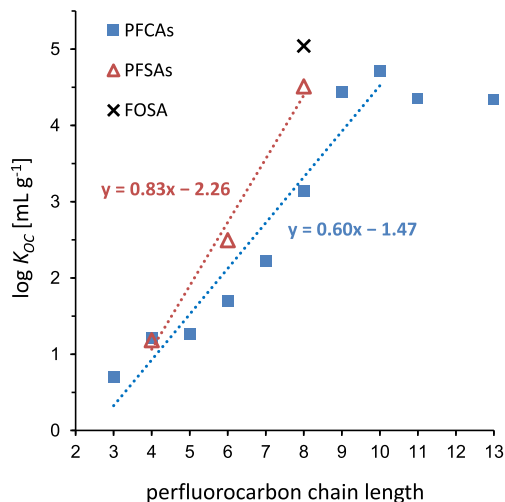


Fig. 2. Relationship between $\log K_{OC}$ [mL g^{-1}] and perfluorocarbon chain length for C_3 – C_{10} PFCAs ($p \leq 0.05$), FOSA, and C_4 , C_6 and C_8 PFSA ($p \leq 0.05$) in the sorption experiment. Each data point represents the average $\log K_{OC}$ ($n = 31$). PFDoDA (C_{11}) and PFTEDA (C_{13}) were excluded from the PFCA regression fit.

PFASs (with the exception of PFPeA), and also for C_7 – C_8 PFCAs and PFHxS, the relationship with the SOM bulk net charge was stronger and provides a better basis for a model able to predict the effects of both pH and cations on PFAS sorption. For the sorption of the most long-chained PFASs, however (i.e. C_9 – C_{11} and C_{13} PFCAs, PFOS and FOSA), the relationship with the SOM bulk net charge was weaker than that with pH alone. This reflects the fact that the added

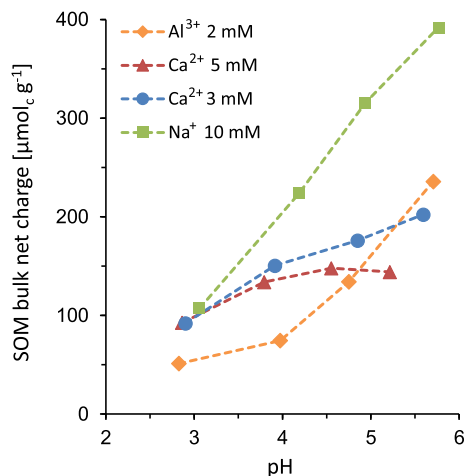


Fig. 3. Calculated SOM bulk net charge as a function of pH and cation treatment in the sorption experiment. Stated cation concentrations are additions of the respective nitrate (NO_3^-) salts. Dashed lines connect the points and are included for clarity.

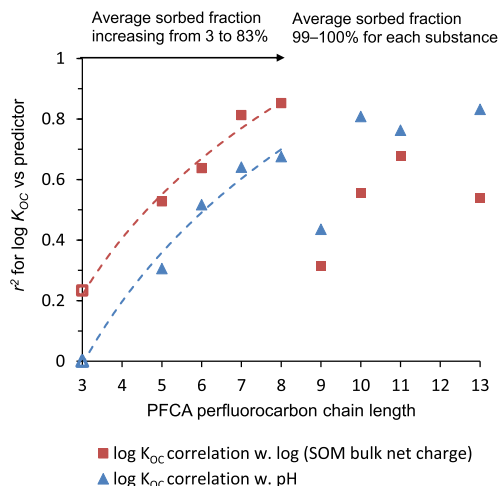


Fig. 4. The Pearson r^2 value for SOM bulk net charge vs. $\log K_{OC}$ and pH vs. $\log K_{OC}$ as influenced by the PFCA perfluorocarbon chain length (C_4 PFPeA excluded). Closed markers represent significant correlations ($p \leq 0.05$) and open markers non-significant relationships ($p > 0.05$).

cations, even though they influenced the SOM bulk net charge as a consequence of their binding, did not alter the PFAS sorption to any large extent. Our hypothesis that the SOM bulk net charge would be a better sorption predictor than pH was thus verified for C_3 and C_5 – C_8 PFCAs and PFHxS, whereas the pH value alone was observed to be the better sorption predictor for C_9 – C_{11} and C_{13} PFCAs, PFOS and FOSA (Fig. 4, Fig. S3 in the Supporting Information). As regards the PFASs for which sorption was better predicted by the SOM bulk net charge, the sorbed fractions ranged, on average, from 3% (PFBA) to 83% (PFNA), whereas for those PFASs for which sorption was better predicted by the pH value alone, sorption ranged, on average, between 99% and 100%.

For the most long-chained PFASs, the observation that pH alone was a better predictor of sorption than the SOM bulk net charge suggests that these PFASs may have had a high affinity for a SOM fraction that did not bind cations such as Ca^{2+} and Al^{3+} to any larger extent, although it possessed pH-dependent charge. A likely candidate is the humin fraction, which is known to be the most important SOM fraction for the sorption of other hydrophobic organic compounds (Gunasekara and Xing, 2003) including PFOS (Zhang et al., 2015). At low pH the degree of dissociation and the number of weak acids of humin is quite small compared to that of HA and FA (López et al., 2012; Cooke et al., 2008; Chang et al., 2014). This explains why a model for SOM bulk net charge, with parameters derived for only HA and FA, may be able to describe the acid-base characteristics of organic soils, including the soil used here, reasonably well as long as low pH is maintained (Gustafsson et al., 2014; Gustafsson and Kleja, 2005; Cooke et al., 2008). It may be hypothesized that the low net charge under low-pH conditions makes the humin fraction a relatively poor sorbent for cations as compared to HA and FA. Thus, the ability of humin to bind HOCs would remain largely unaltered upon cation additions, in accordance with what was observed for the most long-chained PFASs. The high sorption capacity of humin towards HOCs is attributed to its highly condensed aliphatic and aromatic domains (Gunasekara

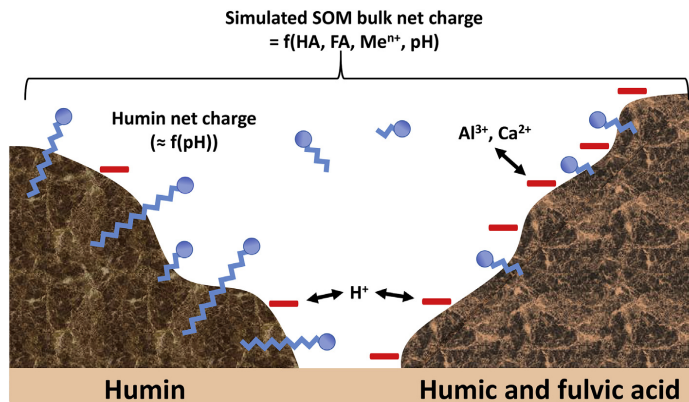


Fig. 5. Conceptual model for the observed PFAS SOM sorption, in which the PFASs (i.e. C₉–C₁₁ and C₁₃ PFCAs, PFOS and FOSA) with a strong SOM sorption ($\geq 99\%$) are preferentially bound to the humin fraction, whereas the PFASs (i.e. C₃ and C₅–C₈ PFCAs and PFHxS) with a weaker SOM sorption are hypothesized to also bind to humic and fulvic acid.

and Xing, 2003; Chen et al., 2007), and thus it is suggested that these domains also bind the longer-chained, relatively more hydrophobic, PFASs.

3.4. Conceptual model

The results shown in Figs. 1 and 4 suggest that the interaction mechanisms between PFASs and SOM may be different depending on PFAS chain length, as conceptually described in Fig. 5. For the majority of the long-chain PFASs (i.e. C₉–C₁₁ and C₁₃ PFCAs, PFOS and FOSA), the pH-dependent sorption in combination with the small effect of cations other than H⁺, suggests that the mechanism is similar to that of other hydrophobic organic compounds, i.e. these PFASs interact preferentially with the most highly condensed domains of the humin fraction, which carry a relatively low – although pH-dependent – net charge and do not bind other cations to any large extent. The extent of sorption of the most long-chained PFASs is poorly predicted by the SOM bulk net charge, simply because the latter does not provide a good representation of the net charge of the highly condensed humin fraction. It can be hypothesized that the most long-chained PFASs may penetrate (limited penetration, as suggested by Higgins and Luthy (2007), or full absorption) into the bulk solid organic phase of the humin fraction. For PFASs of shorter chain length (i.e. C₃ and C₅–C₈ PFCAs and PFHxS), penetration into the condensed domains may be less efficient due to the charge of the head group. This makes preferential sorption to the humin fraction less likely, and instead these PFASs may bind to HAs and FAs as well. This, however, makes sorption increasingly dependent on the sorption of cations such as Ca²⁺ and Al³⁺, as they interact more strongly with HA and FA, causing a reduction in the SOM net charge, which in turn favors PFAS sorption.

HOCs preferentially sorbed to SOM humin-like fractions may be expected to exhibit sorption isotherms with a higher degree of nonlinearity as compared to compounds bound to less condensed, humic-type, carbon domains, and in addition their sorption may be less reversible (with pronounced sorption–desorption hysteresis) (Huang et al., 1997). Such sorption/desorption behavior has been observed for PFOS in previous studies (Wei et al., 2017; Qian et al., 2017; Milinovic et al., 2015) which may further support the suggestion of preferential PFOS binding to the humin fraction (c.f.

Zhang et al., 2015). However, for PFOA, sorption isotherms are linear and the sorption more reversible as compared to that of PFOS (Miao et al., 2017; Milinovic et al., 2015). This may, in agreement with the conceptual model presented here, suggest that PFOA does not exhibit the same preferential affinity for humin and may also bind to humic and fulvic acid.

4. Conclusions

In this study we investigated the effect of the solution pH and SOM bulk net charge on PFAS sorption to an organic soil. The sorption was inversely related to both pH and to SOM bulk net charge, with SOM bulk net charge being more important for mainly short-chained PFASs, while the pH value alone was more important for the majority of the long-chained PFASs since cations had less effect on sorption for the latter group. This suggests that many long-chained PFASs are preferentially bound to the humin fraction of SOM, whereas shorter PFASs may also bind to the humic and fulvic acids. To further explore the role of humin for PFAS sorption to SOM, more knowledge on humin surface chemistry is essential. Of particular importance would be the development of a geochemical surface complexation model with the ability to simulate the acid-base and cation binding characteristics of humin.

Acknowledgements

This research was funded by the Swedish Research Council (grant number 2015-03938). We thank Vera Franke for assistance with parts of the sample analysis, and Lisa Vogel for assisting with the solid-phase extraction procedure.

Appendix A. Supplementary data

Supplementary data related to this article can be found at <https://doi.org/10.1016/j.chemosphere.2018.05.012>.

References

- Ahrens, L., 2011. Polyfluoroalkyl compounds in the aquatic environment: a review of their occurrence and fate. *J. Environ. Monit.* 13, 20–31. <https://doi.org/10.1039/c0em00373e>.
- Ahrens, L., Norström, K., Viktor, T., Palm Cousins, A., Josefsson, S., 2015. Stockholm

- Arlanda Airport as a source of per- and polyfluoroalkyl substances to water, sediment and fish. *Chemosphere* 129, 33–38. <https://doi.org/10.1016/j.chemosphere.2014.03.136>.
- Ahrens, L., Taniyasu, S., Yeung, L.W., Yamashita, N., Lam, P.K., Ebinghaus, R., 2010. Distribution of polyfluoroalkyl compounds in water, suspended particulate matter and sediment from Tokyo Bay, Japan. *Chemosphere* 79 (3), 266–272. <https://doi.org/10.1016/j.chemosphere.2010.01.045>.
- Ahrens, L., Yamashita, N., Yeung, L.W.Y., Taniyasu, S., Horii, Y., Lam, P.K.S., Ebinghaus, R., 2009. Partitioning behavior of per- and polyfluoroalkyl compounds between pore water and sediment in two sediment cores from Tokyo Bay, Jpn. *Environ. Sci. Technol.* 43 (18), 6969–6975. <https://doi.org/10.1021/es901213s>.
- Ahrens, L., Yeung, L.W.Y., Taniyasu, S., Lam, P.K.S., Yamashita, N., 2011. Partitioning of perfluorooctanoate (PFOA), perfluorooctane sulfonate (PFOS) and perfluorooctane sulfonamide (PFOSA) between water and sediment. *Chemosphere* 85 (5), 731–737. <https://doi.org/10.1016/j.chemosphere.2011.06.046>.
- Apelberg, B.J., Witter, F.R., Herbstman, J.B., Calafat, A.M., Halden, R.U., Needham, L.L., Goldman, L.R., 2007. Cord serum concentrations of perfluorooctane sulfonate (PFOS) and perfluorooctanoate (PFOA) in relation to weight and size at birth. *Environ. Health Perspect.* 115 (11), 1670–1676. <https://doi.org/10.1289/ehp.10334>.
- Barzen-Hanson, K.A., Davis, S.E., Kleber, M., Field, J.A., 2017. Sorption of fluorotelomer sulfonates, fluorotelomer sulfonamideobetaines, and a fluorotelomer sulfonamide amine in national foam aqueous film-forming foam to soil. *Environ. Sci. Technol.* 51 (21), 12394–12404. <https://doi.org/10.1021/acs.est.7b03452>.
- Chang, R.R., Mylotte, R., Hayes, M.H.B., McInerney, R., Tzou, Y.M., 2014. A comparison of the compositional differences between humic fractions isolated by the IHSS and exhaustive extraction procedures. *Naturwissenschaften* 101 (3), 197–209. <https://doi.org/10.1007/s00114-013-1140-4>.
- Chen, D., Xing, B., Xie, W., 2007. Sorption of phenanthrene, naphthalene and o-xylene by soil organic matter fractions. *Geoderma* 139 (3–4), 329–335. <https://doi.org/10.1016/j.geoderma.2007.02.011>.
- Chen, H., Chen, S., Quan, X., Zhao, Y., Zhao, H., 2009. Sorption of perfluorooctane sulfonate (PFOS) on oil and oil-derived black carbon: influence of solution pH and $[Ca^{2+}]$. *Chemosphere* 77 (10), 1406–1411. <https://doi.org/10.1016/j.chemosphere.2009.09.008>.
- Chen, W., Wang, H., Gao, Q., Chen, Y., Li, S., Yang, Y., Werner, D., Tao, S., Wang, X., 2017. Association of 16 priority polycyclic aromatic hydrocarbons with humic acid and humin fractions in a peat soil and implications for their long-term retention. *Environ. Pollut.* 230, 882–890. <https://doi.org/10.1016/j.envpol.2017.07.038>.
- Conder, J.M., Hoke, R.A., De Wolf, W., Russel, M.H., Buck, R.C., 2008. Are PFCA's bioaccumulative? A critical review and comparison with regulatory criteria and persistent lipophilic compounds. *Environ. Sci. Technol.* 42, 995–1003. <https://doi.org/10.1021/es070895g>.
- Cooke, J.D., Tipping, E., Hamilton-Taylor, J., 2008. Proton interactions with soil organic matter: the importance of aggregation and the weak acids of humin. *Eur. J. Soil Sci.* 59 (6), 1111–1121. <https://doi.org/10.1111/j.1365-2389.2008.01071.x>.
- Cousins, I.T., Vestergren, R., Wang, Z., Scheringer, M., McLachlan, M.S., 2016. The precautionary principle and chemicals management: the example of perfluoroalkyl acids in groundwater. *Environ. Int.* 94, 331–340. <https://doi.org/10.1016/j.envint.2016.04.044>.
- Ellis, D.A., Denkenberger, K.A., Burrow, T.E., Mabury, S.A., 2004. The use of ^{19}F NMR to interpret the structural properties of perfluorocarboxylate acids: a possible correlation with their environmental disposition. *J. Phys. Chem. A* 108 (46), 10099–10106. <https://doi.org/10.1021/jp049372a>.
- Enell, A., Lundstedt, S., Arp, H.P.H., Josefsson, S., Cornelissen, G., Wik, O., Kleja, D.B., 2016. Combining leaching and passive sampling to measure the mobility and distribution between porewater, DOC, and colloids of native oxy-PAHs, N-PAHs, and PAHs in historically contaminated soil. *Environ. Sci. Technol.* 50 (21), 11797–11805. <https://doi.org/10.1021/acs.est.6b02774>.
- Giesy, J.P., Kannan, K., 2001. Global distribution of perfluorooctane sulfonate in wildlife. *Environ. Sci. Technol.* 35 (7), 1339–1342. <https://doi.org/10.1021/es001834k>.
- Giesy, J.P., Nalje, J.E., Khim, J.S., Jones, K.C., Newsted, J.L., 2010. Aquatic toxicology of perfluorinated chemicals. *Rev. Environ. Contam. Toxicol.* 202, 1–52. https://doi.org/10.1007/978-1-4419-1157-5_1.
- Goss, K.-U., Bronner, G., 2006. What is so special about the sorption behavior of highly fluorinated compounds? *J. Phys. Chem. A* 110 (30), 9518–9522. <https://doi.org/10.1021/jp062684a>.
- Gueffo, J.L., Higgins, C.P., 2013. Subsurface transport potential of perfluoroalkyl acids at aqueous film-forming foam (AFFF)-impacted sites. *Environ. Sci. Technol.* 47 (9), 4164–4171. <https://doi.org/10.1021/es3048043>.
- Gunasekara, A.S., Xing, B., 2003. Sorption and desorption of naphthalene by soil organic matter: importance of aromatic and aliphatic components. *J. Environ. Qual.* 32 (1), 240–246. <https://doi.org/10.2134/jeq2003.2400>.
- Gustafsson, J.P., 2001. Modeling the acid–base properties and metal complexation of humic substances with the Stockholm humic model. *J. Colloid Interface Sci.* 244 (1), 102–112. <https://doi.org/10.1006/jcis.2001.7871>.
- Gustafsson, J.P., 2013. Visual MINTEO – a free equilibrium speciation model [Internet document]. KTH Vis. MINTEQ. URL: <http://vminetq.lwr.kth.se/>. (Accessed 8 June 2015). Version 3.1. Compiled in Visual Basic 2012, 2013.
- Gustafsson, J.P., Kleja, D.B., 2005. Modeling salt-dependent proton binding by organic soils with the NICA–Donnan and Stockholm Humic models. *Environ. Sci. Technol.* 39 (14), 5372–5377. <https://doi.org/10.1021/es050333z>.
- Gustafsson, J.P., Persson, I., Kleja, D.B., van Schaik, J.W.J., 2007. Binding of iron(III) to organic soils: EXAFS spectroscopy and chemical equilibrium modeling. *Environ. Sci. Technol.* 41 (4), 1232–1237. <https://doi.org/10.1021/es0615730>.
- Gustafsson, J.P., Persson, I., Oromieh, A.G., van Schaik, J.W.J., Sjöstedt, C., Kleja, D.B., 2014. Chromium(III) complexation to natural organic matter: mechanisms and modeling. *Environ. Sci. Technol.* 48 (3), 1753–1761. <https://doi.org/10.1021/es404557e>.
- Gustafsson, J.P., van Schaik, J.W.J., 2003. Cation binding in a mor layer: batch experiments and modelling. *Eur. J. Soil Sci.* 54 (2), 295–310. <https://doi.org/10.1046/j.1365-2389.2003.00526.x>.
- Han, W., Luo, L., Zhang, S., 2013. Adsorption of tetrabromobisphenol A on soils: contribution of soil components and influence of soil properties. *Colloids Surf. A Physicochem. Eng. Asp.* 428, 60–64. <https://doi.org/10.1016/j.colsurfa.2013.03.040>.
- Higgins, C.P., Luthy, R.G., 2006. Sorption of perfluorinated surfactants on sediments. *Environ. Sci. Technol.* 40 (23), 7251–7256. <https://doi.org/10.1021/es061000n>.
- Higgins, C.P., Luthy, R.G., 2007. Modeling sorption of anionic surfactants onto sediment materials: an a priori approach for perfluoroalkyl surfactants and linear alkylbenzene sulfonates. *Environ. Sci. Technol.* 41 (9), 3254–3261. <https://doi.org/10.1021/es062449j>.
- Houtz, E.F., Higgins, C.P., Field, J.A., Sedlak, D.L., 2013. Persistence of perfluoroalkyl acid precursors in AFFF-impacted groundwater and soil. *Environ. Sci. Technol.* 47 (15), 8187–8195. <https://doi.org/10.1021/es4018877>.
- Huang, W., Young, T.M., Schlautman, M.A., Yu, H., Weber, W.J., 1997. A distributed reactivity model for sorption by soils and sediments. 9. General isotherm nonlinearity and applicability of the dual reactive domain model. *Environ. Sci. Technol.* 31 (6), 1703–1710. <https://doi.org/10.1021/es960677f>.
- Jafvert, C.T., 1990. Sorption of organic acid compounds to sediments: initial model development. *Environ. Toxicol. Chem.* 9 (10), 1259–1268. <https://doi.org/10.1002/etc.5620091004>.
- Kang, S., Xing, B., 2005. Phenanthrene sorption to sequentially extracted soil humic acids and humins. *Environ. Sci. Technol.* 39 (1), 134–140. <https://doi.org/10.1021/es0490828>.
- Kinniburgh, D.G., van Riemsdijk, W.H., Koopal, L.K., Borkovec, M., Benedetti, M.F., Avena, M.J., 1999. Ion binding to natural organic matter: competition, heterogeneity, stoichiometry and thermodynamic consistency. *Colloids Surf. A Physicochem. Eng. Asp.* 151 (1–2), 147–166. [https://doi.org/10.1016/S0927-7757\(98\)00637-2](https://doi.org/10.1016/S0927-7757(98)00637-2).
- Kohl, S.D., Rice, J.A., 1998. The binding of contaminants to humin: a mass balance. *Chemosphere* 36 (2), 251–261. [https://doi.org/10.1016/S0045-6535\(97\)10005-4](https://doi.org/10.1016/S0045-6535(97)10005-4).
- Labadie, P., Chevreuil, M., 2011. Partitioning behaviour of perfluorinated alkyl contaminants between water, sediment and fish in the Orge River (nearby Paris, France). *Environ. Pollut.* 159 (2), 391–397. <https://doi.org/10.1016/j.envpol.2010.10.039>.
- Lawrance, G.A., 1986. Coordinated trifluoromethanesulfonate and fluorosulfate. *Chem. Rev.* 86 (1), 17–33. <https://doi.org/10.1021/cr00071a002>.
- Li, Y., Oliver, D.P., Kookana, R.S., 2018. A critical analysis of published data to discern the role of soil and sediment properties in determining sorption of per- and polyfluoroalkyl substances (PFASs). *Sci. Total Environ.* 628–629, 110–120. <https://doi.org/10.1016/j.scitotenv.2018.01.167>.
- López, R., Gondar, D., Antelo, J., Fiol, S., Arce, F., 2012. Study of the acid-base properties of a peat soil and its humin and humic acid fractions. *Eur. J. Soil Sci.* 63 (4), 487–494. <https://doi.org/10.1111/j.1365-2389.2012.01461.x>.
- Löfgren, S., Gustafsson, J.P., Bringmark, L., 2010. Decreasing DOC trends in soil solution along the hillslopes at two IM sites in southern Sweden – geochemical modeling of organic matter solubility during acidification recovery. *Sci. Total Environ.* 409 (1), 201–210. <https://doi.org/10.1016/j.scitotenv.2010.09.023>.
- Milunovic, J., Lacorte, S., Vidal, M., Rigol, A., 2015. Sorption behaviour of perfluoroalkyl substances in soils. *Sci. Total Environ.* 511, 63–71. <https://doi.org/10.1016/j.scitotenv.2014.12.017>.
- Miao, Y., Guo, X., Peng, D., Fan, T., Yang, C., 2017. Rates and equilibria of perfluorooctanoate (PFOA) sorption on soils from different regions of China. *Eco-toxicol. Environ. Saf.* 139, 102–108. <https://doi.org/10.1016/j.ecoenv.2017.01.022>.
- Qian, J., Shen, M., Wang, P., Wang, C., Hou, J., Ao, Y., Liu, J., Li, K., 2017. Adsorption of perfluorooctane sulfonate on soils: effects of soil characteristics and phosphate competition. *Chemosphere* 168, 1383–1388. <https://doi.org/10.1016/j.chemosphere.2016.11.114>.
- Steinle-Darling, E., Reinhard, M., 2008. Nanofiltration for trace organic contaminant removal: structure, solution, and membrane fouling effects on the rejection of perfluorochemicals. *Environ. Sci. Technol.* 42 (14), 5292–5297. <https://doi.org/10.1021/es703207s>.
- Tipping, E., Woolf, C., 1991. The distribution of humic substances between the solid and aqueous phases of acid organic soils: a description based on humic heterogeneity and charge-dependent sorption equilibria. *Eur. J. Soil Sci.* 42 (3), 437–448. <https://doi.org/10.1111/j.1365-2389.1991.tb00421.x>.
- Wang, F., Shih, K., Ma, R., Li, X.Y., 2015. Influence of cations on the partition behavior of perfluorooctanoate (PFHpA) and perfluorohexanesulfonate (PFHxS) on wastewater sludge. *Chemosphere* 131, 178–183. <https://doi.org/10.1016/j.chemosphere.2015.03.024>.
- Wei, C., Song, X., Wang, Q., Hu, Z., 2017. Sorption kinetics, isotherms and mechanisms of PFOS on soils with different physicochemical properties. *Ecotoxicol. Environ. Saf.* 142, 40–50. <https://doi.org/10.1016/j.ecoenv.2017.03.040>.

- Yeung, L.W.Y., So, M.K., Jiang, G., Taniyasu, S., Yamashita, N., Song, M., Wu, Y., Li, J., Giesy, J.P., Guruge, K.S., Lam, P.K.S., 2006. Perfluorooctanesulfonate and related fluorochemicals in human blood samples from China. *Environ. Sci. Technol.* 40, 715–720. <https://doi.org/10.1021/es052067y>.
- Zareitalabad, P., Siemens, J., Hamer, M., Amelung, W., 2013. Perfluorooctanoic acid (PFOA) and perfluorooctanesulfonic acid (PFOS) in surface waters, sediments, soils and wastewater – a review on concentrations and distribution coefficients. *Chemosphere* 91, 725–732. <https://doi.org/10.1016/j.chemosphere.2013.02.024>.
- Zhang, C., Yan, H., Li, F., Hu, X., Zhou, Q., 2013. Sorption of short- and long-chain perfluoroalkyl surfactants on sewage sludges. *J. Hazard Mater.* 260, 689–699. <https://doi.org/10.1016/j.jhazmat.2013.06.022>.
- Zhang, R., Yan, W., Jing, C., 2015. Experimental and molecular dynamic simulation study of perfluorooctane sulfonate adsorption on soil and sediment components. *J. Environ. Sci.* 29, 131–138. <https://doi.org/10.1016/j.jes.2014.11.001>.
- Zhao, L., Zhang, Y., Fang, S., Zhu, L., Liu, Z., 2014. Comparative sorption and desorption behaviors of PFHxS and PFOS on sequentially extracted humic substances. *J. Environ. Sci.* 26 (12), 2517–2525. <https://doi.org/10.1016/j.jes.2014.04.009>.

Sorption of perfluoroalkyl substances (PFASs) to an organic soil horizon – effect of cation composition and pH

Hugo Campos Pereira^{a,*}, Malin Ullberg^a, Dan Berggren Kleja^{a,c}, Jon Petter Gustafsson^{a,d},
Lutz Ahrens^b

^aDepartment of Soil and Environment, Swedish University of Agricultural Sciences, Box 7014, SE-75007 Uppsala, Sweden

^bDepartment of Aquatic Sciences and Assessment, Swedish University of Agricultural Sciences, Box 7050, SE-75007 Uppsala, Sweden

^cSwedish Geotechnical Institute, Kornhamnstorg 61, SE-11127 Stockholm, Sweden

^dDepartment of Sustainable Development, Environmental Science and Engineering, KTH Royal Institute of Technology, Teknikringen 10B, 100 44 Stockholm, Sweden

*Corresponding author. E-mail address: hugo.pereira@slu.se. Tel. +46 18671243

Supporting Information

Number of pages: 13

Contents

- S1. Experimental methods – additional description
- S2. Modeling of organic matter surface net charge
- S3. Extracted geochemically active fractions
- S4. Batch recipes
- S5. Modeling input
- S6. Measured PFAS concentrations
- S7. Calculated sorbed amounts
- S8. $\log K_{OC}$ values
- S9. Linear regression analysis – $\log KOC$ vs. pH / \log of SOM bulk net charge
- S10. Paired Student's t-test for evaluation of cation treatment effects

Figure S1 – Measured DOC concentrations in the sorption experiment

Figure S2 – Average sorbed fractions (%) of PFCAs and PFSA as a function of cation treatment (Al^{3+} , Na^+).

Figure S3 – Pearson r^2 values for SOM bulk net charge or pH vs. $\log K_{OC}$ for C_6 and C_8 PFSA and FOSA.

Figure S4 – $\Delta \log K_{OC}$ vs ΔpH and $\Delta(\log \text{SOM bulk net charge})$, as a function of perfluorocarbon chain length

S1. Experimental methods – additional description

After centrifuging the equilibrated PFAS-spiked soil samples and measurement of solution pH, aliquots of 20 mL subsamples were filtered using 0.45 μm syringe filters (Acrodise[®] 32 mm syringe filters with Supor[®] membrane) and subsequently analyzed for dissolved organic carbon (DOC) using a TOC-V CPH analyzer (Shimadzu). The remaining 20 mL supernatant was extracted using solid-phase extraction (SPE) WAX cartridges (Oasis WAX 6cc Cartridge, 150 mg, 30 μg , Waters) as described by Ahrens et al. (2015). The separation and analysis of PFASs were performed with high performance liquid chromatography coupled to tandem mass spectrometry (HPLC-MS/MS) (Agilent Technologies 1200 series and Agilent Technologies 6040 Triple Quad LC/MS) as described previously (Ahrens et al., 2015). All integrations were checked manually.

S2. Modeling of organic matter surface net charge

For the modeling purposes, 25 % of the extracted SOM was assumed to be active (Gustafsson et al., 2014). Further, it was assumed that 75% of the active SOM consisted of humic acid (HA) and 25% of fulvic acid (FA) (Table S1). Also, we assumed that 100 % of the DOC was present as FA. From this, the concentration of active FA in the solid phase was corrected for measured DOC in each sample.

S3. Extracted geochemically active fractions

Table S1. Geochemically active concentrations of the mor sample Risbergshöjden Oe, as determined by Gustafsson et al. (2014). Active cation concentrations do not include any additions. Extraction was made with 0.1 mol L⁻¹ nitric acid using 1 g dw sample to 30 mL solution.

Parameter	Concentration	Unit
Active humic acid	0.0581	g g ⁻¹
Active fulvic acid	0.0194	g g ⁻¹
Ca ²⁺	19.86	μmol g ⁻¹
Mg ²⁺	4.08	μmol g ⁻¹
K ⁺	3.60	μmol g ⁻¹
Mn ²⁺	0.945	μmol g ⁻¹
Al ³⁺	6.84	μmol g ⁻¹
Fe ³⁺	1.05	μmol g ⁻¹
Cr ³⁺	0.0006	μmol g ⁻¹
Cu ²⁺	0.0189	μmol g ⁻¹

S4. Batch recipes

Table S2. Recipes for the four cation treatments in the sorption experiment. 0.45 g dw soil was added to each sample. The stated pH values are the values aimed for, i.e. not the measured pH.

[mL]	30 mM NaNO ₃	20 mM HNO ₃	20 mM NaOH	30 mM Ca(NO ₃) ₂	20 mM Al(NO ₃) ₃	H ₂ O (Milli-Q)
Na, pH 3	13	4.0	0	0	0	23
Na, pH 4	13	0	2.0	0	0	25
Na, pH 5	13	0	6.0	0	0	21
Na, pH 6	13	0	12	0	0	15
Ca, pH 3 [3 mM]	5.3	4.0	0	4.0	0	27
Ca, pH 4 [3 mM]	5.3	0	4.0	4.0	0	27
Ca, pH 5 [3 mM]	5.3	0	10	4.0	0	21
Ca, pH 6 [3 mM]	5.3	0	15	4.0	0	16
Ca, pH 3 [5 mM]	5.3	4.0	0	6.7	0	24
Ca, pH 4 [5 mM]	5.3	0	4.0	6.7	0	24
Ca, pH 5 [5 mM]	5.3	0	10	6.7	0	18
Ca, pH 6 [5 mM]	5.3	0	15	6.7	0	13
Al, pH 3	5.3	0	0	0	4.0	31
Al, pH 4	5.3	0	10	0	4.0	21
Al, pH 5	5.3	0	14	0	4.0	17
Al, pH 6	5.3	0	20	0	4.0	11

S5. Modeling input

Table S3. Visual MINTEQ input and output for the modeling of SOM bulk net charge in the sorption experiment. The input concentrations of Al³⁺, Ca²⁺ and Na⁺ represent the sums of cation additions and geochemically active concentrations as determined by Gustafsson et al. (2014).

Sample	INPUT													OUTPUT
	pH	Mg (mM)	Fe (mM)	Mn (mM)	K (mM)	DOC (mg L ⁻¹)	FA solid (g L ⁻¹)	HA (g L ⁻¹)	Al (mM)	Ca (mM)	Na (mM)	NO ₃ (mM)	Net negative charge (mmol _e L ⁻¹)	
Na pH 3	3.1	0.15	0.04	0.03	0.13	69.1	0.54	2.04	0.24	0.71	10	12	1.21	
Na pH 4	4.2	0.15	0.04	0.03	0.13	35.8	0.61	2.04	0.24	0.71	11	10	2.54	
Na pH 5	4.9	0.15	0.04	0.03	0.13	50.2	0.58	2.04	0.24	0.71	12	10	3.57	
Na pH 6	5.8	0.15	0.04	0.03	0.13	135	0.41	2.04	0.24	0.71	16	10	4.44	
Ca pH 3 [5 mM]	2.9	0.15	0.04	0.03	0.13	72.1	0.54	2.04	0.24	5.71	4	16	1.05	
Ca pH 4 [5 mM]	3.8	0.15	0.04	0.03	0.13	72.5	0.53	2.04	0.24	5.71	6	14	1.52	
Ca pH 5 [5 mM]	4.6	0.15	0.04	0.03	0.13	36.3	0.61	2.04	0.24	5.71	9	14	1.67	
Ca pH 6 [5 mM]	5.2	0.15	0.04	0.03	0.13	51.1	0.58	2.04	0.24	5.71	12	14	1.63	
Ca pH 3 [3 mM]	2.9	0.15	0.04	0.03	0.13	70.3	0.54	2.04	0.24	3.71	4	12	1.04	
Ca pH 4 [3 mM]	3.9	0.15	0.04	0.03	0.13	30.1	0.62	2.04	0.24	3.71	6	10	1.70	
Ca pH 5 [3 mM]	4.9	0.15	0.04	0.03	0.13	44.3	0.59	2.04	0.24	3.71	9	10	1.99	
Ca pH 6 [3 mM]	5.6	0.15	0.04	0.03	0.13	79.9	0.52	2.04	0.24	3.71	12	10	2.29	
Al pH 3	2.8	0.15	0.04	0.03	0.13	70.5	0.54	2.04	2.24	0.71	4	10	0.58	
Al pH 4	4.0	0.15	0.04	0.03	0.13	52.7	0.57	2.04	2.24	0.71	9	10	0.84	
Al pH 5	4.8	0.15	0.04	0.03	0.13	69.1	0.54	2.04	2.24	0.71	11	10	1.52	
Al pH 6	5.7	0.15	0.04	0.03	0.13	108	0.46	2.04	2.24	0.71	14	10	2.67	

S6. Measured PFAS concentrations

Table S4. Aqueous concentrations in positive blanks with similar DOC concentrations (a–e) and pH as compared to the sorption experiment. All blanks contained 10 mM NaNO₃ as background electrolyte.

	pH	DOC	PFBA	PFPeA	PFHxA	PFHpA	PFOA	PFNA	PFDA	PFUnDA	PFDoDA	PFTeDA	FOSA	PFBS	PFHxS	PFOS
	mg L ⁻¹	ng L ⁻¹														
100 % (Milli-Q water reference spike average (n = 2))			522	636	761	897	1234	756	560	368	724	5677	1095	1171	1066	787
Positive blank average (n = 2)																
a	3.2	22	544	628	718	854	1228	864	761	490	768	996	919	761	1111	848
b	4.0	31	534	616	760	901	1260	911	863	553	1021	682	965	863	1078	730
c	4.3	35	565	659	804	909	1283	944	837	418	500	282	507	837	1066	789
d	5.1	74	579	604	818	831	1264	1060	1061	749	1489	1249	1116	1061	1092	787
e	6.0	141	581	615	806	780	1319	1130	1119	775	1418	932	968	1119	1098	839
f (no DOC)	5.6	0	144	184	202	275	339	188	188	134	157	164	163	188	298	211
Average recovery (%) in blanks with DOC			102	98	103	95	103	130	166	162	144	15	82	79	102	101
Recovery standard deviation (% units) in DOC blanks			3.4	3.0	4.9	5.3	2.4	13.0	24.6	38.4	52.1	5.8	18.7	11.8	1.5	5.4

Table S5. Measured dissolved concentrations of PFASs in the sorption experiment. Concentrations in strikethrough style exceeded the initial spiking concentration and were set equal to the initial concentration during the evaluation of results.

Aqueous PFAS concentrations [ng L ⁻¹]																	
Sample	dupl.	pH	DOC [mg L ⁻¹]	PFBA	PFPeA	PFHxA	PFHpA	PFOA	PFNA	PFDA	PFUnDA	PFDoDA	PFTeDA	FOSA	PFBS	PFHsS	PFOS
MDL (S/N = 3)				0.26	0.11	1.01	0.07	0.09	0.08	0.07	0.27	0.44	0.48	0.17	0.20	0.28	0.36
Blank, neg.	A	nd		<MDL	<MDL	<MDL	<MDL	<MDL	<MDL	<MDL	<MDL	<MDL	<MDL	<MDL	<MDL	<MDL	<MDL
Blank, neg.	B	nd		<MDL	<MDL	<MDL	<MDL	<MDL	<MDL	<MDL	<MDL	<MDL	<MDL	<MDL	<MDL	<MDL	<MDL
Reference spike	a			893	765	925	873	856	896	886	771	780	443	836	1020	736	670
Reference spike	b			871	848	928	856	846	887	908	830	802	452	817	889	771	599
AI pH 3	a	2.8	14.6	797	705	711	505	187	27	1.94	1.82	2.23	<MDL	0.20	951	142	2.92
AI pH 4	a	4.0	10.6	795	731	742	575	254	35	5.18	1.13	1.25	0.92	0.40	721	12	1.82
AI pH 5	a	4.8	13.2	811	705	765	599	317	63	6.05	6.85	12.02	4.02	3.78	541	18	4.53
AI pH 6	a	5.7	20.6	815	647	815	682	504	189	14.96	11.35	21.40	13.31	6.80	699	166	6.50
AI pH 3	b	2.8	13.7	830	756	718	504	170	21	1.75	0.26	<MDL	<MDL	0.17	954	43	3.15
AI pH 4	b	4.0	10.5	830	750	763	597	282	44	7.75	0.37	1.35	0.58	0.36	678	23	2.50
AI pH 5	b	4.7	14.5	820	729	772	638	364	87	12.99	15.15	18.37	10.29	6.06	656	53	10.53
AI pH 6	b	5.7	22.5	830	645	796	668	480	194	25.10	13.46	25.93	14.63	7.17	672	107	6.33
Ca pH 3 [5 mM]	a	2.9	13.7	842	740	774	578	294	55	6.68	1.00	2.06	0.72	0.71	4444	341	0.99
Ca pH 4 [5 mM]*	a																
Ca pH 5 [5 mM]	a	4.5	7.7	879	762	858	699	501	107	0.60	1.49	5.12	3.35	0.46	4022	383	<MDL
Ca pH 6 [5 mM]	a	5.2	10.7	852	714	848	704	508	114	12.54	10.41	18.62	11.03	5.16	872	365	5.79
Ca pH 3 [5 mM]	b	2.9	15.1	881	778	800	579	281	43	1.25	0.30	<MDL	<MDL	0.39	4448	343	1.94
Ca pH 4 [5 mM]	b	3.8	15.1	882	786	863	714	416	64	0.58	1.33	3.2	1.29	0.59	4094	348	1.13
Ca pH 5 [5 mM]	b	4.6	0.9	907	765	857	724	504	102	9.45	7.55	12.0	7.40	2.52	4085	381	5.23
Ca pH 6 [5 mM]	b	5.2	9.7	889	734	865	713	519	112	6.24	5.91	15.4	12.68	4.01	927	370	3.29
Ca pH 3 [3 mM]	a	2.9	13.1	853	718	775	571	281	43	2.19	<MDL	0.5	<MDL	0.27	4442	342	0.61
Ca pH 4 [3 mM]	a	3.8	5.45	837	732	853	712	523	174	4.97	0.98	3.2	0.85	1.08	892	477	1.74
Ca pH 5 [3 mM]	a	4.6	8.87	942	781	883	815	595	259	14.02	3.98	5.8	3.81	2.60	4295	536	3.81
Ca pH 6 [3 mM]	a	5.2	15.4	944	738	901	781	685	319	23.86	19.24	25.8	12.87	8.20	921	550	12.51
Ca pH 3 [3 mM]	b	2.9	15	867	717	773	548	284	46	4.54	0.45	1.5	1.96	0.77	892	345	2.14
Ca pH 4 [3 mM]	b	3.9	6.6	878	758	880	713	515	165	5.50	1.84	5.3	2.56	2.79	4442	510	2.94
Ca pH 5 [3 mM]	b	4.9	8.9	907	775	886	766	621	242	10.63	5.51	11.5	7.83	1.76	933	504	6.78
Ca pH 6 [3 mM]	b	5.6	16.5	922	745	910	786	674	297	9.37	8.38	17.4	12.39	3.99	922	517	5.19
Na pH 3	a	3.1	13.4	862	768	794	590	313	46	21.33	20.39	21.0	1.41	0.68	4429	331	15.45
Na pH 4	a	4.2	6.4	867	758	841	708	543	195	5.96	3.12	7.3	1.59	1.75	961	505	5.61
Na pH 5	a	5.0	8.7	881	757	880	751	660	321	7.01	5.11	11.2	7.99	2.30	940	555	5.23
Na pH 6	a	5.8	26.2	887	677	874	755	681	377	12.27	9.73	21.8	16.08	7.14	853	588	6.90
Na pH 3	b	3.1	14.2	908	788	826	627	304	20	5.56	0.32	1.7	0.73	0.17	4429	284	2.64
Na pH 4	b	4.2	8.0	928	852	919	769	582	221	6.27	2.41	7.2	2.57	1.32	4029	522	5.58
Na pH 5	b	4.9	11.4	889	755	881	761	634	324	8.63	5.55	12.0	6.27	3.13	4008	555	5.57
Na pH 6	b	5.8	27.7	905	683	876	749	590	304	36.7	8.31	18.7	12.61	5.68	670	171	4.85

*Sample omitted from results
nd = not determined

S7. Calculated sorbed amounts

Table S6. Calculated sorbed amounts (ng g⁻¹ dw soil) with the method of aqueous loss.

Calculated sorbed amounts [ng g ⁻¹ dw]																
Sample	dupl.	soil (g dw)	PFBA	PFPeA	PFHxA	PFHpA	PFOA	PFNA	PFDA	PFUnDA	PFDoDA	PFTeDA	FOSA	PFBS	PFHxS	PFOS
Al pH 3	a	0.454	7.5	8.9	19.0	31.7	58.5	76.2	78.9	70.4	69.5	39.4	72.8	0.3	53.8	55.6
Al pH 4	a	0.453	7.7	6.7	16.3	25.6	52.7	75.7	78.8	70.7	69.8	39.5	73.0	20.7	65.5	55.9
Al pH 5	a	0.453	6.3	9.0	14.3	23.4	47.1	73.1	78.7	70.1	68.8	39.2	72.6	36.5	64.9	55.6
Al pH 6	a	0.454	5.9	14.0	9.8	16.1	30.6	61.8	77.7	69.5	67.8	38.3	72.2	22.5	51.7	55.3
Al pH 3	b	0.454	4.6	4.5	18.3	31.8	60.0	76.7	78.9	70.6	69.7	39.4	72.8	0.1	62.6	55.6
Al pH 4	b	0.453	4.6	5.0	14.4	23.6	50.3	74.9	78.6	70.8	69.8	39.5	73.0	24.5	64.5	55.9
Al pH 5	b	0.454	5.5	6.8	13.6	20.0	42.9	70.9	77.9	69.2	68.1	38.6	72.3	26.4	61.7	55.0
Al pH 6	b	0.454	4.6	14.3	11.5	17.4	32.6	61.4	76.8	69.3	67.4	38.1	72.2	24.9	56.9	55.3
Ca pH 3 [5 mM]	a	0.454	3.5	5.9	13.5	25.2	49.1	73.7	78.5	70.5	69.6	39.4	72.8	0.0	36.3	55.8
Ca pH 4 [5 mM]*	a	0.454														
Ca pH 5 [5 mM]	a	0.453	0.2	3.9	6.0	14.6	30.8	69.2	79.1	70.6	69.4	39.2	72.9	0.0	32.7	56.0
Ca pH 6 [5 mM]	a	0.454	2.7	8.2	6.9	14.2	30.2	68.6	78.0	69.7	68.2	38.5	72.4	7.3	34.3	55.4
Ca pH 3 [5 mM]	b	0.454	0.1	2.6	11.1	25.2	50.2	74.8	79.0	70.6	69.8	39.5	72.9	0.0	36.2	55.8
Ca pH 4 [5 mM]	b	0.453	0.0	1.9	5.6	13.3	38.4	73.1	79.2	70.6	69.6	39.4	73.0	0.0	35.8	55.9
Ca pH 5 [5 mM]	b	0.453	0.0	3.7	6.1	12.4	30.7	69.7	78.4	70.1	68.8	38.9	72.8	0.0	32.9	55.6
Ca pH 6 [5 mM]	b	0.453	0.0	6.4	5.4	13.4	29.3	68.8	78.6	70.2	68.5	38.4	72.6	2.5	33.8	55.7
Ca pH 3 [3 mM]	a	0.452	2.6	7.8	13.4	26.0	50.4	75.1	79.2	70.8	70.0	39.6	73.1	0.0	36.3	56.1
Ca pH 4 [3 mM]	a	0.454	4.0	6.6	6.5	13.5	28.9	63.3	78.7	70.6	69.5	39.4	72.8	5.5	24.3	55.8
Ca pH 5 [3 mM]	a	0.453	0.0	2.3	3.8	4.4	22.6	55.9	77.9	70.3	69.3	39.2	72.7	0.0	19.1	55.7
Ca pH 6 [3 mM]	a	0.454	0.0	6.0	2.3	7.4	14.6	50.5	77.0	68.9	67.5	38.3	72.1	3.0	17.9	54.8
Ca pH 3 [3 mM]	b	0.454	1.4	7.9	13.5	27.9	49.9	74.4	78.6	70.5	69.6	39.3	72.7	5.5	36.0	55.7
Ca pH 4 [3 mM]	b	0.452	0.3	4.3	4.1	13.4	29.7	64.3	78.9	70.7	69.5	39.4	72.9	0.0	21.5	55.9
Ca pH 5 [3 mM]	b	0.452	0.0	2.7	3.6	8.7	20.3	57.4	78.4	70.4	69.0	38.9	73.0	1.9	22.1	55.5
Ca pH 6 [3 mM]	b	0.454	0.0	5.4	1.4	7.0	15.6	52.4	78.2	69.8	68.2	38.4	72.5	2.9	20.8	55.4
Na pH 3	a	0.453	1.8	3.4	11.7	24.3	47.5	74.7	77.4	69.0	68.1	39.5	73.0	0.0	37.3	54.7
Na pH 4	a	0.453	1.3	4.3	7.5	13.8	27.2	61.6	78.8	70.5	69.3	39.4	72.9	0.0	21.9	55.6
Na pH 5	a	0.453	0.1	4.4	4.1	10.1	16.9	50.4	78.7	70.3	69.0	38.9	72.9	1.3	17.5	55.6
Na pH 6	a	0.454	0.0	11.4	4.6	9.6	15.0	45.4	78.0	69.8	67.9	38.1	72.3	9.0	14.6	55.3
Na pH 3	b	0.453	0.0	1.7	8.8	21.0	48.3	77.0	78.8	70.7	69.8	39.5	73.0	0.0	41.5	55.8
Na pH 4	b	0.453	0.0	0.0	0.7	8.5	23.7	59.2	78.6	70.5	69.2	39.3	72.8	0.0	20.4	55.5
Na pH 5	b	0.454	0.0	4.6	4.0	9.1	19.1	50.1	78.4	70.1	68.7	38.9	72.6	0.0	17.4	55.5
Na pH 6	b	0.453	0.0	10.9	4.4	10.2	23.0	51.8	75.9	70.0	68.2	38.4	72.4	25.2	51.4	55.6

*Omitted from results

S8. log K_{oc} values

Table S7. Log K_{oc} [mL g⁻¹ dw] values obtained from sorption experiment. Concentrations below the respective MDLs, as well as aqueous concentrations higher than initial spiking concentration, were omitted in the determination of partitioning coefficients.

Log K_{oc} [mL g ⁻¹ dw]																
Sample	dupl.	pH	PFBA	PFPeA	PFHxA	PFHpA	PFOA	PFNA	PFDA	PFUnDA	PFDoDA	PFTeDA	FOSA	PFBS	PFHxS	PFOS
Al pH 3	a	2.8	1.3	1.4	1.8	2.1	2.8	3.8	5.0	4.9	4.8		5.9	-0.1	2.9	4.6
Al pH 4	a	4.0	1.3	1.3	1.7	2.0	2.7	3.7	4.5	5.1	5.1	5.0	5.6	1.8	4.1	4.8
Al pH 5	a	4.8	1.2	1.5	1.6	1.9	2.5	3.4	4.5	4.4	4.1	4.3	4.6	2.2	3.9	4.4
Al pH 6	a	5.7	1.2	1.7	1.4	1.7	2.1	2.9	4.1	4.1	3.8	3.8	4.4	1.9	2.8	4.3
Al pH 3	b	2.8	1.1	1.1	1.8	2.1	2.9	3.9	5.0	5.8			6.0	-0.7	3.5	4.6
Al pH 4	b	4.0	1.1	1.2	1.6	1.9	2.6	3.6	4.4	5.6	5.1	5.2	5.7	1.9	3.8	4.7
Al pH 5	b	4.7	1.2	1.3	1.6	1.8	2.4	3.3	4.1	4.0	3.9	3.9	4.4	2.0	3.4	4.1
Al pH 6	b	5.7	1.1	1.7	1.5	1.8	2.2	2.8	3.8	4.1	3.8	3.8	4.3	1.9	3.1	4.3
Ca pH 3 [5 mM]	a	2.9	1.0	1.2	1.6	2.0	2.6	3.5	4.4	5.2	4.9	5.1	5.4		2.4	5.1
Ca pH 4 [5 mM]*	a	4.0														
Ca pH 5 [5 mM]	a	4.5	-0.2	1.1	1.2	1.7	2.1	3.2	5.5	5.0	4.5	4.4	5.5		2.3	
Ca pH 6 [5 mM]	a	5.2	0.8	1.4	1.3	1.7	2.1	3.1	4.1	4.2	3.9	3.9	4.5	1.3	2.3	4.3
Ca pH 3 [5 mM]	b	2.9	-0.8	0.9	1.5	2.0	2.6	3.6	5.1	5.7			5.6		2.4	4.8
Ca pH 4 [5 mM]	b	3.8		0.7	1.2	1.6	2.3	3.4	5.5	5.1	4.7	4.8	5.4		2.4	5.0
Ca pH 5 [5 mM]	b	4.6		1.0	1.2	1.6	2.1	3.2	4.3	4.3	4.1	4.1	4.8		2.3	4.4
Ca pH 6 [5 mM]	b	5.2		1.3	1.1	1.6	2.1	3.1	4.4	4.4	4.0	3.8	4.6	0.8	2.3	4.6
Ca pH 3 [3 mM]	a	2.9	0.8	1.4	1.6	2.0	2.6	3.6	4.9		5.5		5.8		2.4	5.3
Ca pH 4 [3 mM]	a	3.9	1.0	1.3	1.2	1.6	2.1	2.9	4.5	5.2	4.7	5.0	5.2	1.1	2.1	4.9
Ca pH 5 [3 mM]	a	4.9		0.8	1.0	1.1	1.9	2.7	4.1	4.6	4.4	4.4	4.8		1.9	4.5
Ca pH 6 [3 mM]	a	5.6		1.3	0.7	1.3	1.7	2.5	3.9	3.9	3.8	3.8	4.3	0.9	1.9	4.0
Ca pH 3 [3 mM]	b	2.9	0.5	1.4	1.6	2.1	2.6	3.6	4.6	5.5	5.0	4.6	5.3	1.1	2.4	4.8
Ca pH 4 [3 mM]	b	3.9	-0.1	1.1	1.0	1.6	2.1	2.9	4.5	4.9	4.5	4.5	4.8		2.0	4.6
Ca pH 5 [3 mM]	b	4.8		0.9	0.9	1.4	1.9	2.7	4.2	4.5	4.1	4.0	5.0	0.7	2.0	4.3
Ca pH 6 [3 mM]	b	5.6		1.2	0.5	1.3	1.7	2.6	4.3	4.3	3.9	3.8	4.6	0.8	2.0	4.4
Na pH 3	a	3.1	0.7	1.0	1.5	2.0	2.5	3.6	3.9	3.9	3.9	4.8	5.4		2.4	3.9
Na pH 4	a	4.2	0.5	1.1	1.3	1.6	2.0	2.8	4.5	4.7	4.3	4.7	5.0		2.0	4.3
Na pH 5	a	4.9	-0.6	1.1	1.0	1.5	1.8	2.5	4.4	4.5	4.1	4.0	4.8	0.5	1.8	4.4
Na pH 6	a	5.8		1.6	1.1	1.5	1.7	2.4	4.2	4.2	3.8	3.7	4.4	1.4	1.7	4.3
Na pH 3	b	3.1		0.7	1.4	1.9	2.5	3.9	4.5	5.7	5.0	5.1	6.0		2.5	4.7
Na pH 4	b	4.2			0.2	1.4	2.0	2.8	4.4	4.8	4.3	4.5	5.1		1.9	4.3
Na pH 5	b	4.9		1.1	1.0	1.4	1.8	2.5	4.3	4.4	4.1	4.1	4.7		1.8	4.3
Na pH 6	b	5.8		1.5	1.1	1.5	1.9	2.6	3.7	4.3	3.9	3.8	4.5	1.9	2.8	4.4
Average		4.3	0.7	1.2	1.3	1.7	2.2	3.1	4.4	4.7	4.3	4.3	5.0	1.2	2.5	4.5

*Omitted from results

S9. Linear regression analysis – log K_{OC} vs. pH / log of SOM bulk net charge

Table S8. Pearson r^2 values, significance and regression slopes for the two sorption (log K_{OC}) predictors pH and SOM bulk net charge.

Sorption predictor	pH (n = 31)				SOM bulk net charge, (simulated with SHM) (n = 16, i.e. averaged over duplicates)			
	Substance	r^2 (log K_{OC} vs pH)	Significance ($p \leq 0.05$)	Slope ($\Delta K_{OC}/\Delta pH$)	Intercept	r^2 (log K_{OC} vs log net charge (mol $_e$ g $^{-1}$))	Significance ($p \leq 0.05$)	Slope ($\Delta K_{OC}/\Delta(\log$ mol $_e$ g $^{-1}$))
PFBA	0	-	0.055	0.48	0.23	NS-	-1.26	-4.31
PFPeA	0.16	S+	0.10	0.78	0.04	NS+	0.24	2.10
PFHxA	0.26	S-	-0.18	2.05	0.53	S-	-1.05	-2.75
PFHpA	0.51	S-	-0.19	2.53	0.64	S-	-0.93	-1.88
PFOA	0.63	S-	-0.27	3.41	0.81	S-	-1.38	-3.05
PFNA	0.66	S-	-0.36	4.70	0.85	S-	-1.82	-3.85
PFDA	0.35	S-	-0.25	5.53	0.31	S-	-1.02	0.56
PFUnDA	0.57	S-	-0.44	6.62	0.56	S-	-1.66	-1.61
PFDoDa	0.64	S-	-0.40	6.11	0.68	S-	-1.81	-2.53
PFTeDA	0.79	S-	-0.48	6.50	0.54	S-	-1.77	-2.32
PFBS ^a	0.22	S+	0.35	-0.47	0.08	NS+	0.77	4.06
PFHxS	0.03	NS-	-0.11	2.96	0.30	S-	-1.49	-3.21
PFOS	0.35	S-	-0.18	5.30	0.30	S-	-0.70	1.84
FOSA	0.78	S-	-0.46	7.05	0.66	S-	-1.83	-1.98

S+/- = significant positive/negative correlation, NS = non-significant relationship

^aHigh uncertainty in linear regression for both pH and SOM net charge due to $n = 13$ omitted measurements of aqueous concentrations (higher than initial spiking).

S10. Paired Student's t-test for evaluation of cation treatment effects

Table S9. Paired Student's t-test (double-sided, type 1) testing significance ($p \leq 0.05$) for differences in $\log K_{oc}$ averages between the four cation treatments in the sorption experiment. S corresponds to a significant difference in average $\log K_{oc}$ and blanks correspond to a non-significant difference. The $\log K_{oc}$ values of this study roughly followed log-normal distributions. The sign of any significant difference between two cation treatments was determined by comparison of the respective $\log K_{oc}$ means. The results should be viewed as indicative as paired samples from different cation treatments have similar, but not equal, pH values.

Tested hypothesis	$\log K_{oc}(Al^{3+})$ [2 mM] > Ca^{2+} [3 mM]	$\log K_{oc}(Al^{3+})$ [2 mM] > Na^{+} [10 mM]	$\log K_{oc}(Ca^{2+})$ [5 mM] > Ca^{2+} [3 mM]	$\log K_{oc}(Ca^{2+})$ [5 mM] > Na^{+} [10 mM]	$\log K_{oc}(Ca^{2+})$ [3 mM] > Na^{+} [10 mM]
PFBA		S			
PFPeA	S		S		
PFHxA	S	S	S		
PFHpA	S	S	S	S	
PFOA	S	S	S	S	
PFNA	S	S	S	S	
PFDA				S	
PFUnDA				S	
PFDoDA				S	
PFTeDA				S	
FOSA					
PFBS					
PFHxS	S	S	S	S	
PFOS	S (Ca^{2+} [5 mM] > Al^{3+} [2 mM])				S

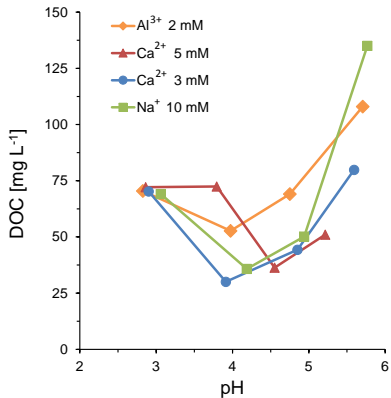


Figure S1. DOC concentrations in the sorption experiment as a function of pH and cation additions (stated concentrations). Each data point represents the average of duplicates. Lines connect the points and are included for clarity.

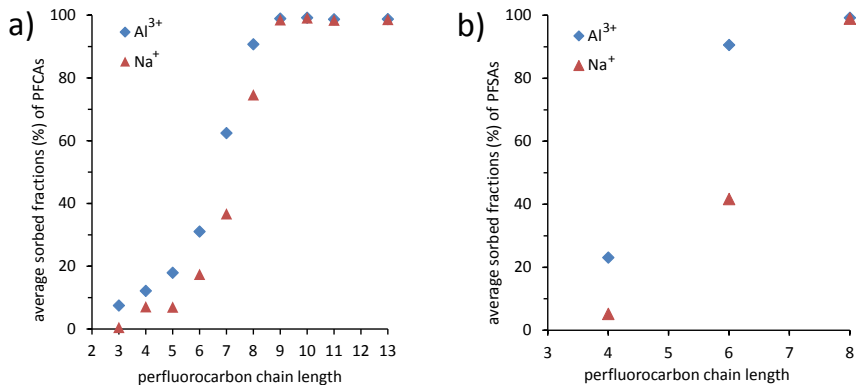


Figure S2. Average sorption of PFCA (a) and PFSA (b) in the Al³⁺ (2 mM) and Na⁺ (10 mM) treatments for the pH range 2.8–5.8.

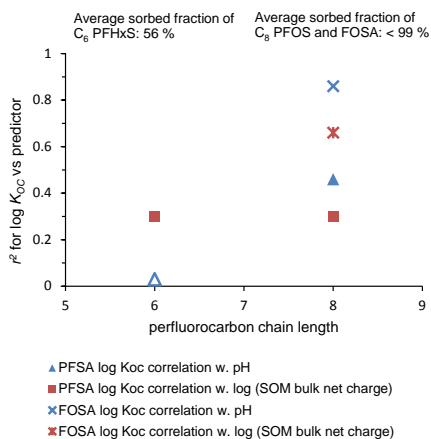


Figure S3. The Pearson r^2 value for SOM bulk net charge or pH vs. log K_{oc} as influenced by the perfluorocarbon chain length and functional group of C₆ and C₈ PFSA and FOSA. Closed markers represent significant correlations ($p \leq 0.05$) and the open marker a non-significant relationship.

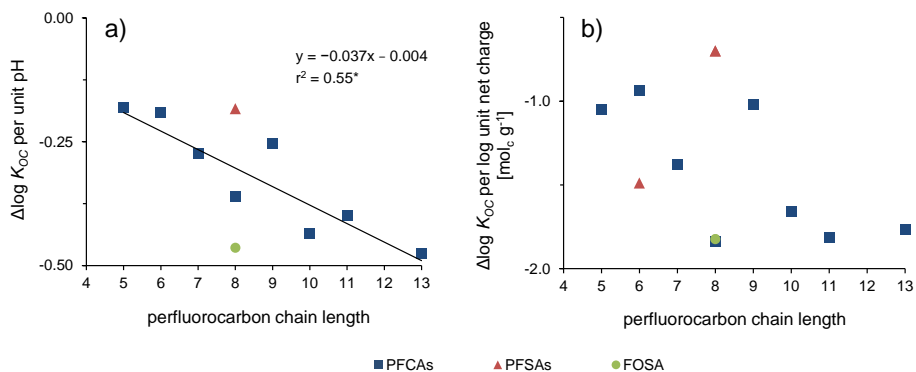


Figure S4. $\Delta \log K_{oc}$, with respect to pH (a) and SOM bulk net charge (b), as a function of perfluorocarbon chain length. Included are the substances for which sorption showed a significant relationship ($p \leq 0.05$) with the respective sorption predictor.

The Adsorption of Per- and Polyfluoroalkyl Substances (PFASs) onto Ferrihydrite Is Governed by Surface Charge

Hugo Campos-Pereira,* Dan B. Kleja, Carin Sjöstedt, Lutz Ahrens, Wantana Klysubun, and Jon Petter Gustafsson

Cite This: *Environ. Sci. Technol.* 2020, 54, 15722–15730

Read Online

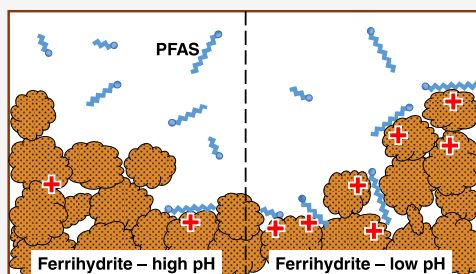
ACCESS |

Metrics & More

Article Recommendations

Supporting Information

ABSTRACT: An improved quantitative and qualitative understanding of the interaction of per- and polyfluoroalkyl substances (PFASs) and short-range ordered Fe (hydr)oxides is crucial for environmental risk assessment in environments low in natural organic matter. Here, we present data on the pH-dependent sorption behavior of 12 PFASs onto ferrihydrite. The nature of the binding mechanisms was investigated by sulfur K-edge X-ray absorption near-edge structure (XANES) spectroscopy and by phosphate competition experiments. Sulfur K-edge XANES spectroscopy showed that the sulfur atom of the head group of the sulfonated PFASs retained an oxidation state of +V after adsorption. Furthermore, the XANES spectra did not indicate any involvement of inner-sphere surface complexes in the sorption process. Adsorption was inversely related to pH ($p < 0.05$) for all PFASs (i.e., C₃–C₅ and C₇–C₉ perfluorocarboxylates, C₄, C₆, and C₈ perfluorosulfonates, perfluorooctane sulfonamide, and 6:2 and 8:2 fluorotelomer sulfonates). This was attributed to the pH-dependent charge of the ferrihydrite surface, as reflected in the decrease of surface ζ -potential with increasing pH. The importance of surface charge for PFAS adsorption was further corroborated by the observation that the adsorption of PFASs decreased upon phosphate adsorption in a way that was consistent with the decrease in ferrihydrite ζ -potential. The results show that ferrihydrite can be an important sorbent for PFASs with six or more perfluorinated carbons in acid environments (pH ≤ 5), particularly when phosphate and other competitors are present in relatively low concentrations.



INTRODUCTION

Accurate prediction of the binding of per- and polyfluoroalkyl substances (PFASs) in soil is essential for environmental risk assessment. However, information on PFAS binding to poorly crystalline iron (hydr)oxides such as ferrihydrite is scarce up to date, despite that these phases are known to be important for contaminant and trace element soil retention^{1–3} due to their large surface area^{4,5} and high reactivity.⁶ The poorly crystalline Fe (hydr)oxide ferrihydrite has a high abundance in many young soils, particularly in cool or temperate climates with high moisture and occurrence of Si and/or organic matter.⁷ For example, ferrihydrite is present in concentrations up to 2% in the B horizon of Swedish Podzols.^{8,9} Because of its high reactivity and high surface area, ranging from 250 to 1260 m² g⁻¹, ferrihydrite is an important adsorbent in many soils, particularly for anions.⁶ Subsoils are conceptually interesting environments as they delay the transport of solutes between the soil surface horizon and ground- and surface waters. As PFASs such as perfluorooctane sulfonate (PFOS) and perfluorooctane carboxylate (PFOA) are common ground-water contaminants,^{10–12} it is of importance for environmental risk assessment to gain more knowledge on PFAS sorption

behavior to subsoil materials, especially as regards sorption to poorly crystalline Fe (hydr)oxides like ferrihydrite.

Up to date, studies on PFAS binding to mineral surfaces have mostly focused on the sorption properties of crystalline minerals such as alumina (Al₂O₃), silica (SiO₂),^{13–15} hematite (α -Fe₂O₃),^{16,17} boehmite (γ -AlOOH),^{18,19} and goethite (α -FeOOH),^{14,20,21} and of minerals that are typical of aquatic sediments such as, for example, the silicates kaolinite and montmorillonite.^{16,22,23} Besides, many studies up to date have been limited to include one single PFAS, i.e., PFOS. As regards binding mechanisms responsible for adsorption onto mineral surfaces, previous works have often emphasized the outer-sphere or electrostatic contributions^{13,20,21} over those of hydrophobic interactions or specific (inner-sphere) complexes. However, using attenuated total reflection infrared spectro-

Received: March 16, 2020

Revised: October 30, 2020

Accepted: November 8, 2020

Published: November 27, 2020



copy, specific binding of PFOA has been reported to take place on hematite¹⁷ and on ferrihydrite²⁴ under acidic conditions, although the results of Zhang et al.²⁵ suggest outer-sphere complexes on oxidized zero-valent iron. For PFOS, inner-sphere complexes on Fe oxides have not been reported. Instead outer-sphere complexes and/or electrostatic attractions may predominate.^{17,25} The ferrihydrite surface is positively charged at pH values below its point of zero charge (PZC), which is pH ~8.1 for pure ferrihydrite.^{4,26} Hence, it may be expected that the adsorption of anionic PFASs by ferrihydrite is stronger at low pH. Furthermore, it may be hypothesized that PFAS adsorption onto ferrihydrite decreases in the presence of other adsorbed anions at the ferrihydrite surface, as specific binding of such species lowers the positive surface charge. For example, phosphate (PO_4^{3-}) is a common oxyanion in the environment, which forms strong surface complexes; hence, phosphate may affect PFAS binding both by direct competition for sites and by modifying the surface charge.²⁷

PFASs such as PFOS and perfluorooctane sulfonamide (FOSA) contain a sulfur (S) atom as part of their head group. The chemistry and speciation of sulfur-containing compounds may be investigated using spectroscopic methods such as, e.g., X-ray absorption near-edge structure (XANES) and extended X-ray absorption fine structure (EXAFS) spectroscopy.^{28–33} The absorption edge, corresponding to the excitation of an inner-shell electron, exhibits several identifiable features that change depending on the chemical environment of the sulfur atom. For example, inner-sphere complexes involving Fe give rise to a so-called pre-edge due to orbital hybridization, as, for example, observed for the inner-sphere complexes of sulfate on ferrihydrite.^{32,33} Hence, in the present study, we employed S K-edge XANES spectroscopy to investigate the bonding characteristics of sulfonated PFASs onto ferrihydrite.

To our knowledge, this is the first study to investigate the adsorption behavior of a range of different PFASs onto ferrihydrite (Fh). The specific objectives were to (1) investigate the pH-dependent Fh binding of PFASs in the absence and presence of phosphate (PO_4^{3-}) as a competing anion and (2) reveal the adsorption mechanism of selected sulfonated PFASs onto Fh using S K-edge XANES spectroscopy in combination with ζ -potential measurements and results from batch experiments.

MATERIALS AND METHODS

Target PFASs. Twelve PFASs (standards purchased from Sigma-Aldrich) were analyzed, i.e., C_3 – C_5 and C_7 – C_9 perfluoroalkyl carboxylates (PFCAs), C_4 , C_6 , and C_8 perfluoroalkyl sulfonates (PFASs), perfluorooctane sulfonamide (FOSA), and 6:2 and 8:2 fluorotelomer sulfonates (6:2 and 8:2 FTSA). For quantification as well as for quality assurance and control (QA/QC), eight mass-labeled internal standards (ISs) (i.e., $^{13}\text{C}_4$ -PFBA, $^{15}\text{C}_2$ -PFHxA, $^{13}\text{C}_4$ -PFOA, $^{13}\text{C}_2$ -PFNA, $^{13}\text{C}_2$ -PFDA, $^{18}\text{O}_2$ -PFHxS, $^{13}\text{C}_4$ -PFOS, $^{13}\text{C}_2$ -FOSA, purities > 99%, Wellington Laboratories, Guelph, ON) were also included. For details on the included PFASs and their internal standards, see Table S1 in the Supporting Information.

Ferrihydrite and Al Hydroxide Preparation. 2-Line ferrihydrite was synthesized using the method of Swedlund and Webster³⁴ and Schwertmann and Cornell³⁵ with minor modifications. In short, a solution containing 36 mmol $\text{Fe}(\text{NO}_3)_3$ L^{-1} was brought to pH 8.0 through dropwise addition of freshly prepared sodium hydroxide (4 mol NaOH L^{-1}) under magnetic stirring. The resulting suspension was left

to settle and age for about 16 h at 20 °C in a tightly capped high-density polyethylene (HDPE) bottle (500 mL, Nalgene). Iron (hydr)oxide particles from such a suspension have previously been studied by Fe K-edge EXAFS spectroscopy^{3,36} and were confirmed to be poorly crystalline 2-line ferrihydrite. After synthesis, the Fh suspension was back-titrated to pH 4.6 with dropwise addition of 0.1 mol nitric acid (HNO_3) L^{-1} under magnetic stirring and stirred for some additional 30 min before the start of the batch experiments to remove CO_2 . For the preparation of Fh subjected to S K-edge XANES spectroscopy, high-purity HNO_3 (purchased from Sigma-Aldrich) was used to minimize trace element (in particular S) contamination. The properties of the Fh synthesized in this way (e.g., surface area, aggregation state, etc.) have been described by Hiemstra.^{6,26} For example, the surface area for the Fh produced in our laboratory has been estimated at 650 or 611 $\text{m}^2 \text{g}^{-1}$, depending on the assumption made on the molar weight of ferrihydrite.^{2,6} Furthermore, for use in the spectroscopic measurements, poorly crystalline aluminum hydroxide (Alhox) was synthesized with the same method as was used for the preparation of ferrihydrite, with the only modifications being that $\text{Fe}(\text{NO}_3)_3$ was substituted for $\text{Al}(\text{NO}_3)_3$, and that the suspension was titrated to pH 7.0 before aging and back-titrated to pH 5.0 after aging.

X-ray Absorption Spectroscopy. For the S K-edge XANES measurements, PFASs adsorbed to Fh and Alhox were sampled in their wet paste state from sorption batch experiments. The purpose of including Alhox in these experiments was that a pre-edge peak, resulting from inner-sphere complexation of SO_4^{2-} , would be expected on Fh, but not on Alhox.^{30,33} Hence, the existence of a pre-edge peak resulting from orbital hybridization on Fh could more easily be separated from other features in the S K-edge XANES spectrum. Spectra for adsorbed sulfate (SO_4^{2-}) were also collected for comparison, as were those of pure PFAS standards and potassium sulfate (K_2SO_4) salt in their solid states. The batch experiments were performed immediately before the spectroscopic measurements. In brief, concentrations of 200 $\mu\text{mol L}^{-1}$ of selected sulfonated PFASs (i.e., PFHxS (counterion K), PFOS(K), FOSA, or sulfate (added as K_2SO_4)) were equilibrated for 24 h with either Fh or Alhox (1 mmol L^{-1} Fe or Al, respectively) before phase separation. Supernatant residual sulfate and PFASs were quantified to determine adsorbed concentrations (Table S13 in the Supporting Information). Sulfate was determined with ion chromatography according to ISO 10 304-1:2009 (accredited). The S K-edge XANES spectra were collected in fluorescence mode over the energy range of 2400–2550 eV at beamline BL8 at the Synchrotron Light Research Institute (SLRI), Nakhon Ratchasima, Thailand,³⁷ in May 2017. Details on beamline equipment are given in Section S1.1 in the Supporting Information, and instrument settings are provided elsewhere.³¹ Samples were diluted with boron nitride (BN), placed into Al frames, and sealed with X-ray film using sulfur-free Kapton tape (Lanmar, Inc.). Energy calibration was done using the sulfate white-line of FeSO_4 at 2482.5 eV.³¹ All XANES spectra were corrected for energy shift and normalized using the Athena software³⁸ (version 0.9.26). Multiple scans were merged and subsequently normalized to yield a K-edge intensity step of unity. This was done by subtracting linear and quadratic baseline functions over the pre-edge and normalization (post-edge) range, respectively. Relative to the white-line position, the employed pre-edge ranges were from –70 to

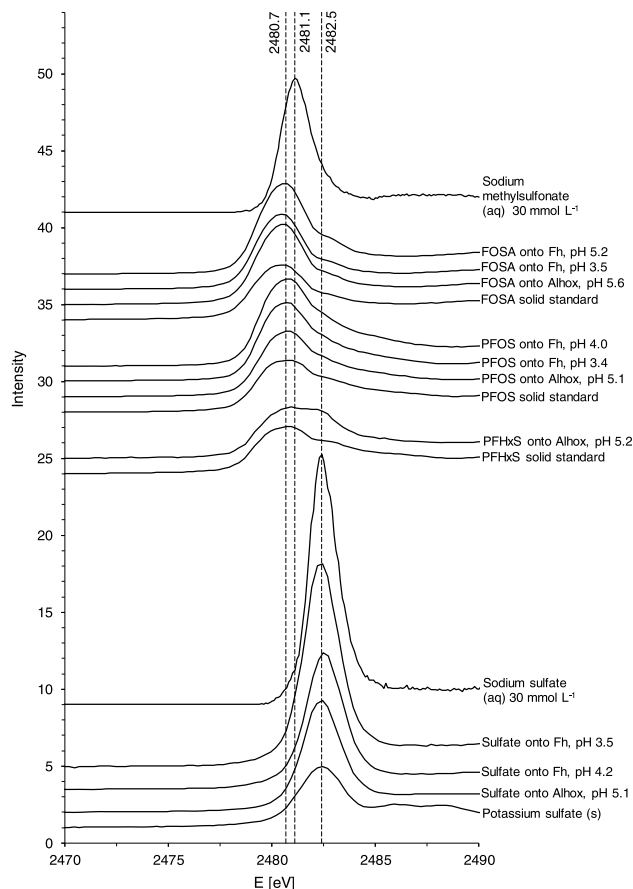


Figure 1. Stacked normalized S K-edge XANES spectra for sulfonated PFASs adsorbed to ferrihydrite (Fh) and poorly crystalline aluminum hydroxide (Alhox). Dashed white-line positions are, from lower to higher energies, those of PFOS onto Fh and Alhox, of dissolved dilute sodium methylsulfonate (NaCH_3SO_3), and of sulfate onto Fh and Alhox. Spectra for sodium sulfate (Na_2SO_4) (aq) and sodium methylsulfonate were provided by Almkvist et al.,⁵² and their intensities were set to unity at 2490 eV for the purpose of comparison.

−25 eV for PFASs and from −65 to −25 eV for sulfate, whereas the normalization range was from +40 to +60 eV.

BATCH EXPERIMENTS

pH-Dependent Binding in the Absence and Presence of Phosphate.

A ferrihydrite stock suspension was mixed with Milli-Q water and NaNO_3 solution in 50 mL reactors (polypropylene centrifuge tubes) to obtain final concentrations of 3.2 mmol Fe L^{-1} as ferrihydrite and 10 mmol nitrate L^{-1} . Various amounts of acid (HNO_3) or base (NaOH , prepared the same day) were then added to reach pH values between 4.0 and 7.6 after equilibration. Subsequently, 0 or 200 $\mu\text{mol L}^{-1}$ phosphate (as NaH_2PO_4) was added. For details, see Table S2 in the Supporting Information. Finally, triplicate sets of centrifuge tubes were spiked with 20 μL of a stock mixture of 12 PFASs dissolved in methanol (analytical grade, Merck) so that the initial aqueous concentrations of individual PFASs

ranged from 1.6 nmol L^{-1} (PFDA) to 5.5 nmol L^{-1} (PFBS) (Table S3 in the Supporting Information). The additions were sufficiently low to ensure that sorption occurred in the linear range (cf. below). Duplicate negative controls were included for quality assurance and control. Suspensions were end-over-end shaken (45 rpm, 21 °C) for 24 h prior to centrifugation at $\sim 2000g$ for about 30 min. The pH was measured in the supernatant of subsamples using a Red Rod Ag/AgCl electrode (Radiometer Analytical SAS). The ferrihydrite ζ -potential was measured at 21 °C (Zetasizer Nano-ZS, Malvern) on nonspiked suspensions (pH 3.9–9.5) having the same solution chemistry and phosphate additions as samples in the sorption experiment (Table S10 in the Supporting Information). Aqueous phosphate and Fe (0.45 μm filtration, Sartorius Minisart hydrophilic regenerated cellulose, \varnothing 25 mm) were analyzed using inductively coupled plasma-optical emission spectroscopy (ICP-OES) (Table S4 in the Supporting

Information). Iron was quantified ($LoQ = 40 \mu\text{g L}^{-1}$) to ensure efficient filter retention of ferrihydrite particles and to check that no iron dissolution of significance occurred in the investigated pH range.

Sorption Isotherms. Varying volumes of either PFOA, PFOS, or FOSA dissolved in methanol (20 mmol L^{-1}) were added to Fh suspensions ($10 \text{ mmol Fe L}^{-1}$) prior to equilibration for 24 h using end-over-end shaking. Initial additions of the individual PFASs were chosen so that aqueous concentrations after equilibration spanned approximately 3 orders of magnitude (i.e., ca. $1\text{--}700 \text{ nmol PFOS L}^{-1}$, $1\text{--}2000 \text{ nmol PFOA L}^{-1}$, $0.3\text{--}1000 \text{ nmol FOSA L}^{-1}$). After centrifugation, pH was measured in supernatants of sample aliquots, and was confirmed to be 4.5 ± 0.1 .

PFAS Analysis. For quantification of aqueous PFAS concentrations, 5 ng of each of the mass-labeled ISs was added to sample aliquots prior to gentle filtration ($0.45 \mu\text{m}$, Sartorius Minisart hydrophilic regenerated cellulose^{39,40}). The PFAS concentrations were measured by the means of IS isotope dilution using direct injection in a Dionex UltiMate 3000 ultrahigh-performance liquid chromatography (UPLC) system (Thermo Fisher Scientific, Massachusetts) coupled to a triple-quadrupole tandem mass spectrometer (MS/MS) (TSQ Quantiva, Thermo Fisher Scientific, Massachusetts). Sorption to ferrihydrite was calculated as the difference between added and dissolved PFASs, with the exception of that of substances that showed recoveries below 90% in the positive controls, for which losses to reactor walls were also taken into account (see below).

Quality Assurance and Control. All experiments used Milli-Q water, which was filtered through a cartridge containing powdered activated carbon (PAC) (Milli-Q LC-Pak, Merck) to minimize contamination. For the same purpose, no fluorinated materials (e.g., tetrafluoroethylene, Teflon) were used in the experiments. All PFASs in the negative controls ($n = 2$) were below the limit of quantification (LoQ), as defined as the lowest quantifiable calibration point (i.e., the lowest calibration point having a response factor within $\pm 30\%$ of the average response factor of the calibration curve). The method recovery was calculated from the losses of ISs due to sample preparation and matrix effects, as determined by comparison with the calibration curve, and was, for individual PFASs, on average $86 \pm 3\%$. The percent standard deviation of individual aqueous PFAS concentrations was, on average, 7% in the pH-dependent sorption experiment ($n = 3$), and 5% as regards the sorption isotherms ($n = 2$). The fraction of spiked co-solvent methanol in the isotherm and the pH-dependent sorption experiments was $<0.3\%$ (v/v), and thus the effect of methanol on PFAS partitioning could be considered negligible.⁴¹

Aqueous recoveries in positive controls without ferrihydrite ($n = 4$, 10 mM NaNO_3 , pH 5.8, equilibration 24 h) were typically higher than 90% of the total added amount of PFASs (sum of amounts in the solution phase and in MeOH extract of the empty control reactor). For substances that showed control recoveries below 90%, i.e., PFNA (86%), PFDA (87%), and FOSA (80%), the calculated pH-dependent sorption to ferrihydrite was corrected for losses to the reactor walls using a three-compartment equilibrium-based approach (Section S1.3 and Figure S1 in the Supporting Information). However, as reactor losses of organic chemicals (including PFOA) generally decrease with increasing aqueous concentrations,^{39,42,43} the sorption isotherm of FOSA was not

recalculated according to the above method, as we in this experiment employed significantly higher concentrations compared to those used in the pH-dependent sorption test and in the positive controls (i.e., most nominal isotherm additions were 50–2500 times larger).

RESULTS AND DISCUSSION

X-ray Absorption Spectroscopy. As shown in Figure 1, the sulfur K-edge white-line positions for adsorbed sulfonated PFASs (e.g., that of PFOS; 2480.7 eV) were close to that of dissolved dilute methylsulfonate (2481.1 eV), in which the sulfur atom has a formal and electronic oxidation state of +V. All of these white-line positions were also similar to those of the pure, solid PFAS standards (i.e., $2480.4\text{--}2480.9 \text{ eV}$; Table S13 in the Supporting Information). As the electronic oxidation state of S increases linearly with the white-line position relative to that of elemental (0) sulfur,^{28,44–49} it can be concluded that the sulfur atom in all measured PFASs (i.e., PFOS, FOSA, PFHxS) retained an oxidation state of +V after the adsorption of these PFASs onto both ferrihydrite and poorly crystalline Al hydroxide. In agreement with previous studies, sulfate onto Fh showed a pre-edge (Figure S6 in the Supporting Information), which reflects the involvement of inner-sphere complexes.^{30,33,50,51} A similar pre-edge was not observed for any of the three S-containing PFASs onto ferrihydrite, as no clear feature could be identified on the low-energy side of the main absorption peak, and as the spectra for the S-containing PFASs onto the Al hydroxide were identical in shape (Figures S7–S13 in the Supporting Information). Therefore, these results rule out a significant role of inner-sphere complexes for S-containing PFASs on ferrihydrite, in agreement with previous infrared evidence for PFOS on Fe oxides.^{17,25} Still, it is possible, or even likely, that the head group can form an outer-sphere complex.¹⁷ However, such an interaction is normally weak and would imply a strong role of electrostatic interactions in the PFAS binding process.

pH-Dependent Adsorption onto Ferrihydrite. The adsorption of all 12 investigated PFASs (i.e., PFBA, PFPeA, PFHxA, PFOA, PFNA, PFDA, PFBS, PFHxS, PFOS, FOSA, 6:2 FTSA, 8:2 FTSA) was inversely related to pH ($p < 0.05$) (Figure 2 and Tables S4–S8 in the Supporting Information). This was attributed to the pH-dependent charge of the ferrihydrite surface, i.e., the lower the pH value, the larger the positive surface net charge (Figure 3) and thus the larger the attraction between the ferrihydrite surface and the negatively charged PFAS anions. At pH values between 4 and 5, the ζ -potential was $>27 \text{ mV}$, which decreased to nearly zero at pH 7.7, in agreement with the PZC of pH ~ 8.1 reported for 2-line ferrihydrite.²⁶ At pH values ≤ 5 , there was a stronger adsorption of long-chained PFASs (i.e., PFOA, PFNA, PFDA, PFHxS, PFOS, FOSA, 6:2 FTSA, 8:2 FTSA) compared to that of the short-chained PFASs (i.e., PFBA, PFPeA, PFHxA, PFBS) (Figures 2 and S2–S4 and Table S7 in the Supporting Information). For example, at pH 4, the sorption percentage of the long-chained PFASs was between 60% (PFOA) and 100% (PFDA), whereas it ranged from 31% (PFPeA) to 43% (PFHxA) for the short-chained PFASs. However, at pH values higher than 5, the overall sorption was low, and there was no evident difference in the degree of adsorption between long-chained and short-chained PFASs (Figures 2 and S2–S4 and Table S7 in the Supporting Information). This indicates that to achieve $> 50\%$ sorption to ferrihydrite, a strongly positively charged surface is required (ζ -

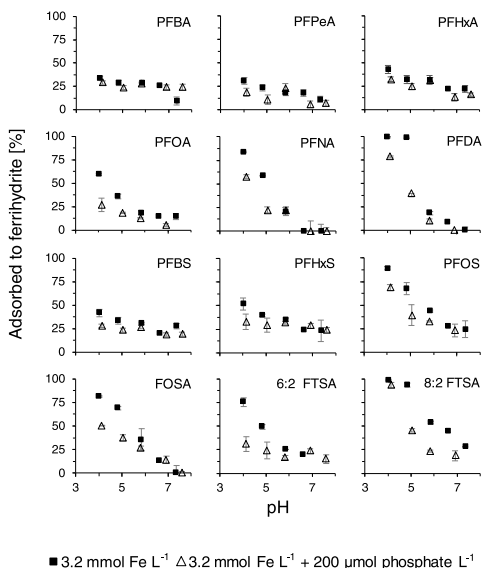


Figure 2. Effect of pH on PFAS adsorption onto ferrihydrite in the absence and presence of phosphate. PFAS additions ranged from 1.6 nmol L⁻¹ (PFDA) to 5.5 nmol L⁻¹ (PFBS). The error bars represent the standard error of the mean ($n = 3$).

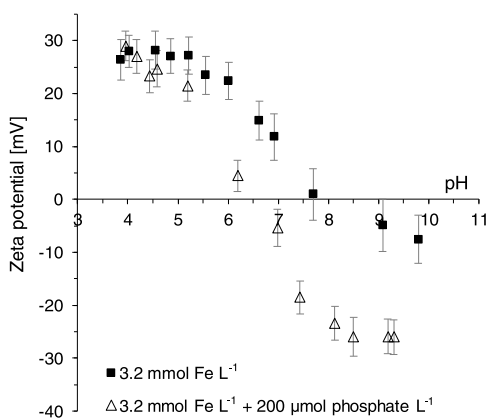


Figure 3. Ferrihydrite ζ -potential as a function of pH and added phosphate. The error bars represent the standard deviation within each measurement.

potential $> +20$ to 25 mV, Figure 3), and in addition, the PFAS molecule needs to be of sufficient chain length in terms of its number of perfluorinated carbons (i.e., C₆ or longer).

At low pH, the binding of the long-chained PFASs was significant despite the fact that the sulfonate and carboxylate head groups are weakly charged and likely not able to compete strongly with the electrolyte anions (0.01 M NO₃⁻) in the studied systems, if only electrostatic interactions of the head

group were involved. Hence, such a mechanism is not sufficient to explain PFAS binding. Further, the observation that long-chained PFASs are sorbed more strongly than short-chained PFASs to ferrihydrite strongly suggests that the role of specific interactions (i.e., as inner-sphere or outer-sphere complexes), although they may exist, is rather small, despite earlier research showing surface complex formation between the head group of a PFAS (PFOS and PFOA) and Fe oxide.^{17,24,25}

Instead, the stronger adsorption of the long-chained PFASs is consistent with a substantial additional contribution of the weakly negatively charged fluorine moieties to the overall electrostatic interaction, as suggested by Johnson et al.²¹ and Xiao et al.²³ Although the charge excess for dissolved PFOS has been reported to be only around -0.1 to -0.2 per fluorine atom,^{23,53} the electron density should be sufficient to induce hydrogen bonding between the fluorine moieties and positively charged $-\text{OH}_2^{1/2+}$ or $-\text{O}_3\text{H}^{1/2+}$ groups of ferrihydrite, which may act as proton donors. The probable significance of a strong involvement of the tail in the sorption process is underlined also by the strong sorption of FOSA at low pH, as the head group of FOSA (i.e., SO₂NH₂) is not charged under low-pH conditions ($\text{p}K_a = 6.24$,⁵⁴ 6.52⁵⁵). The differences between different PFASs may be explained by multiple F⁻HO sorptive contacts for long-chained PFASs, which would stabilize sorption. A related mechanism has earlier been suggested for PAH sorption on goethite, based on DFT calculations.⁵⁶ For a short-chained PFAS such as PFBS, there are fewer fluorine atoms available for binding, which makes sorption rather inefficient also at low pH.

Effects of Phosphate and Surface Charge. In general, the adsorption of PFASs onto ferrihydrite decreased with the addition of phosphate (Figure 2). The decreased PFAS binding can be related to the ζ -potential, which also decreased with increasing pH at pH > 5 (Figure 3). With the exception of PFBA, the decrease in adsorption of all investigated PFASs upon the addition of phosphate anions was significantly ($p < 0.05$) related to the decrease in positive charge on the ferrihydrite surface (ζ -potential) due to the presence of adsorbed phosphate (Figures 4 and S5, linear regression given in Table S9 in the Supporting Information). The strong relationship with the ζ -potential for the sorption of individual PFASs in both phosphate-containing and phosphate-free systems provides further support to the idea forwarded in the previous section, i.e., that electrostatic interactions are important for PFAS sorption. However, for two of the weakest binding PFASs, i.e., PFBS and PFBA, the relationship with the ζ -potential was less convincing (Figure 4), and in the case of PFBA statistically nonsignificant (Table S9 in the Supporting Information). Whether this is due to uncertainties in the analytical measurements or reflects the presence of an additional weak sorption mechanism (e.g., oleophobic) cannot be determined from the current data.

Sorption Isotherms. As evident from Figure 5, the sorption isotherms of PFOS and PFOA onto ferrihydrite were both nonlinear (Tables S11 and S12 in the Supporting Information), and for both isotherms, the Langmuir equation provided a better fit compared to the Freundlich equation (Table S12 in the Supporting Information). Hence, the isotherms may be interpreted as being consistent with adsorption in the form of a monolayer, as also suggested by Tang et al.¹⁴ and Johnson et al.²¹ for nonlinear adsorption of PFOS onto goethite. In this study, the Langmuir maximum

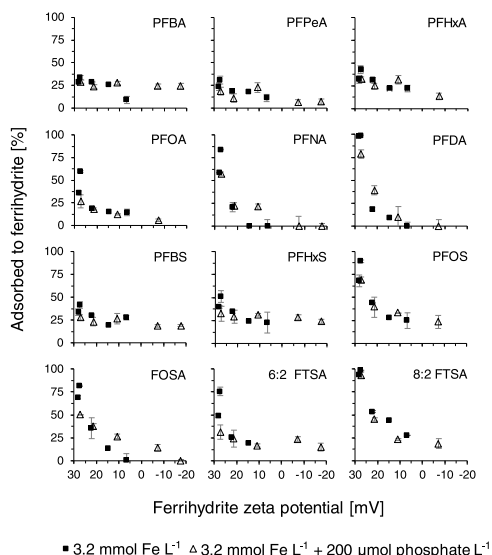


Figure 4. PFAS adsorption onto ferrihydrite as a function of ζ -potential in the absence and presence of added phosphate. ζ -potential values on the horizontal axis are given in reverse order, to reflect the negative relationship with the pH value.

ferrihydrite surface coverage Q_{\max} was calculated to be 180 and $160 \mu\text{mol mol}^{-1} \text{Fe}$, equivalent to 1.6 and $1.4 \mu\text{g m}^{-2}$ for PFOS and PFOA, respectively, when a surface area of $650 \text{ m}^2 \text{ g}^{-1}$ for ferrihydrite is used. These values are low in comparison to the calculated net positive charge of the ferrihydrite of $\sim 10 \text{ mol mol}^{-1} \text{Fe}$, as calculated by the model of Tiberghien et al.² for the experimental conditions given in Figure 5, but for PFOS, they are reasonably close to the Langmuir maxima previously given for goethite, i.e., 1.2 and $2.4 \mu\text{g m}^{-2}$ by Johnson et al.²¹ and Tang et al.,¹⁴ respectively. The K_d value (i.e., the solid–solution distribution coefficient) for adsorption of PFOS onto ferrihydrite at pH 4.5 is about $3300 \text{ L kg}^{-1} \text{Fe}$ at an aqueous equilibrium concentration of $0.75 \mu\text{mol PFOS L}^{-1}$. This is essentially the same value as that obtained for “nanosized

Fe_2O_3 ” (K_d recalculated from the work of Lu et al.³⁷), despite the higher pH (7.0) of the Fe_2O_3 system. Still, the estimated Q_{\max} values obtained in our work are surprisingly low compared to what would be expected for inorganic ions. This suggests that not all of the charged sites were readily accessible to the PFASs, for steric reasons or because of the aggregated and microporous structure of our ferrihydrite, which may have prevented the PFASs from binding to a large part of the charged ferrihydrite structure.

The sorption isotherm of FOSA onto ferrihydrite was relatively linear up to an approximate aqueous equilibrium concentration of $0.65 \mu\text{mol L}^{-1}$ (Figure 5). In the isotherm experiments, the overall order of sorption affinity to ferrihydrite was PFOS > FOSA \approx PFOA. Thus, the presence of a negatively charged head group (SO_3^- in PFOS) was generally observed to favor sorption compared to the presence of an uncharged functional group (SO_2NH_2 (FOSA)), suggesting that for PFOS, both the charged head group and the fluorine moieties were important for sorption. However, at the highest aqueous concentration of the respective isotherm, the adsorption of FOSA was significantly larger compared to that of PFOS and PFOA. A possible explanation for the higher adsorption of FOSA at high aqueous concentration may be that the FOSA molecules self-aggregated, i.e., formed hemimicelles,^{23,58} at the ferrihydrite–solution interface. For amphiphilic compounds, it has been estimated that hemimicelles may be formed at mineral surfaces when the aqueous concentration exceeds between 0.1 and 1% of the critical micelle concentration (CMC).⁴¹ While no values for the CMC of FOSA were found in the literature, the CMC of PFOS has been reported to lie in the range of $6.3\text{--}9 \text{ mmol L}^{-1}$.^{59–61} However, given the stronger hydrophobic character of the neutral FOSA molecule compared to that of the charged PFOS anion, one may assume that FOSA would exhibit a somewhat lower CMC in relation to PFOS. If so, this could make FOSA hemimicelle formation on ferrihydrite possible at aqueous concentrations of approximately $1 \mu\text{mol L}^{-1}$, consistent with the observed isothermal sorption of the substance.

Environmental Implications. The results presented here indicate that at low pH, ferrihydrite and other poorly crystalline Fe and Al (hydr)oxides could contribute significantly to binding of PFASs in soils. For example, $\log K_d$ values ($\text{L kg}^{-1} \text{Fe}$) for PFOS and PFOA at pH 5 were approximately 4.1 and 3.5, respectively, in the absence of phosphate. Hence, partitioning onto pure ferrihydrite was $1.4 \pm 0.1 \text{ log units}$

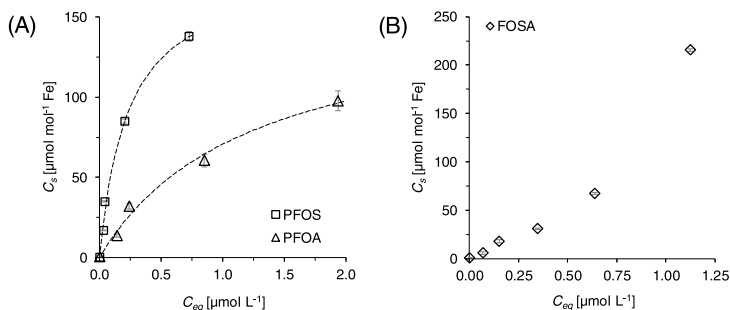


Figure 5. Sorption isotherms for (A) PFOS and PFOA, and (B) FOSA, onto ferrihydrite ($10 \text{ mmol Fe L}^{-1}$) at pH 4.4–4.6. The dashed lines represent the fitted Langmuir isotherms.

larger than the corresponding organic carbon-normalized sorption ($\log K_{OC}$ ($/L\ kg^{-1}\ C$)) commonly found for midrange soil and sediment concentrations, i.e., ~ 2.8 and ~ 2.0 log units for PFOS and PFOA, respectively.^{62–68}

However, it needs to be acknowledged that the properties of pure ferrihydrite systems will differ from those found in the field. Perhaps most crucially, the net positive surface charge of Fe and Al (hydr)oxides in soils and sediments is expected to be lower than for the pure minerals, due to the presence of adsorbed phosphate and organic matter. For example, the PZC of naturally occurring ferrihydrite has been reported to be between pH 5.3 to 7.5 with emphasis on the lower values,^{69,70} i.e., significantly lower than that of laboratory-derived ferrihydrite. Consequently, under field conditions, the contribution of Fe and Al (hydr)oxides to PFAS binding is likely to be smaller than under laboratory conditions with isolated, pure mineral phases. The surface charge of natural ferrihydrite is critical not least because PFAS sorption is predominantly electrostatic in nature, and that surface complexes with the head group, if they are formed, are weak: if stronger inner-sphere complexes had formed, the PFAS binding would have been stronger and less sensitive to the surface charge. Although some studies do indicate a role of Fe and Al (hydr)oxides for PFAS sorption, for example, in tropical soils,⁷¹ additional research is needed to more accurately determine the relative roles of organic matter and (hydr)oxide surfaces.

In summary, the above findings allow us to conclude that Fe oxides such as ferrihydrite could be important for PFAS sorption in acidic environments (pH 5 or lower), especially if the content of organic matter and phosphate (that decrease the surface charge) is low, and if the PFAS in question is of sufficient chain length, C_6 or longer.

■ ASSOCIATED CONTENT

Supporting Information

The Supporting Information is available free of charge at <https://pubs.acs.org/doi/10.1021/acs.est.0c01646>.

Beamline equipment for S K-edge XANES measurements; details on PFAS analytical method; positive control recoveries and method to correct for losses to reactors; PFAS native and internal standards; chemical recipe for pH-dependent sorption experiment; pH-dependent sorption data; linear regressions; ζ -potentials; phosphate adsorption onto ferrihydrite; isotherm sorption data and its derived parameters; details on samples measured with S K-edge XANES spectroscopy and their spectra; and normalized spectra, and spectra derivatives, for adsorbed individual PFASs and sulfate (PDF)

■ AUTHOR INFORMATION

Corresponding Author

Hugo Campos-Pereira – Department of Soil and Environment, Swedish University of Agricultural Sciences (SLU), SE-750 07 Uppsala, Sweden; orcid.org/0000-0002-8023-0767; Phone: +46 (0)18 671243; Email: hugo.pereira@slu.se

Authors

Dan B. Kleja – Department of Soil and Environment, Swedish University of Agricultural Sciences (SLU), SE-750 07

Uppsala, Sweden; Swedish Geotechnical Institute (SGI), SE-581 93 Linköping, Sweden

Carin Sjöstedt – Department of Soil and Environment, Swedish University of Agricultural Sciences (SLU), SE-750 07 Uppsala, Sweden; orcid.org/0000-0001-6490-1658

Lutz Ahrens – Department of Aquatic Sciences and Assessment, Swedish University of Agricultural Sciences (SLU), SE-750 07 Uppsala, Sweden; orcid.org/0000-0002-5430-6764

Wantana Klysubun – Synchrotron Light Research Institute, Nakhon Ratchasima 30000, Thailand

Jon Petter Gustafsson – Department of Soil and Environment, Swedish University of Agricultural Sciences (SLU), SE-750 07 Uppsala, Sweden; Department of Sustainable Development, Environmental Science and Engineering, KTH Royal Institute of Technology, SE-100 44 Stockholm, Sweden

Complete contact information is available at: <https://pubs.acs.org/10.1021/acs.est.0c01646>

Notes

The authors declare no competing financial interest.

■ ACKNOWLEDGMENTS

This research was gratefully supported by the Swedish Research Council (Vetenskapsrådet) (grant number 2015-03938). The authors further acknowledge Geert Cornelis and Jani Tuoriniemi at the Swedish University of Agricultural Sciences (SLU), for initial assistance with ζ -potential measurements. G. Almkvist, K. Boye, and I. Persson are acknowledged for kindly providing S K-edge XANES spectra for reference. The authors thank the staff at Beamline 8 (BL8), Synchrotron Light Research Institute (Nakhon Ratchasima, Thailand), for support during the XANES data collection. The authors also thank Farid Jan (SLU) for quantification of aqueous iron and phosphate, and Vera Franke and Mattias Söregård (SLU) for assistance with parts of the PFAS analyses.

■ REFERENCES

- Jambor, J. L.; Dutrizac, J. E. Occurrence and Constitution of Natural and Synthetic Ferrihydrite, a Widespread Iron Oxyhydroxide. *Chem. Rev.* **1998**, *98*, 2549–2586.
- Tiberg, C.; Sjöstedt, C.; Persson, I.; Gustafsson, J. P. Phosphate Effects on Copper(II) and Lead(II) Sorption to Ferrihydrite. *Geochim. Cosmochim. Acta* **2013**, *120*, 140–157.
- Tiberg, C.; Gustafsson, J. P. Phosphate Effects on Cadmium(II) Sorption to Ferrihydrite. *J. Colloid Interface Sci.* **2016**, *471*, 103–111.
- Davis, J. A.; Leckie, J. O. Surface Ionization and Complexation at the Oxide/Water Interface II. Surface Properties of Amorphous Iron Oxyhydroxide and Adsorption of Metal Ions. *J. Colloid Interface Sci.* **1978**, *67*, 90–107.
- Goldberg, S. Competitive Adsorption of Arsenate and Arsenite on Oxides and Clay Minerals. *Soil Sci. Soc. Am. J.* **2002**, *66*, 413–421.
- Hiemstra, T.; Zhao, W. Reactivity of Ferrihydrite and Ferritin in Relation to Surface Structure, Size, and Nanoparticle Formation Studied for Phosphate and Arsenate. *Environ. Sci. Nano* **2016**, *3*, 1265–1279.
- Schwertmann, U. Occurrence and Formation of Iron Oxides in Various Pedoenvironments. In *Iron in Soils and Clay Minerals*; Stucki, J. W.; Goodman, B. A.; Schwertmann, U., Eds.; Springer: Netherlands: Dordrecht, 1988; pp 267–308.
- Karlton, E.; Bain, D. C.; Gustafsson, J. P.; Mannerkoski, H.; Murad, E.; Wagner, U.; Fraser, A. R.; McHardy, W. J.; Starr, M. Surface Reactivity of Poorly-Ordered Minerals in Podzol B Horizons. *Geoderma* **2000**, *94*, 265–288.

- (9) Tiberg, C.; Sjöstedt, C.; Gustafsson, J. P. Metal Sorption to Spodosol Bs Horizons: Organic Matter Complexes Predominate. *Chemosphere* **2018**, *196*, 556–565.
- (10) Banzhaf, S.; Filipovic, M.; Lewis, J.; Sparrenbom, C. J.; Barthel, R. A Review of Contamination of Surface, Ground-, and Drinking Water in Sweden by Perfluoroalkyl and Polyfluoroalkyl Substances (PFASs). *Ambio* **2017**, *46*, 335–346.
- (11) Park, S.; Lee, L. S.; Medina, V. F.; Zull, A.; Waisner, S. Heat-Activated Persulfate Oxidation of PFOA, 6:2 Fluorotelomer Sulfonate, and PFOS under Conditions Suitable for in-Situ Groundwater Remediation. *Chemosphere* **2016**, *145*, 376–383.
- (12) von der Trenck, K. T.; Konietzka, R.; Biegel-Engler, A.; Brodsky, J.; Hädicke, A.; Quadflieg, A.; Stockerl, R.; Stahl, T. Significance Thresholds for the Assessment of Contaminated Groundwater: Perfluorinated and Polyfluorinated Chemicals. *Environ. Sci. Eur.* **2018**, *30*, No. 19.
- (13) Helsing, M. S.; Josefsson, S.; Hughes, A. V.; Ahrens, L. Sorption of Perfluoroalkyl Substances to Two Types of Minerals. *Chemosphere* **2016**, *159*, 385–391.
- (14) Tang, C. Y.; Shiang, F. Q.; Gao, D.; Criddle, C. S.; Leckie, J. O. Effect of Solution Chemistry on the Adsorption of Perfluorooctane Sulfonate onto Mineral Surfaces. *Water Res.* **2010**, *44*, 2654–2662.
- (15) Wang, F.; Shih, K. Adsorption of Perfluorooctanesulfonate (PFOS) and Perfluorooctanoate (PFOA) on Alumina: Influence of Solution pH and Cations. *Water Res.* **2011**, *45*, 2925–2930.
- (16) Zhao, L.; Bian, J.; Zhang, Y.; Zhu, L.; Liu, Z. Comparison of the Sorption Behaviors and Mechanisms of Perfluorosulfonates and Perfluorocarboxylic Acids on Three Kinds of Clay Minerals. *Chemosphere* **2014**, *114*, 51–58.
- (17) Gao, X.; Chorover, J. Adsorption of Perfluorooctanoic Acid and Perfluorooctanesulfonic Acid to Iron Oxide Surfaces as Studied by Flow-through ATR-FTIR Spectroscopy. *Environ. Chem.* **2012**, *9*, 148–157.
- (18) Wang, F.; Liu, C.; Shih, K. Adsorption Behavior of Perfluorooctanesulfonate (PFOS) and Perfluorooctanoate (PFOA) on Boehmite. *Chemosphere* **2012**, *89*, 1009–1014.
- (19) Wang, F.; Shih, K.; Leckie, J. O. Effect of Humic Acid on the Sorption of Perfluorooctane Sulfonate (PFOS) and Perfluorobutane Sulfonate (PFBS) on Boehmite. *Chemosphere* **2015**, *118*, 213–218.
- (20) Uwayezu, J.-N.; Yeung, L. W. Y.; Bäckström, M. Sorption of PFOS Isomers on Goethite as a Function of pH, Dissolved Organic Matter (Humic and Fulvic Acid) and Sulfate. *Chemosphere* **2019**, *233*, 896–904.
- (21) Johnson, R. L.; Anschutz, A. J.; Smolen, J. M.; Simcik, M. F.; Penn, R. L. The Adsorption of Perfluorooctane Sulfonate onto Sand, Clay, and Iron Oxide Surfaces. *J. Chem. Eng. Data* **2007**, *52*, 1165–1170.
- (22) Jeon, J.; Kannan, K.; Lim, B. J.; An, K. G.; Kim, S. D. Effects of Salinity and Organic Matter on the Partitioning of Perfluoroalkyl Acid (PFAs) to Clay Particles. *J. Environ. Monit.* **2011**, *13*, 1803–1810.
- (23) Xiao, F.; Zhang, X.; Penn, L.; Gulliver, J. S.; Simcik, M. F. Effects of Monovalent Cations on the Competitive Adsorption of Perfluoroalkyl Acids by Kaolinite: Experimental Studies and Modeling. *Environ. Sci. Technol.* **2011**, *45*, 10028–10035.
- (24) Xu, T.; Ji, H.; Gu, Y.; Tong, T.; Xia, Y.; Zhang, L.; Zhao, D. Enhanced Adsorption and Photocatalytic Degradation of Perfluorooctanoic Acid in Water Using Iron (Hydr)Oxides/Carbon Sphere Composite. *Chem. Eng. J.* **2020**, *388*, No. 124230.
- (25) Zhang, Y.; Zhi, Y.; Liu, J.; Ghoshal, S. Sorption of Perfluoroalkyl Acids to Fresh and Aged Nanoscale Zerovalent Iron Particles. *Environ. Sci. Technol.* **2018**, *52*, 6300–6308.
- (26) Hiemstra, T.; Van Riemsdijk, W. H. A Surface Structural Model for Ferrihydrite I: Sites Related to Primary Charge, Molar Mass, and Mass Density. *Geochim. Cosmochim. Acta* **2009**, *73*, 4423–4436.
- (27) Goldberg, S.; Sposito, G. A Chemical Model of Phosphate Adsorption by Soils: II. Noncalcareous Soils. *Soil Sci. Soc. Am. J.* **1984**, *48*, 779–783.
- (28) Xia, K.; Weesner, F.; Bleam, W. F.; Helmke, P. A.; Bloom, P. R.; Skyllberg, U. L. XANES Studies of Oxidation States of Sulfur in Aquatic and Soil Humic Substances. *Soil Sci. Soc. Am. J.* **1998**, *62*, 1240–1246.
- (29) Boye, K.; Almkvist, G.; Nilsson, S. I.; Eriksen, J.; Persson, I. Quantification of Chemical Sulphur Species in Bulk Soil and Organic Sulphur Fractions by S K-Edge XANES Spectroscopy. *Eur. J. Soil Sci.* **2011**, *62*, 874–881.
- (30) Majzlan, J.; Alpers, C. N.; Koch, C. B.; McCleskey, R. B.; Myneni, S. C. B.; Neil, J. M. Vibrational, X-Ray Absorption, and Mössbauer Spectra of Sulfate Minerals from the Weathered Massive Sulfide Deposit at Iron Mountain, California. *Chem. Geol.* **2011**, *284*, 296–305.
- (31) Prietzel, J.; Wu, Y.; Dümig, A.; Zhou, J.; Klysubun, W. Soil Sulphur Speciation in Two Glacier Forefield Soil Chronosequences Assessed by S K-Edge XANES Spectroscopy. *Eur. J. Soil Sci.* **2013**, *64*, 260–272.
- (32) Zhu, M.; Northrup, P.; Shi, C.; Billings, S. J. L.; Sparks, D. L.; Waychunas, G. A. Structure of Sulfate Adsorption Complexes on Ferrihydrite. *Environ. Sci. Technol. Lett.* **2014**, *1*, 97–101.
- (33) Gu, C.; Wang, Z.; Kubicki, J. D.; Wang, X.; Zhu, M. X-Ray Absorption Spectroscopic Quantification and Speciation Modeling of Sulfate Adsorption on Ferrihydrite Surfaces. *Environ. Sci. Technol.* **2016**, *50*, 8067–8076.
- (34) Swedlund, P. J.; Webster, J. G. Adsorption and Polymerisation of Silicic Acid on Ferrihydrite, and Its Effect on Arsenic Adsorption. *Water Res.* **1999**, *33*, 3413–3422.
- (35) Schwertmann, U.; Cornell, R. M. *Iron Oxides in the Laboratory*; Wiley Books, 2000.
- (36) Gustafsson, J. P.; Persson, I.; Kleja, D. B.; van Schaik, J. W. J. Binding of Iron(III) to Organic Soils: EXAFS Spectroscopy and Chemical Equilibrium Modeling. *Environ. Sci. Technol.* **2007**, *41*, 1232–1237.
- (37) Klysubun, W.; Tarawarakarn, P.; Thamsanong, N.; Amonpattaratkit, P.; Cholsuk, C.; Lapboonrueng, S.; Chaichuay, S.; Wongtepa, W. Upgrade of SLRI BL8 Beamline for XAFS Spectroscopy in a Photon Energy Range of 1–13 keV. *Radiat. Phys. Chem.* **2020**, *175*, No. 108145.
- (38) Ravel, B.; Newville, M. ATHENA, ARTEMIS, HEPHAESTUS: Data Analysis for X-Ray Absorption Spectroscopy Using IFEFFIT. *J. Synchrotron Radiat.* **2005**, *12*, 537–541.
- (39) Lath, S.; Knight, E. R.; Navarro, D. A.; Kookana, R. S.; McLaughlin, M. J. Sorption of PFOA onto Different Laboratory Materials: Filter Membranes and Centrifuge Tubes. *Chemosphere* **2019**, *222*, 671–678.
- (40) Söregård, M.; Franke, V.; Tröger, R.; Ahrens, L. Losses of Poly- and Perfluoroalkyl Substances to Syringe Filter Materials. *J. Chromatogr. A* **2020**, *1609*, No. 460430.
- (41) Schwarzenbach, R. P.; Gschwend, P. M.; Imboden, D. M. *Environmental Organic Chemistry*; John Wiley & Sons, 2016.
- (42) Sharom, M. S.; Solomon, K. R. Adsorption and Desorption of Permethrin and Other Pesticides on Glass and Plastic Materials Used in Bioassay Procedures. *Can. J. Fish Aquat. Sci. Can.* **1981**, *199*–204.
- (43) Chlebowski, A. C.; Tanguay, R. L.; Simonich, S. L. M. Quantitation and Prediction of Sorptive Losses during Toxicity Testing of Polycyclic Aromatic Hydrocarbon (PAH) and Nitrated PAH (NPAH) Using Polystyrene 96-Well Plates. *Neurotoxicol. Teratol.* **2016**, *57*, 30–38.
- (44) Waldo, G.; Carlson, R. M. K.; Moldovan, J. M.; Peters, K. E.; Penner-Hahn, J. E. Sulfur Speciation in Heavy Petroleum: Information from X-Ray Absorption near-Edge Structure. *Geochim. Cosmochim. Acta* **1991**, *55*, 801–814.
- (45) Waldo, G. S.; Mullins, O. C.; Penner-Hahn, J. E.; Cramer, S. P. Determination of the Chemical Environment of Sulphur in Petroleum Asphaltenes by X-Ray Absorption Spectroscopy. *Fuel* **1992**, *71*, 53–57.
- (46) Spiro, C. L.; Wong, J.; Lytle, F. W.; Greigor, R. B.; Maylotte, D. H.; Lamson, S. H. X-Ray Absorption Spectroscopic Investigation of Sulfur Sites in Coal: Organic Sulfur Identification. *Science* **1984**, *226*, 48–50.

- (47) Huffman, G. P.; Shah, N.; Huggins, F. E.; Stock, L. M.; Chatterjee, K.; Kilbane, J. J.; Chou, M.-I. M.; Buchanan, D. H. Sulfur Speciation of Desulfurized Coals by XANES Spectroscopy. *Fuel* **1995**, *74*, 549–555.
- (48) Vairavamurthy, A.; Manowitz, B.; Luther, G. W.; Jeon, Y. Oxidation State of Sulfur in Thiosulfate and Implications for Anaerobic Energy Metabolism. *Geochim. Cosmochim. Acta* **1993**, *57*, 1619–1623.
- (49) Vairavamurthy, A.; Zhou, W.; Eglinton, T.; Manowitz, B. Sulfonates: A Novel Class of Organic Sulfur Compounds in Marine Sediments. *Geochim. Cosmochim. Acta* **1994**, *58*, 4681–4687.
- (50) Okude, N.; Nagoshi, M.; Noro, H.; Baba, Y.; Yamamoto, H.; Sasaki, T. A. P and S K-Edge XANES of Transition-Metal Phosphates and Sulfates. *J. Electron Spectrosc. Relat. Phenom.* **1999**, *101*–*103*, 607–610.
- (51) Majzlan, J.; Myneni, S. C. B. Speciation of Iron and Sulfate in Acid Waters: Aqueous Clusters to Mineral Precipitates. *Environ. Sci. Technol.* **2005**, *39*, 188–194.
- (52) Almkvist, G.; Boye, K.; Persson, I. K-Edge XANES Analysis of Sulfur Compounds: An Investigation of the Relative Intensities Using Internal Calibration. *J. Synchrotron Radiat.* **2010**, *17*, 683–688.
- (53) Erkoç, Ş.; Erkoç, F. Structural and Electronic Properties of PFOS and LiPFOS. *J. Mol. Struct.: THEOCHEM* **2001**, *549*, 289–293.
- (54) Rayne, S.; Forest, K. A New Class of Perfluorinated Acid Contaminants: Primary and Secondary Substituted Perfluoroalkyl Sulfonamides Are Acidic at Environmentally and Toxicologically Relevant PH Values. *J. Environ. Sci. Health, Part A: Toxic/Hazard. Subst. Environ. Eng.* **2009**, *44*, 1388–1399.
- (55) Steinle-Darling, E.; Reinhard, M. Nanofiltration for Trace Organic Contaminant Removal: Structure, Solution, and Membrane Fouling Effects on the Rejection of Perfluorochemicals. *Environ. Sci. Technol.* **2008**, *42*, 5292–5297.
- (56) Tunega, D.; Gerzabek, M. H.; Haberhauer, G.; Totsche, K. U.; Lischka, H. Model Study on Sorption of Polycyclic Aromatic Hydrocarbons to Goethite. *J. Colloid Interface Sci.* **2009**, *330*, 244–249.
- (57) Lu, X.; Deng, S.; Wang, B.; Huang, J.; Wang, Y.; Yu, G. Adsorption Behavior and Mechanism of Perfluorooctane Sulfonate on Nanosized Inorganic Oxides. *J. Colloid Interface Sci.* **2016**, *474*, 199–205.
- (58) Rayne, S.; Forest, K. Perfluoroalkyl Sulfonic and Carboxylic Acids: A Critical Review of Physicochemical Properties, Levels and Patterns in Waters and Wastewaters, and Treatment Methods. *J. Environ. Sci. Health, Part A: Toxic/Hazard. Subst. Environ. Eng.* **2009**, *44*, 1145–1199.
- (59) Sorli, J. B.; Låg, M.; Ekeren, L.; Perez-Gil, J.; Haug, L. S.; Da Silva, E.; Matrod, M. N.; Gützkow, K. B.; Lindeman, B. Per- and Polyfluoroalkyl Substances (PFASs) Modify Lung Surfactant Function and pro-Inflammatory Responses in Human Bronchial Epithelial Cells. *Toxicol. In Vitro* **2020**, *62*, No. 104656.
- (60) Shinoda, K.; Hato, M.; Hayashi, T. Physicochemical Properties of Aqueous Solutions of Fluorinated Surfactants. *J. Phys. Chem. A.* **1972**, *76*, 909–914.
- (61) Kissa, E. *Fluorinated Surfactants and Repellents*; Marcel Dekker, 2001.
- (62) Brusseau, M. L. Estimating the Relative Magnitudes of Adsorption to Solid-Water and Air/Oil-Water Interfaces for per- and Poly-Fluoroalkyl Substances. *Environ. Pollut.* **2019**, *254*, No. 113102.
- (63) Guelfo, J. L.; Higgins, C. P. Subsurface Transport Potential of Perfluoroalkyl Acids at Aqueous Film-Forming Foam (AFFF)-Impacted Sites. *Environ. Sci. Technol.* **2013**, *47*, 4164–4171.
- (64) Higgins, C. P.; Luthy, R. G. Sorption of Perfluorinated Surfactants on Sediments. *Environ. Sci. Technol.* **2006**, *40*, 7251–7256.
- (65) Chen, Y.-C.; Lo, S.-L.; Li, N.-H.; Lee, Y.-C.; Kuo, J. Sorption of Perfluoroalkyl Substances (PFASs) onto Wetland Soils. *Desalination Water Treat.* **2013**, *51*, 7469–7475.
- (66) Milinovic, J.; Lacorte, S.; Vidal, M.; Rigol, A. Sorption Behaviour of Perfluoroalkyl Substances in Soils. *Sci. Total Environ.* **2015**, *511*, 63–71.
- (67) Zhao, L.; Zhang, Y.; Fang, S.; Zhu, L.; Liu, Z. Comparative Sorption and Desorption Behaviors of PFHxS and PFOS on Sequentially Extracted Humic Substances. *J. Environ. Sci.* **2014**, *26*, 2517–2525.
- (68) Zhi, Y.; Liu, J. Sorption and Desorption of Anionic, Cationic and Zwitterionic Polyfluoroalkyl Substances by Soil Organic Matter and Pyrogenic Carbonaceous Materials. *Chem. Eng. J.* **2018**, *346*, 682–691.
- (69) Schwertmann, U.; Fechter, H. The Point of Zero Charge of Natural and Synthetic Ferrihydrites and Its Relation to Adsorbed Silicate. *Clay Miner.* **1982**, 471–476.
- (70) Rhoton, F. E.; Bigham, J. M. Natural Ferrihydrite as an Agent for Reducing Turbidity Caused by Suspended Clays. *J. Environ. Qual.* **2009**, *38*, 1887–1891.
- (71) Oliver, D. P.; Li, Y.; Orr, R.; Nelson, P.; Barnes, M.; McLaughlin, M. J.; Kookana, R. S. The Role of Surface Charge and PH Changes in Tropical Soils on Sorption Behaviour of Per- and Polyfluoroalkyl Substances (PFASs). *Sci. Total Environ.* **2019**, *673*, 197–206.

Supporting Information

**THE ADSORPTION OF PER- AND POLYFLUOROALKYL SUBSTANCES (PFASs)
ONTO FERRIHYDRITE IS GOVERNED BY SURFACE CHARGE**

Hugo Campos-Pereira ^{a*}, Dan B. Kleja ^{a,c}, Carin Sjöstedt ^a, Lutz Ahrens ^d, Wantana Klysubun ^e, Jon Petter Gustafsson ^{a,b}

* Corresponding author

^a Department of Soil and Environment, Swedish University of Agricultural Sciences (SLU), Box 7014, SE-750 07 Uppsala, Sweden

^b KTH Royal Institute of Technology, Department of Sustainable Development, Environmental Science and Engineering, Teknikringen 10B, SE-100 44 Stockholm, Sweden

^c Swedish Geotechnical Institute (SGI), SE-581 93 Linköping, Sweden

^d Department of Aquatic Sciences and Assessment, Swedish University of Agricultural Sciences (SLU), Box 7014, SE-750 07 Uppsala, Sweden

^e Synchrotron Light Research Institute, 111 Moo 6, Suranaree, Muang, Nakhon Ratchasima, 30000, Thailand

Number of pages: 24

Content summary

The Supporting Information includes 13 tables and 13 figures:

Tables

- Table S1.** PFAS native and internal standards – page S5
- Table S2.** pH-dependent sorption – recipe for sample preparation – page S6
- Table S3.** pH-dependent sorption – initial additions of individual PFASs [nmol L⁻¹] – page S7
- Table S4.** pH-dependent sorption – measured aqueous concentrations (PFASs, pH, phosphate, Fe) – page S7
- Table S5.** pH-dependent sorption – calculated adsorbed concentrations (PFASs, phosphate) – page S8
- Table S6.** pH-dependent sorption – percent adsorbed PFASs and phosphate – page S9
- Table S7.** pH-dependent sorption – log K_d values – page S10
- Table S8.** pH-dependent sorption – linear regression log K_d vs pH – page S14
- Table S9.** pH-dependent sorption – linear regression log K_d vs zeta potential – page S14
- Table S10.** pH-dependent sorption – zeta potential as a function of pH and added phosphate – page S15
- Table S11.** Sorption isotherms – PFOS, PFOA and FOSA – pages S17–S18
- Table S12.** Sorption isotherm parameters – PFOS, PFOA and FOSA – page S18
- Table S13.** S K-edge XANES spectroscopy – sample properties, and features of spectra – page S19

Figures

- Figure S1.** Recoveries in positive controls, solution–reactor partitioning coefficients – page S11
- Figure S2.** PFCA log K_d values as affected by chain length and pH – page S12
- Figure S3.** log K_d values for PFASs as affected by chain length and pH, log K_d values for FOSA as affected by pH – page S12
- Figure S4.** log K_d values for 6:2 and 8:2 FTSA as affected by chain length and pH – page S13
- Figure S5.** Phosphate adsorption onto ferrihydrite as affected by pH – page S16
- Figure S6.** Sulfur K-edge XANES first derivative of the pre-edge of sulfate on ferrihydrite – page S20
- Figure S7.** Sulfur K-edge XANES first derivative of PFOS on ferrihydrite – page S20
- Figure S8.** Sulfur K-edge XANES first derivative of FOSA on ferrihydrite – page S21
- Figure S9.** Sulfur K-edge XANES first derivative of PFOS on poorly crystalline aluminum hydroxide – page S21
- Figure S10.** Stacked normalized sulfur K-edge XANES spectra for FOSA on ferrihydrite and poorly crystalline aluminum hydroxide – page S22
- Figure S11.** Stacked normalized sulfur K-edge XANES spectra for PFOS on ferrihydrite and poorly crystalline aluminum hydroxide – page S22
- Figure S12.** Stacked normalized sulfur K-edge XANES spectra for PFHxS on poorly crystalline aluminum hydroxide – page S23
- Figure S13.** Stacked normalized sulfur K-edge XANES spectra for sulfate on ferrihydrite and poorly crystalline aluminum hydroxide – page S23

Section S1. Additional information – Material and methods (text)

- Section S1.1.** Beamline equipment – sulfur K-edge XANES spectroscopy – page S3
- Section S1.2.** Analysis of aqueous PFAS concentrations – additional information – page S3
- Section S1.3.** Calculation of ferrihydrite sorption – accounting for losses to reactors – pages S3–S4

S1. Additional information – Materials and methods

S1.1 Beamline equipment – sulfur K-edge XANES (X-ray absorption near-edge structure) spectroscopy

The beamline (BL-8, Synchrotron Light Research Institute (SLRI), Nakhon Ratchasima, Thailand) was equipped with an InSb(111) double crystal monochromator yielding a beam flux of $1.3 \times 10^9 - 6 \times 10^{10}$ photons s^{-1} (100 mA) $^{-1}$ in a 17.7×0.9 mm 2 beam 1 . To minimize X-ray absorption by air, the sample chamber was filled with helium (He) gas. Data was collected using a solid-state, 13-element Ge fluorescence detector. 1

S1.2 Additional information – analysis of aqueous PFAS concentrations

The injected volume (10 μ L) was separated on an Acquity UPLC BEH-C18 analytical column (1.7 μ m, 50 mm, Waters, UK) using an eluent gradient of 12 min. Mobile phase was milli-Q water (LC-PAC quality) with 5 mmol L $^{-1}$ ammonium acetate and 2% (v/v) acetonitrile. All integrations were checked manually and concentrations were evaluated using a 9-point calibration curve (0.01–100 ng mL $^{-1}$, all r^2 values ≥ 0.99).

S1.3 Calculation of ferrihydrite sorption – accounting for losses to reactors

For substances that showed recoveries below 90% in the positive controls, i.e. PFNA (86%), PFDA (87%) and FOSA (80%), the calculated pH-dependent sorption to ferrihydrite was corrected for losses to the reactor walls. A reactor–solution distribution coefficient $K_{reactor}$ [mL] was calculated from the aqueous PFAS concentration of the positive control ($C_{W,control}$) and the amount of PFAS extracted from the walls of the empty reactor ($m_{reactor,control}$) (24h shaking with MeOH):

$$K_{reactor} = \frac{m_{reactor,control}}{C_{W,control}}$$

Subsequently, the $K_{reactor}$ coefficient was used to calculate the amount of PFASs sorbed to the reactor walls ($m_{reactor}$) in the pH-dependent sorption experiment:

$$m_{reactor} = C_W \cdot K_{reactor}$$

where C_W is the measured aqueous PFAS concentration.

The K_d values for the sorption onto ferrihydrite were then corrected according to

$$K_{d,ferrihydrite} = ((total\ sorbed - m_{reactor}) / \text{mass of Fe in system}) / C_W$$

where *total sorbed* denotes the total aqueous loss in the sorption experiment, i.e. the sum of the losses to ferrihydrite and to the reactor walls.

In cases where this corrected mass balance yielded a negative value for the sorbed amount of PFASs onto ferrihydrite, the sorption onto ferrihydrite was assigned the value zero if the mass balance corresponded to a figure between <0% to -10% sorption. If the corrected value corresponded to < -10% sorption onto ferrihydrite, the data point was excluded.

Positive control recoveries and calculated K_{reactor} values are given in Fig. S1 in the Supporting Information.

S2. Sorption experiments

S2.1

Table S1. PFAS native and internal standards.

Substance	Acronym	Chemical formula (dissociated)	Internal standard for quantification
Perfluorobutanoate	PFBA	C ₃ F ₇ COO ⁻	¹³ C ₄ -PFBA
Perfluoropentanoate	PFPeA	C ₄ F ₉ COO ⁻	¹³ C ₂ -PFHxA
Perfluorohexanoate	PFHxA	C ₅ F ₁₁ COO ⁻	¹³ C ₂ -PFHxA
Perfluorooctanoate	PFOA	C ₇ F ₁₅ COO ⁻	¹³ C ₄ -PFOA
Perfluorononanoate	PFNA	C ₈ F ₁₇ COO ⁻	¹³ C ₅ -PFNA
Perfluorodecanoate	PFDA	C ₉ F ₁₉ COO ⁻	¹³ C ₂ -PFDA
Perfluorobutanoate	PFBS	C ₄ F ₉ SO ₃ ⁻	¹⁸ O ₂ -PFHxS
Perfluorohexane sulfonate	PFHxS	C ₆ F ₁₃ SO ₃ ⁻	¹⁸ O ₂ -PFHxS
Perfluorooctane sulfonate	PFOS	C ₈ F ₁₇ SO ₃ ⁻	¹³ C ₄ -PFOS
Perfluorooctane sulfonamide	FOSA	C ₈ F ₁₇ SO ₂ NH ₂ ^a	¹³ C ₈ -FOSA
6:2 fluorotelomer sulfonate	6:2 FTSA	C ₆ F ₁₃ CH ₂ CH ₂ SO ₃ ⁻	¹⁸ O ₂ -PFHxS
8:2 fluorotelomer sulfonate	8:2 FTSA	C ₈ F ₁₇ CH ₂ CH ₂ SO ₃ ⁻	¹³ C ₄ -PFOS

^aThe non-ionic species is expected to predominate in the larger part of the investigated pH range of 4 to 7.6 (pK_a(*n*-FOSA) = 6.52²).

S2.2 pH-dependent sorption experiment in the absence and presence of phosphate

S2.2.1 Recipe for sample preparation

Table S2. Recipe for pH-dependent sorption experiment in batch mode. Stated pH values were targeted values.

Samples:	Vol. (mL) of 20 mM HNO ₃	Vol. (mL) of 100 mM NaOH	Vol. (mL) of 36 mM Fe(NO ₃) ₃	Vol. (mL) of 20 mM NaH ₂ PO ₄	Vol. (mL) of 0.1 M NaNO ₃	Vol. (mL) Milli-Q water	Total vol. (mL) of suspension
3.2 mM Fe as Fh							
Fh pH 4	0.160	0	3.50	0	0.219	36.1	40.0
Fh pH 5	0	0.040	3.50	0	0.220	36.2	40.0
Fh pH 6	0	0.110	3.50	0	0.220	36.2	40.0
Fh pH 7	0	0.140	3.50	0	0.220	36.1	40.0
Fh pH 8	0	0.160	3.50	0	0.220	36.1	40.0
3.2 mM Fe as Fh + 200 μM PO ₄ ³⁻							
Fh + PO ₄ ³⁻ pH 4	0.160	0	3.50	0.400	0.219	35.7	40.0
Fh + PO ₄ ³⁻ pH 5	0	0.020	3.50	0.400	0.220	35.9	40.0
Fh + PO ₄ ³⁻ pH 6	0	0.040	3.50	0.400	0.220	35.8	40.0
Fh + PO ₄ ³⁻ pH 7	0	0.080	3.50	0.400	0.220	35.8	40.0
Fh + PO ₄ ³⁻ pH 8	0	0.133	3.50	0.400	0.220	35.7	40.0

S2.2.2 Measured aqueous concentrations

Table S3. Initial additions (positive blanks) of individual PFASs [nmol L^{-1}] employed in the multi-solute pH-dependent sorption experiment. A pH- and ionic strength-adjusted supernatant (filtered at $0.2 \mu\text{m}$) from the synthesis of ferrihydrite was used as matrix.

	PFBA	PFPeA	PFHxA	PFOA	PFNA	PFDA	PFBS	PFHxS	PFOS	FOSA	6:2 FTSA	8:2 FTSA
nmol L^{-1}	2.0	1.8	2.1	2.8	1.7	1.6	5.5	3.7	3.9	2.9	4.1	2.2

Table S4. Measured aqueous concentrations in the pH-dependent sorption experiment.

Measured aqueous concentrations (C_{eq})																
Unit	n	pH	Fe^{a}	mg L^{-3} PO_4^{3-}	ng L^{-1} PFBA	ng L^{-1} PFPeA	ng L^{-1} PFHxA	ng L^{-1} PFOA	ng L^{-1} PFNA	ng L^{-1} PFDA	ng L^{-1} PFBS	ng L^{-1} PFHxS	ng L^{-1} PFOS	ng L^{-1} FOSA	ng L^{-1} 6:2 FTSA	ng L^{-1} 8:2 FTSA
LoQ			0.04 mg L^{-1}	0.02	100	25	15	20	10	10	74	15	10	10	100	10
Negative blank	2	4.60		<LoQ	<LoQ	<LoQ	<LoQ	<LoQ	<LoQ	<LoQ	<LoQ	<LoQ	<LoQ	<LoQ	<LoQ	<LoQ
Positive blank ^a	2	6.80	nd		433	480	649	1140	773	794	1657	1486	1968	1465	1747	1179
Fh 4	3	4.01	0.02%	n.d.	288	331	371	459	107	6.50^{c}	969	722	142	217	428	17
Fh 5	3	4.83	<LoQ	n.d.	309	367	441	728	274	11.5	1103	896	634	362	889	76
Fh 6	3	5.85	nd	n.d.	309	392	446	929	524	562	1156	971	1105	756	1082	547
Fh 7	1 ^b	6.62	nd	n.d.	322	393	505	968	698	627	1334	1130	1423	1014	1408	655
Fh 8	3	7.36	nd	n.d.	393	427	506	974	668	770	1200	1143	1483	1163	1872^{d}	844
Fh + 200 $\mu\text{M PO}_4^{3-}$ 4	3	4.13	<LoQ	<LoQ	307	391	440	834	282	146	1198	1001	626	584	1201	78
Fh + 200 $\mu\text{M PO}_4^{3-}$ 5	3	5.04	<LoQ	<LoQ	331	429	489	931	516	420	1272	1052	1190	732	1382	646
Fh + 200 $\mu\text{M PO}_4^{3-}$ 6	3	5.82	<LoQ	<LoQ	312	371	444	997	519	618	1219	1017	1320	860	1454	904
Fh + 200 $\mu\text{M PO}_4^{3-}$ 7	3	6.91	<LoQ	0.099	328	456	564	1075	694	726	1349	1061	1509	1006	1333	959
Fh + 200 $\mu\text{M PO}_4^{3-}$ 8	3	7.60	<LoQ	1.25	329	447	545	901	698	774	1343	1125	1146	1263	1482	729

^a% of initial addition for ferrihydrite synthesis ($3.2 \text{ mmol Fe L}^{-1}$), if not stated otherwise.

^bpH- and ionic strength-adjusted supernatant (filtered at $0.2 \mu\text{m}$) from the synthesis of ferrihydrite was used as matrix.

^cTwo samples were removed due to suspected carry-over from the calibration curve.

^d<LoQ

^eThe measured concentration was higher than the initial addition (i.e. concentration of positive blank).

Thus the value was removed from subsequent data treatment.

LoQ = Limit of Quantification

nd = not determined

S2.2.3 Calculated adsorbed concentrations of PFASs

Table S5. Calculated adsorbed concentrations of PFASs in the pH-dependent sorption experiment.

Sample	pH	PO ₄ ³⁻	PFBA	PFPeA	PFHxA	PFOA	PFNA	PFDA	PFBS	PFHxS	PFOS	FOSA	6:2 FTSA	8:2 FTSA
Unit		mg g ⁻¹ Fe	ng g ⁻¹ Fe											
Fh 4	4.0		825	848	1581	3869	3768	4470	3915	4343	10378	6783	7498	6604
Fh 5	4.8		705	645	1185	2338	2582	4438	3153	3359	7582	5754	4878	6271
Fh 6	5.9		705	502	1154	1197	922	833	2849	2930	4907	2949	3778	3595
Fh 7	6.6		633	496	820	974	0	408	1839	2026	3094	1116	1934	2976
Fh 8	7.4		227	304	812	940	0	^d	2601	1953	2753	54	^b	1902
Fh + 200 μM PO ₄ ³⁻ 4	4.1	108.0	717	508	1191	1735	2527	3555	2610	2760	7627	4176	3102	6258
Fh + 200 μM PO ₄ ³⁻ 5	5.0	108.0	583	291	909	1185	980	1765	2190	2467	4423	3119	2076	3030
Fh + 200 μM PO ₄ ³⁻ 6	5.8	107.9	687	624	1168	811	955	463	2492	2668	3685	2211	1666	1562
Fh + 200 μM PO ₄ ³⁻ 7	6.9	106.2	596	141	487	368	0	0	1750	2418	2609	1171	2350	1250
Fh + 200 μM PO ₄ ³⁻ 8	7.6	86.1	594	193	595	*	0	^d	1784	2052	*	0	1504	*

n.d. = not determined

^a2 samples were removed due to suspected carry-over from the calibration curve.

^bThe measured aqueous concentration > the initially spiked concentration. Value was removed from subsequent data treatment.

^cAqueous concentration <LoQ, strikethrough value excluded from subsequent data treatment.

^dWhen sorption was corrected for losses to reactor walls, the sorbed amount was calculated to be negative (< -10% sorption), why this data was removed from the subsequent data treatment.

*Outlier excluded from data treatment. Large scattering among triplicates prevented any closer evaluation of sorption.

S2.2.4 Percent adsorbed

Table S6. Percent adsorbed PFASs in the pH-dependent sorption experiment.

sample	pH	PO ₄ ³⁻	PFBA	PFPeA	PFHxA	PFOA	PFNA	PFDA	PFBS	PFHxS	PFOS	FOSA	6:2 FTSA	8:2 FTSA
Unit		% sorbed	% sorbed	% sorbed	% sorbed	% sorbed	% sorbed	% sorbed	% sorbed	% sorbed	% sorbed	% sorbed	% sorbed	% sorbed
Fh 4	4.0		33.5	31.0	42.8	59.7	83.9	100 ^b	41.6	51.4	92.8	81.5	75.5	98.6
Fh 5	4.8		28.7	23.6	32.1	36.1	58.8	98.3	33.5	39.8	67.8	69.1	49.1	93.6
Fh 6	5.9		28.6	18.4	31.3	18.5	21.0	18.5	30.2	34.7	43.9	35.4	38.1	53.6
Fh 7	6.6		25.7	18.1	22.2	15.0	0	9.0	19.5	24.0	27.7	13.4	19.4	44.4
Fh 8	7.4		9.2	11.1	22.0	14.5	0	^d	27.6	23.1	24.6	0.7	^c	28.0
Fh + 200 μM PO ₄ ³⁻ 4	4.1	100 ^b	29.1	18.6	32.3	26.8	57.5	78.8	27.7	32.7	68.2	50.1	31.2	93.4
Fh + 200 μM PO ₄ ³⁻ 5	5.0	100 ^b	23.7	10.6	24.6	18.3	22.3	39.1	23.2	29.2	39.5	37.4	20.9	45.2
Fh + 200 μM PO ₄ ³⁻ 6	5.8	100 ^b	27.9	22.8	31.6	12.5	21.7	10.3	26.5	31.6	32.9	26.6	16.8	23.3
Fh + 200 μM PO ₄ ³⁻ 7	6.9	98.4	24.2	5.2	13.2	5.7	0	0	18.6	28.6	23.3	14.1	23.7	18.7
Fh + 200 μM PO ₄ ³⁻ 8	7.6	93.4	24.1	7.1	16.1	*	0	^d	18.9	24.3	*	0	15.1	*

^a2 samples were removed due to suspected carry-over from the calibration curve.

^bAqueous concentrations <LoQ (Table S4) are reported as 100% adsorption.

*Outlier excluded from data treatment. Large scattering among triplicates prevented any closer evaluation of sorption.

^cThe measured aqueous concentration > the initially spiked concentration. Value was removed from subsequent data treatment.

^dWhen sorption was corrected for losses to reactor walls, the sorbed amount was calculated to be negative (< -10% sorption), why this data was removed from the subsequent data treatment.

S2.2.5 log K_d values ($L\ kg^{-1}\ Fe$)

Table S7. log K_d values ($L\ kg^{-1}\ Fe$) for the pH-dependent sorption experiment.

sample	pH	PFBA	PFPeA	PFHxA	PFOA	PFNA	PFDA	PFBS	PFHxS	PFOS	FOSA	6:2 FTSA	8:2 FTSA
Fh 4	4.0	3.46	3.41	3.63	3.93	4.54	≥5.84	3.61	3.78	4.86	4.49	4.24	5.59
Fh 5	4.8	3.36	3.25	3.43	3.51	3.97	5.59	3.46	3.57	4.08	4.20	3.74	4.92
Fh 6	5.9	3.36	3.11	3.41	3.11	3.25	3.17	3.39	3.48	3.65	3.59	3.54	3.82
Fh 7	6.6	3.29	3.10	3.21	3.00	n.a.	2.81	3.14	3.25	3.34	3.04	3.14	3.66
Fh 8	7.4	2.76	2.85	3.20	2.98	n.a.	^b	3.34	3.23	3.27	1.67	^a	3.35
Fh + 200 $\mu M\ PO_4^{3-}$ 4	4.1	3.37	3.11	3.43	3.32	3.95	4.39	3.34	3.44	4.09	3.85	3.41	4.90
Fh + 200 $\mu M\ PO_4^{3-}$ 5	5.0	3.25	2.83	3.27	3.10	3.28	3.62	3.24	3.37	3.57	3.62	3.18	3.67
Fh + 200 $\mu M\ PO_4^{3-}$ 6	5.8	3.34	3.23	3.42	2.91	3.27	2.87	3.31	3.42	3.45	3.41	3.06	3.24
Fh + 200 $\mu M\ PO_4^{3-}$ 7	6.9	3.26	2.49	2.94	2.53	n.a.	n.a.	3.11	3.36	3.24	3.07	3.25	3.12
Fh + 200 $\mu M\ PO_4^{3-}$ 8	7.6	3.26	2.63	3.04	*	n.a.	^b	3.12	3.26	*	n.a.	3.01	*

*Outlier excluded from data treatment. Large scattering among triplicates prevented any closer evaluation of sorption.

^aThe measured aqueous concentration > the initially spiked concentration. Value was removed from subsequent data treatment.

^bWhen sorption was corrected for losses to reactor walls, the sorbed amount was calculated to be negative (< -10% sorption), why this data was removed from the subsequent data treatment.
n.a. not available

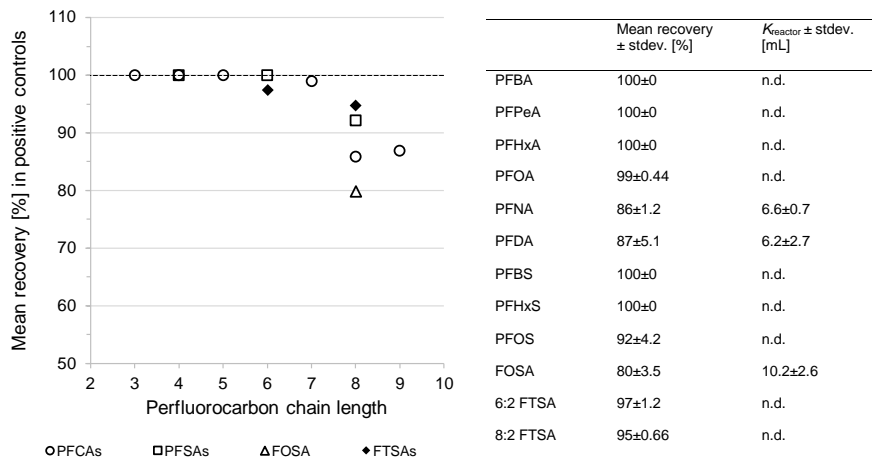


Figure S1. Recoveries [%] for positive controls ($n = 4$, 10 mM NaNO₃, pH 5.8). Note that the vertical axis is broken at 50% recovery. For substances that showed recoveries below 90% in the positive controls (i.e. PFNA, PFDA, FOSA), solution–reactor distribution coefficients K_{reactor} were calculated from the aqueous PFAS concentration in the positive control and the amount of PFAS extracted (MeOH, 24h of shaking) from the walls of the empty reactor. This coefficient was then used to calculate the amounts of these three PFASs that were sorbed to the reactor walls in the pH-dependent sorption experiment.

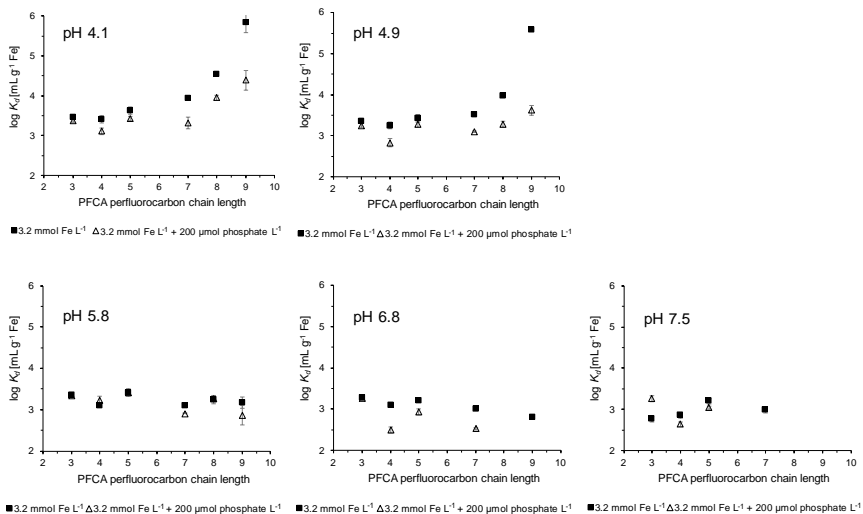


Figure S2. PFCAs ferrihydrite–water partitioning coefficients $\log K_d$ [L kg⁻¹ Fe] in the absence and presence of added phosphate. $\sum[\text{NO}_3^-] = 10 \text{ mmol L}^{-1}$. At pH 4.1, the measured aqueous concentration of C₉ PFDA was below the limit of quantification (LoQ), and thus, the above shown K_d value corresponds to an assumed aqueous concentration equal to that of the LoQ.

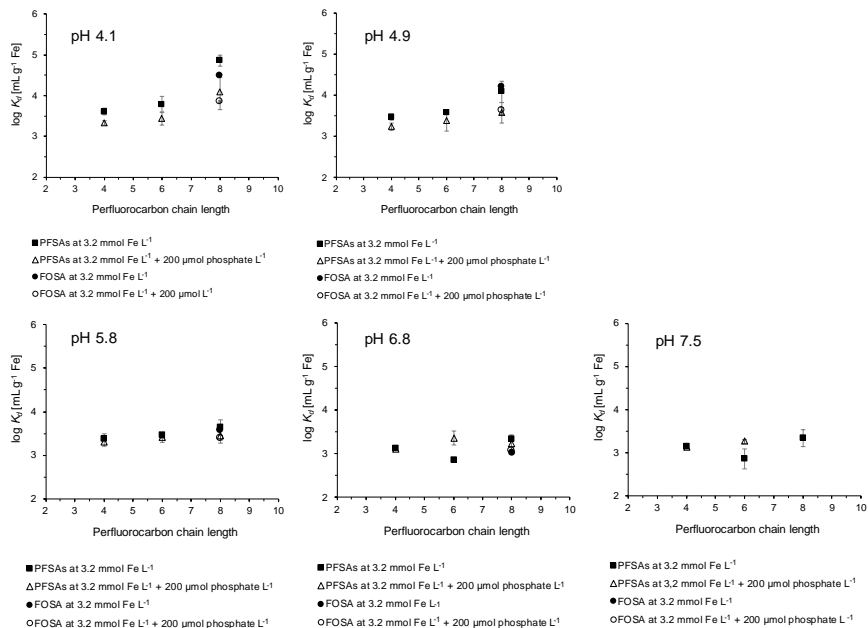


Figure S3. Ferrihydrite–water partitioning coefficients $\log K_d$ [L kg⁻¹ Fe] for PFSA and FOSA in the absence and presence of added phosphate. $\sum[\text{NO}_3^-] = 10 \text{ mmol L}^{-1}$.

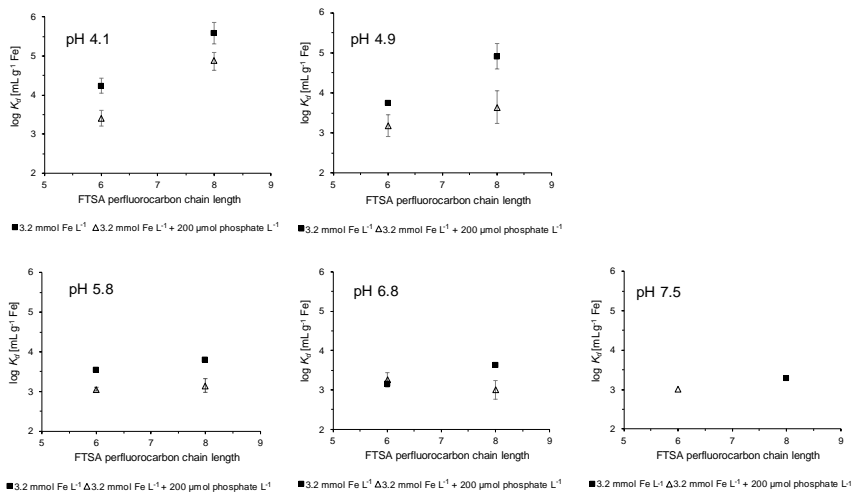


Figure S4. Ferrihydrite–water partitioning coefficients $\log K_d$ [$\text{L kg}^{-1} \text{Fe}$] for 6:2 and 8:2 FTSA in the absence and presence of added phosphate. $\Sigma[\text{NO}_3^-] = 10 \text{ mmol L}^{-1}$.

S2.2.6 Linear regression – effects of pH and zeta potential

Table S8. Linear regression for the relationship between pH and the partitioning coefficient $\log K_d$ (L kg⁻¹ Fe) for the untreated batches *Fh 4* through *Fh 8* (c.f. Table S7).

	$\Delta \log K_d$ unit pH ⁻¹	Pearson r^2	Significant (S) or nonsignificant (NS) relationship ($\alpha = 0.05$)
PFBA	-0.17	0.65	S
PFPeA	-0.15	0.93	S
PFHxA	-0.13	0.91	S
PFOA	-0.29	0.90	S
PFNA	-0.68	0.99	S
PFDA	-1.32	0.93	S
PFBS	-0.10	0.65	S
PFHxS	-0.32	0.84	S
PFOS	-0.47	0.92	S
FOSA	-0.78	0.91	S
6:2 FTSA	-0.39	0.96	S
8:2 FTSA	-0.68	0.96	S

Table S9. Linear regression for the relationship between the ferrihydrite zeta potential [mV] and the partitioning coefficient $\log K_d$ [L kg⁻¹ Fe].

	$\Delta \log K_d$ mV ⁻¹ zeta potential	Pearson r^2	Significant (S) or nonsignificant (NS) relationship ($\alpha = 0.05$)
PFBA	0.0045	0.13	NS ($p = 0.30$)
PFPeA	0.015	0.65	S
PFHxA	0.012	0.73	S
PFOA*	0.029	0.73	S
PFNA*	0.057	0.51	S
PFDA*	0.16	0.72	S
PFBS	0.0076	0.55	S
PFHxS	0.0073	0.17	S
PFOS*	0.034	0.56	S
FOSA	0.047	0.48	S
6:2 FTSA*	0.021	0.36	S
8:2 FTSA	0.060	0.65	S

*The value of the regressed linear slope [$\Delta \log K_d$ mV⁻¹ zeta potential] should be viewed as indicative due to the pronounced nonlinearity of the relationship between $\log K_d$ and the zeta potential, i.e. due to larger positive values of the slope $\Delta \log K_d$ mV⁻¹ upon larger zeta potentials.

S2.2.7 Zeta potential measurements

Table S10. The zeta potential of the ferrihydrite suspensions after 24 h of shaking. The measured samples had the same solution chemistries as those of the pH-dependent sorption experiment, with the exception of not having any PFASs added.

	pH	Zeta potential (mV)	Standard deviation (mV)
3.2 mmol Fe L ⁻¹ as ferrihydrite	3.86	26.4	3.82
	4.02	28.0	3.09
	4.55	28.2	3.59
	4.85	27.1	3.29
	5.21	27.2	3.52
	5.55	23.5	3.60
	6.01	22.4	3.50
	6.62	14.9	3.61
	6.92	11.8	4.38
	7.69	0.98	4.85
	9.08	-4.89	4.98
	9.79	-7.51	4.52
3.2 mmol Fe L ⁻¹ as ferrihydrite + 200 μmol PO ₄ ³⁻ L ⁻¹	3.96	29.0	2.82
	4.18	27.1	3.19
	4.44	23.3	3.09
	4.58	24.7	3.38
	5.19	21.5	2.95
	6.19	4.46	2.94
	6.98	-5.37	3.54
	7.43	-18.5	3.17
	8.13	-23.4	3.21
	8.50	-25.9	3.69
	9.18	-25.9	3.30
	9.31	-26	3.21

S2.2.8 Measured and modelled phosphate adsorption onto ferrihydrite in the pH-dependent sorption experiment.

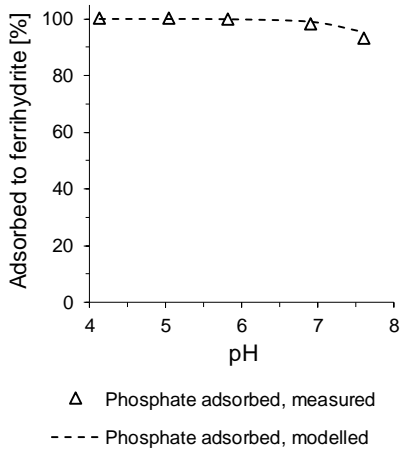


Figure S5. Measured and equilibrium-modelled phosphate ($200 \mu\text{mol L}^{-1}$) adsorption onto ferrihydrite ($3.2 \text{ mmol Fe L}^{-1}$). For the modelling, geochemical software Visual MINTEQ³ (ver. 3.1) was employed, using phosphate–ferrihydrite surface complexation constants from Tiberg et al⁴.

S2.3 Sorption isotherms

S2.3.1 Measured aqueous and adsorbed concentrations of PFASs

Table S11. PFOS, PFOA and FOSA sorption isotherms onto ferrihydrite (10 mmol Fe L⁻¹, with the exception of samples 1A–1C for which [Fe] was 3.2 mmol L⁻¹).

Sample	pH	C_{eq} : Measured aqueous conc. (µg/L)	$C_{adsorbed}$: Calculated sorbed concentration (µg g ⁻¹ Fe)	$\log(C_{adsorbed}/C_{eq})$ (/L kg ⁻¹ Fe)
PFOS				
1A	4.93	0.697	7.22	4.02
1B	4.76	0.337	9.27	4.44
1C	4.81	0.868	6.25	3.86
2A	4.61	15.8	150	3.98
2B	4.42	18.2	146	3.90
3A	4.45	24.8	313	4.10
3B	4.44	19.8	322	4.21
4A	4.48	95.0	758	3.90
4B	4.44	111	729	3.82
5A	4.42	349	1230	3.55
5B	4.39	378	1180	3.49
PFOA				
1A	4.01	0.431	4.02	3.97
1B	4.02	0.489	3.70	3.88
1C	4.02	0.457	3.88	3.93
2A	4.37	55.8	107	3.28
2B	4.35	61.3	97	3.20
3A	4.36	94.1	245	3.41
3B	4.35	104	227	3.34
4A	4.37	339	467	3.14
4B	4.35	362	427	3.07
5A	4.36	780	752	2.97
5B	4.33	815	689	2.93

Table S11, cont.	pH	C_{eq} : Measured aqueous conc. ($\mu\text{g/L}$)	C_s : Calculated sorbed concentration [$\mu\text{g g}^{-1} \text{Fe}$]	$\log(C_{adsorbed}/C_{eq})$
FOSA				
1A	4.01	0.237	6.98	4.47
1B	4.02	0.199	7.19	4.56
1C	4.02	0.215	7.11	4.52
2A	4.46	30.1	58.9	3.29
2B	4.36	38.3	44.3	3.06
3A	4.47	70.2	168	3.38
3B	4.35	81.5	147	3.26
4A	4.44	172	278	3.21
4B	4.34	176	272	3.19
5A	4.45	316	607	3.28
5B	4.36	322	597	3.27
6A	4.54	566	1920	3.53
6B	4.36	556	1940	3.54

S2.3.2 Derived sorption isotherm parameters

Table S12. Summary of fitted sorption isotherm parameters for adsorption of PFOS, PFOA and FOSA onto ferrihydrite. RMSE = root-mean-square error.

Sorption isotherm equation	PFOS	PFOA	FOSA
Freundlich equation: $C_s = K_F \cdot C_{eq}^n$	$K_F = 190 \mu\text{mol}^{1-n} \text{L}^n$ $\text{mol}^{-1} \text{Fe}$; $n = 0.63$ RMSE of fit = $11.4 \mu\text{mol mol}^{-1} \text{Fe}$	$K_F = 66 \mu\text{mol}^{1-n} \text{L}^n$ $\text{mol}^{-1} \text{Fe}$; $n = 0.69$ RMSE of fit = $4.81 \mu\text{mol mol}^{-1} \text{Fe}$	n.d.
Langmuir equation: $C_s = Q_{max} \cdot$ $C_{eq} / (K_{Langmuir} + C_{eq})$	$Q_{max} = 180 \mu\text{mol mol}^{-1} \text{Fe}$, $K_{Langmuir} = 0.24 \mu\text{mol L}^{-1}$ RMSE of fit = $5.52 \mu\text{mol mol}^{-1} \text{Fe}$	$Q_{max} = 160 \mu\text{mol mol}^{-1} \text{Fe}$, $K_{Langmuir} = 1.20 \mu\text{mol L}^{-1}$ RMSE of fit = $4.27 \mu\text{mol mol}^{-1} \text{Fe}$	n.d.
Linear model ^a $C_s = K_d \cdot C_{eq}$	n.d.	n.d.	$K_d =$ $1800 \text{L kg}^{-1} \text{Fe}$ Pearson r^2 of fit = 0.988

^aThe highest aqueous concentration of the FOSA sorption isotherm did not allow fitting to the linear model. The shown K_d value is the regressed value when the highest aqueous concentration was excluded. n.d. = not determined.

S3. Sulfur K-edge XANES spectroscopy

S3.1. Sample properties and features of XANES spectra

Table S13. Properties and spectra characteristics of samples studied with S K-edge XANES spectroscopy (BL-8, Synchrotron Light Research Institute (SLRI), Thailand, May 2017).

Sample	pH	Adsorbed PFAS or sulfate [$\mu\text{mol per mmol}$ Fe or Al]	White-line [eV]	Pre-edge* [eV]	Post-edge shoulder [eV]
PFOS onto Fh	4.0	79	2480.67		2482.5
	3.4	17	2480.68		2482.5
PFOS onto Alhox	5.1	nd ^a	2480.68		2482.5
KPFOS solid standard			2480.72		2483.0
FOSA onto Fh	5.2	185	2480.39		2482.8
	3.5	147	2480.43		2483.0
FOSA onto Alhox	5.6	134	2480.44		2482.8
FOSA solid standard			2480.43		2483.0
PFHxS onto Alhox	5.2	nd ^b	2480.93		
KPFHxS solid standard			2480.93		2482.7
Sulfate onto Fh	4.2	75	2482.47	2478.46	
	3.5	nd ^c	2482.44	Possible pre-edge at 2478.4 eV	
Sulfate onto Alhox	5.1	55	2482.44		
Sodium sulfate (Na ₂ SO ₄) (aq) 30 mM			2482.4		
Potassium sulfate (K ₂ SO ₄) solid standard			2482.39		
Sodium methyl sulfonate (aq) 30 mM			2481.1		

*Determined as the local minima of the second derivative of the normalized spectra.

^aNot determined. 200 μM of KPFOS was equilibrated with Alhox at a concentration of 1 mM Al.

^bNot determined. 200 μM of KPFHxS was equilibrated with Alhox at a concentration of 1 mM Al.

^cNot determined. 200 μM of sulfate (added as K₂SO₄) was equilibrated with Fh at a concentration of 1 mM Fe.

S3.2 Derivatives of normalized spectra for sulfate, PFOS and FOSA onto ferrihydrite

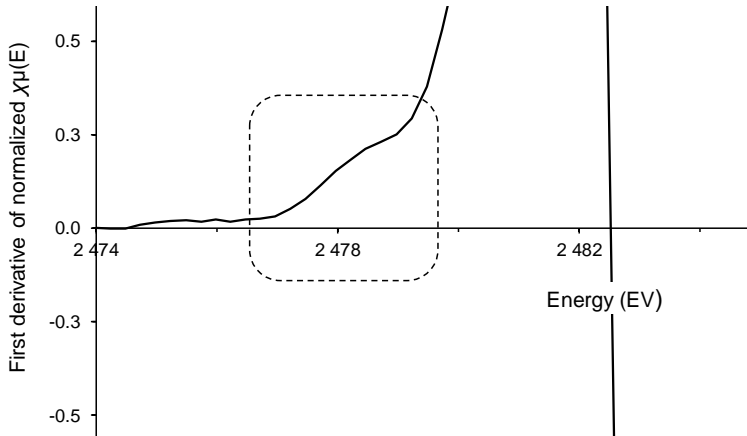


Figure S6. Sulfur K-edge XANES first derivative of the pre-edge (dashed domain) of sulfate adsorbed to ferrihydrite ($75 \mu\text{mol adsorbed mmol}^{-1} \text{Fe}$). pH = 4.2.

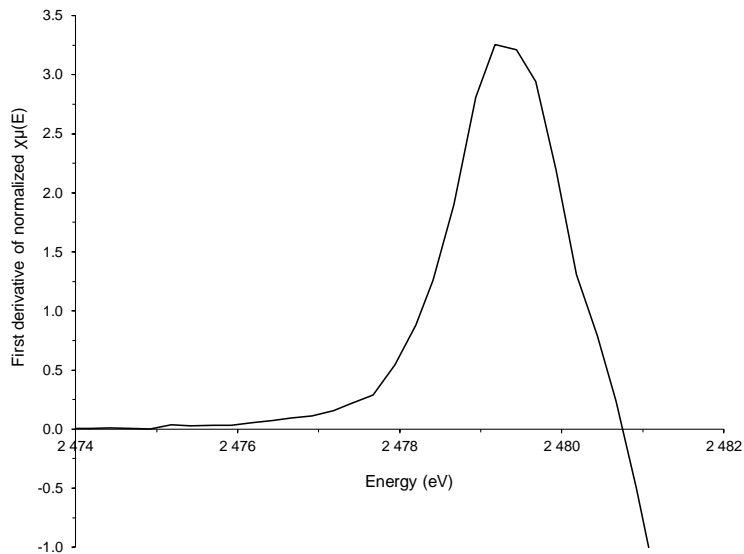


Figure S7. Sulfur K-edge XANES first derivative of PFOS adsorbed to ferrihydrite ($79 \mu\text{mol adsorbed mmol}^{-1} \text{Fe}$). pH = 4.0.

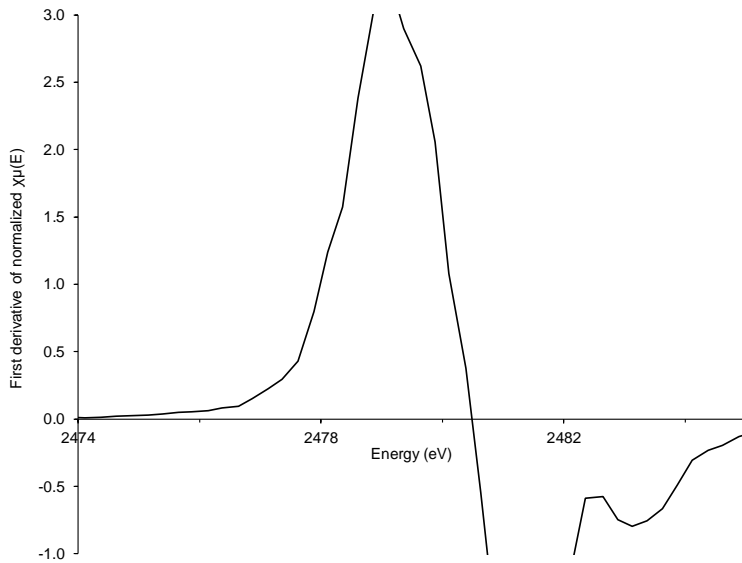


Figure S8. Sulfur K-edge XANES first derivative of FOSA adsorbed to ferrihydrite (185 μmol adsorbed mmol^{-1} Fe). pH = 5.2.

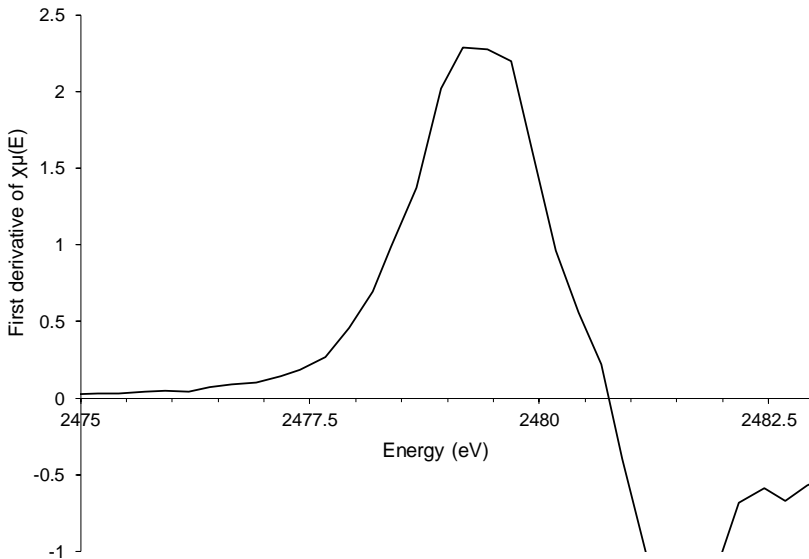


Figure S9. Sulfur K-edge XANES first derivative of PFOS adsorbed to poorly crystalline aluminum hydroxide (Alhox). pH = 5.1. 200 μM of KPFOS was equilibrated with Alhox at a concentration of 1 mM Al.

S3.3 S K-edge XANES spectra for individual PFASs and sulfate

S3.3.1 S K-edge XANES spectra for FOSA

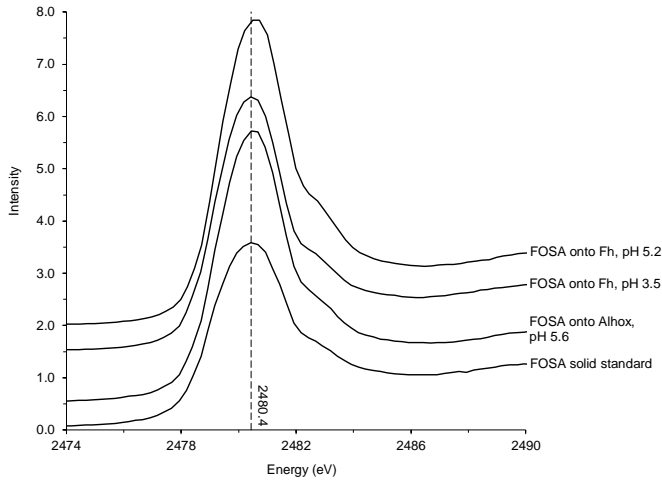


Figure S10. Stacked normalized sulfur K-edge XANES spectra for FOSA onto ferrihydrite (Fh) and poorly crystalline aluminum hydroxide (Alhox).

S3.3.2 S K-edge XANES spectra for PFOS

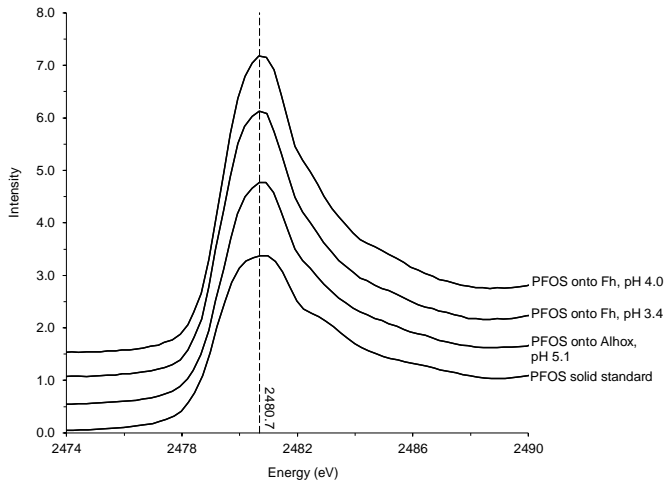


Figure S11. Stacked normalized sulfur K-edge XANES spectra for PFOS onto ferrihydrite (Fh) and poorly crystalline aluminum hydroxide (Alhox).

S3.3.3 S K-edge XANES spectra for PFHxS

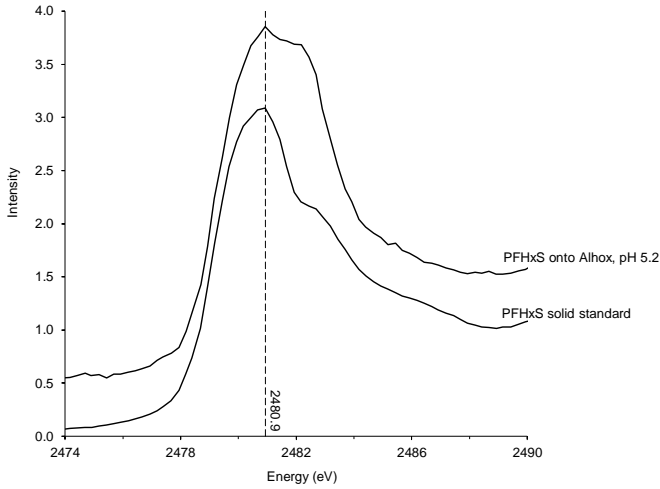


Figure S12. Stacked normalized sulfur K-edge XANES spectra for PFHxS onto poorly crystalline aluminum hydroxide (Alhox).

S3.3.4 S K-edge XANES spectra for sulfate

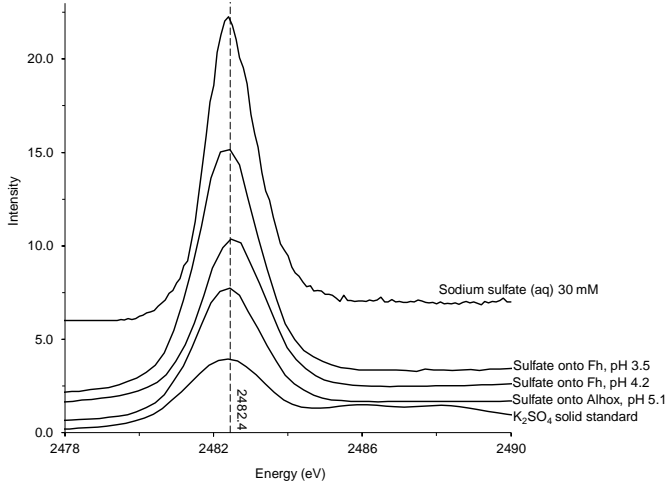


Figure S13. Stacked normalized sulfur K-edge XANES spectra for sulfate (added as K₂SO₄) onto ferrihydrite (Fh) and poorly crystalline aluminum hydroxide (Alhox). The reference spectrum of dissolved sodium sulfate (30 mM Na₂SO₄) was provided by Almkvist et al.⁵

S4. References

- (1) Eriksson, A. K.; Hesterberg, D.; Klysubun, W.; Gustafsson, J. P. Phosphorus Dynamics in Swedish Agricultural Soils as Influenced by Fertilization and Mineralogical Properties: Insights Gained from Batch Experiments and XANES Spectroscopy. *Sci. Total Environ.* **2016**, 566–567, 1410–1419. <https://doi.org/10.1016/j.scitotenv.2016.05.225>.
- (2) Steinle-Darling, E.; Reinhard, M. Nanofiltration for Trace Organic Contaminant Removal: Structure, Solution, and Membrane Fouling Effects on the Rejection of Perfluorochemicals. *Environ. Sci. Technol.* **2008**, 42 (14), 5292–5297. <https://doi.org/10.1021/es703207s>.(3)
- (3) Gustafsson, J.P., 2013. Visual MINTEQ e a free equilibrium speciation model [Internet document]. KTH Vis. MINTEQ. URL. <http://vminteq.lwr.kth.se/>. (Accessed 8 June 2019). Version 3.1. Compiled in Visual Basic 2012, 2013.
- (4) Tiberg, C.; Sjöstedt, C.; Persson, I.; Gustafsson, J. P. Phosphate Effects on Copper(II) and Lead(II) Sorption to Ferrihydrite. *Geochim. Cosmochim. Acta* **2013**, 120, 140–157. <https://doi.org/10.1016/j.gca.2013.06.012>.
- (5) Almkvist, G., Boye, K., Persson, I. K-edge XANES analysis of sulfur compounds: an investigation of the relative intensities using internal calibration. *Journal of Synchrotron Radiation* 2010, 17; 683–688. <https://doi.org/10.1107/S0909049510022946>

ACTA UNIVERSITATIS AGRICULTURAE SUECIAE

DOCTORAL THESIS NO. 2021:75

Understanding the soil retention and mobility of per- and polyfluoroalkyl substances (PFASs) is crucial for their environmental risk assessment. PFASs are bound in soil by a combination of hydrophobic and electrostatic interactions, where pH and soil/sorbent net charge substantially affects their binding. Although organic matter was indicated to be an important sorbent for some PFASs, extrapolations from organic soil materials to mineral soils consistently underestimated the binding, highlighting possible contributions from mineral surfaces, high-affinity binding sites and/or component interactions effects.

Hugo de Campos Pereira received his graduate degree at the Department of Soil and Environment, SLU, Uppsala. He holds a degree of Master of Science (M.Sc.) in Engineering, Environmental and Water Engr., from the Faculty of Science and Technology, Uppsala University.

Acta Universitatis Agriculturae Sueciae presents doctoral theses from the Swedish University of Agricultural Sciences (SLU).

SLU generates knowledge for the sustainable use of biological natural resources. Research, education, extension, as well as environmental monitoring and assessment are used to achieve this goal.

Online publication of thesis summary: <http://pub.epsilon.slu.se/>

ISSN 1652-6880

ISBN (print version) 978-91-7760-827-1

ISBN (electronic version) 978-91-7760-828-8